2P(mx

ELECTROMAGNETIC FREE SUSPENSION SYSTEM FOR SPACE MANUFACTURING

VOL. I: Technology Development

FINAL REPORT

December 22, 1972

Contract No. NAS 8-27228

Prepared For

NATIONAL AERONAUTICS AND SPACE ADMINISTRATION
Product Engineering and Technology Laboratory
Marshall Space Flight Center

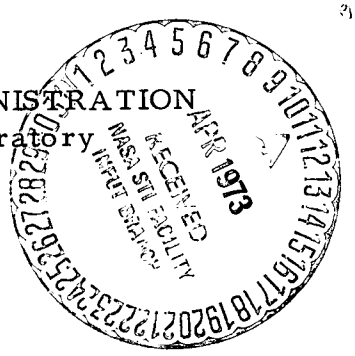

GENERAL ELECTRIC
SPACE DIVISION
Valley Forge Space Center
P. O. Box 8555 • Philadelphia, Penna. 19101

ELECTROMAGNETIC FREE SUSPENSION SYSTEM FOR SPACE MANUFACTURING

VOL. I: Technology Development

BY

E. H. Buerger
R. T. Frost
R. H. Lambert
M. F. O'Connor
E. L. G. O'Dell
L. J. Napaluch
E. H. Stockhoff
G. Wouch

FINAL REPORT

December 22, 1972

Contract No. NAS 8-27228

Prepared For

NATIONAL AERONAUTICS AND SPACE ADMINISTRATION
Product Engineering and Technology Laboratory
Marshall Space Flight Center

GENERAL ELECTRIC
SPACE DIVISION
Valley Forge Space Center
P. O. Box 8555 • Philadelphia, Penna. 19101

TABLE OF CONTENTS

LIST OF ILLUSTRATIONS

FOREWORD

This report (Volume I) is a technical summary of the effort on Modification 3 of Contract NAS 8-27228 carried out between May 18, 1972 and November 21, 1972. The contract was begun on August 25, 1971 as a continuation of the technological development efforts carried out under Contracts No. NAS 8-24683 and NAS 8-26157. On September 14, 1971 the work was verbally redirected by Marshall Space Flight Center to cover definition, design, manufacture, test and flight qualification of an experiment package which would permit the carrying out of zero gravity supercooling and nucleation experiments in the Skylab mission as an extension of the M512-related experiments. The objectives of the supercooling and nucleation experiments are described in an Experiment Proposal dated June 18, 1971 submitted to Marshall Space Flight Center by Dr. R. T. Frost and Professor D. J. Turnbull as Principal Investigators. This document served as the initial guide for the redirected effort.

On December 10, 1971 Marshall Space Flight Center approved a number of specific tasks (Modification 1) which served as a more detailed framework for the new redirection. Work was greatly accelerated in order to meet the very stringent deadlines set by the M512 qualification and launch schedule.

In February 1972 NASA made a decision to terminate the accelerated effort aimed at furnishing a supercooling and nucleation experiment for the

Skylab and issued a stop work order on February 18. On May 18, 1972, a completion effort was defined and mutually agreed upon (Modification 3) which would result in preserving those parts of the technical effort which would be most useful with regard to further technology developments in the zero gravity melting and solidification of metals and semiconductors. Since a large amount of the technical effort had been determined by the specific compatibility requirements with the existing M512 experiment apparatus and the Skylab interfaces, this termination effort was primarily directed to documenting and preserving technology and hardware which would be of most general interest for future experiment developments rather than documentation of the details of the technical effort most specifically related to the M512 and Skylab constraints. To this end, attention was concentrated upon assembly and delivery of laboratory breadboard hardware consisting of a working device for automatic position sensing and control of freely floating diamagnetic spheres compatible with the Marshall Space Flight Center 400 foot drop tower test program. The new documentation of the various phases of the engineering work was limited to only those few items of most general interest for further work in this new technology area.

In Volume I, brief summaries are given of the selected technical areas as well as descriptions of the breadboard hardware and drop test package which is being delivered as part of this effort. Volume II of the report contains the documentation on the Modification 1 contract work specifically related to the Skylab experiment as it existed at the time of contract completion.

1.0 INTRODUCTION

The material which follows describes briefly the technology development done in conjunction with defining a facility to be used on the Skylab mission for electromagnetic suspension of small, molten spheres in the weightless space environment. This facility was planned as an add-on for the M553 sphere-forming experiment. That experiment utilizes an electron beam for melting the specimen and it was planned to use the same source of energy for the electromagnetic suspension demonstration. Electromagnetic suspension and position was to be employed to control the position of the specimens so that they would not contact any other materials or objects during solidification.

In the proposed add-on system, electromagnetic forces are developed by the interaction of the fields from a system of current-carrying coils, with the dipole moment induced by this same coil system in the floating melted specimen. Position and velocity of the levitated spherule are continuously monitored by an optical position sensor. A temperature history of the melt during cooling and solidification was to be provided by means of a simple radiation pyrometer measuring the ratio of radiance in two infrared wave bands. A position control system introduces position and position rate information into a servo loop to control the current levels in several nearby magnetic coils. Although positioning forces as high as 50 to 100 dynes would be utilized for initial deployment of the spherule at the instant of melting and for recovery of the specimen after solidification, it was expected that position

and velocity errors would be nulled within the first few seconds after melting so that only miniscule forces would have to be applied to this spheroid during solidification, provided that solidification did not begin for several seconds after melting. "Miniscule forces" here refers to those forces required to overcome residual accelerations of the Skylab facility which are expected to be in the 10^{-5} g range.

1.1 GENERAL DESCRIPTION

The Electromagnetic Levitation System (EMLS) was to utilize the spherical work chamber of the sphere-forming experiment. Figure 1.1-1 illustrates, schematically, the various elements of the proposed system positioned in this chamber and includes a perspective view of the specimen wheel with the electromagnetic positioning coils, position sensors and control electronics. The electron beam of the facility enters the sphere at the lower left end as indicated by a broken line. Also shown by a broken line is a small cylinder which was to serve to capture the specimens after solidification. A detailed description of the Electromagnetic Levitation System as planned for the Skylab is given in the Experiment Implementation Plan, Section A of Volume II of this report and will not be repeated here.

1.2 BACKGROUND

Under Contract NAS 8-24683 analyses and experiments were carried out on a position control system consisting of six coils mounted as three orthogonal pairs. The coils consisted of typically hundreds of turns of relatively small

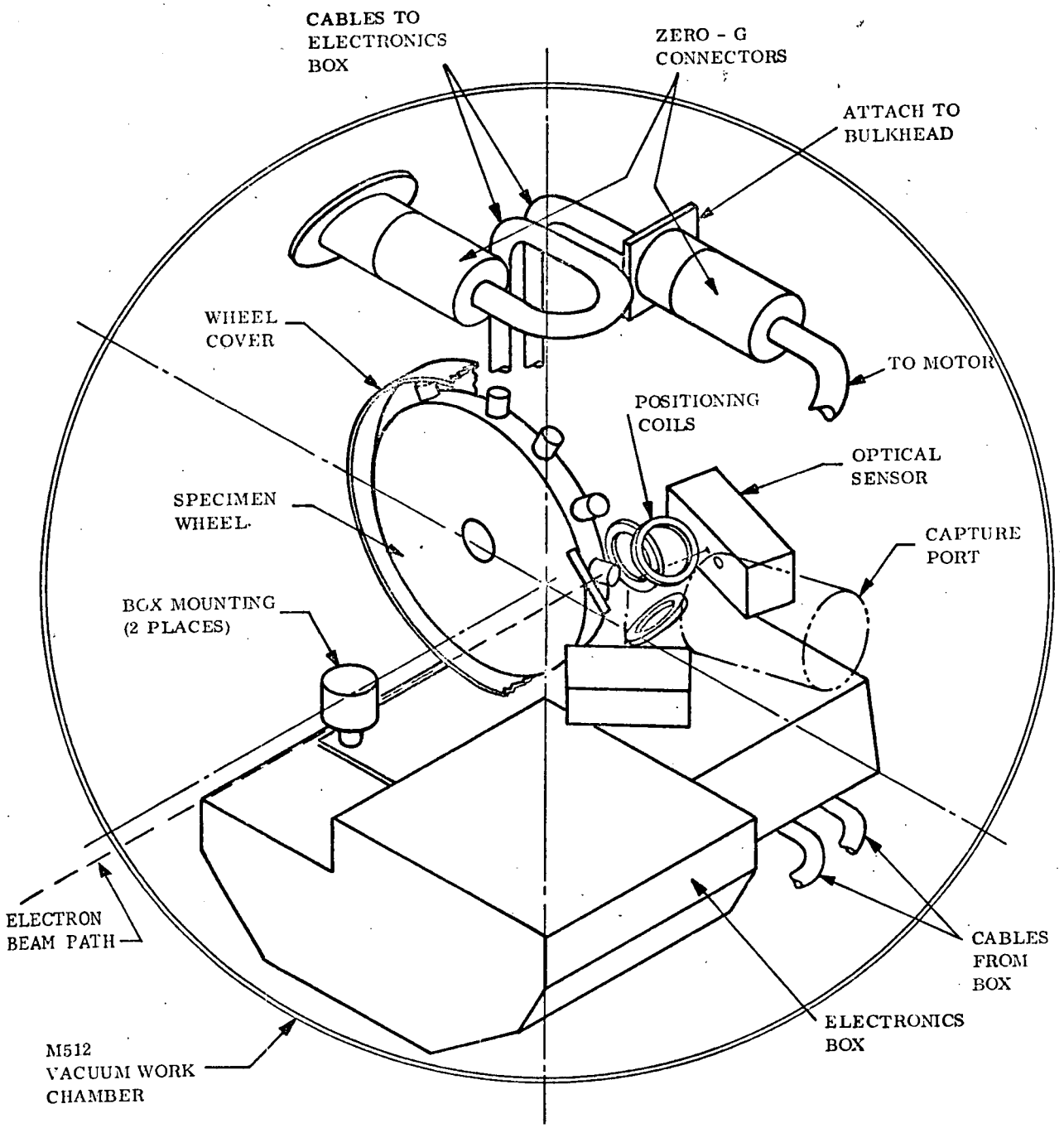

Figure 1.1-1. EMLS in M512 Vacuum Chamber

diameter wire and were operated at frequencies in the 10 kHz region. The coils could be considered to lie on the faces of a cube circumscribing the specimen position. The position of the conducting sphere relative to the center of the cube was monitored by means of the change in inductance of the individual coils due to the reflected impedance of the eddy current paths in the spherical specimen. The position error signals, consisting of the relative changes in impedance of the six coils, was fed into a servo system which automatically regulated the relative power inputs to the six coils in such a manner as to urge the spherical specimen to the center of the cube and to damp oscillatory motions.

Under Contract NAS 8-26157, this concept was developed into a zero gravity position and velocity control servo which was tested in the MSFC 400 foot drop test facility and in the KC135 USAF ballistic flight program. This package incorporated electro-optical sensors for determining the position errors and error rates for the freely floating specimen. Six coils were again used for position control and simultaneously served as the inductor in resonant tuned circuits to improve power coupling efficiency at operating frequencies in the 100 kHz regime. The electro-optical position sensing development was undertaken to widen the range of specimen resistivities which could be handled by the facility since the electromagnetic position sensing scheme is restricted to relatively good conductors. The use of the coils simultaneously as producers of the magnetic field for position control and as tank circuit inductors resulted in only relatively weak available electromagnetic forces because of the high

tank inductance required for use with available capacitors, causing the coil configuration to be solenoids having appreciable length.

1.3 SUMMARY

At the beginning of the contract work reported here, it was decided to separate the field producing and tank circuit inductor functions by use of ferrite core transformers which coupled a resonant tank circuit to the field producing coils. It was also decided to explore the relative merits of employing only four position control coils arranged so as to lie on the faces of an imaginary tetrahedron. This configuration has the advantage of giving a somewhat more open structure to the coil assembly and reduce the number of power amplifiers required. Mock-ups and tests as well as analyses were carried out and a comparison with the six coil configuration was begun. When the contract was redirected towards furnishing a flight model equipment for the Skylab Supercooling and Nucleation experiment it was decided that the more open structure of the tetrahedron as well as a saving in number of power amplifiers was more compatible with the constraints of the already existing M553 specimen changing wheel, electron beam heater and vacuum chamber. For that reason most of the work directed towards the Skylab experiment application was based upon the assumption of a four coil tetrahedral configuration. The tetrahedral configuration required implementation of coordinate converter circuitry since there exist only three independent coordinates describing the position error of the specimen, whereas excitation of the separate coils results in force components

lying in the four non-orthogonal directions described by the coil axes. The requirement for this additional signal circuitry was considered to be a disadvantage outweighed by the superiority in terms of coil geometry and number of high powered circuits and coil leads as compared to the six coil system.

At the time the Skylab Supercooling and Nucleation experiment effort was terminated, the coordinate conversion signal processing electronics had not passed the conceptual design stage. In the interest of furnishing a working drop tower demonstration package for future experiment development in this area on the limited funds available, it was determined that a six coil unit could be assembled more readily because of the relatively large expense that would be entailed in detailed design and construction of the coordinate converter electronics. It was also considered that the advantages of coil configuration and reduced number of power amplifiers were associated primarily with the constraints determined by the existing Skylab equipment and would probably not outweigh the disadvantage of the coordinate converter electronics for future experiment development unconstrained by details such as the M553 specimen selector wheel. A comparison of the four-coil and six-coil configurations is considered in Section 2.2 of this report.

Because of the necessity for performing certain basic tests on the electromagnetic force field configuration with the four-coil system on the accelerated program aimed at the Skylab opportunity, it was necessary to carry out tests on a four-coil servo mock-up at a time before the coordinate converter

electronics was to be available. To this end, a demonstration servo controlling the position of a neutrally buoyant sphere floating in liquid of controlled density was carried out with the four-coil configuration. A simplified position error sensing system and position control servo without coordinate converter was assembled for these tests. Although the position sensing and control servo circuits were somewhat different than those adopted as the reference design for the Skylab experiment, it was agreed to deliver this working four-coil position servo as part of the Mod 3 termination effort in order to preserve the four-coil breadboard hardware development which had been carried out to that date.

The position error sensor which was adopted as the reference design for the Skylab Supercooling and Nucleation experiment consisted of two separate electro-optical sensors viewing the specimen in two orthogonal directions. Each sensor incorporated a quadrant silicon detector which could determine the specimen position transverse to the viewing axis. With the two detectors the three orthogonal position errors of the specimen could be measured with some redundancy. It was decided to incorporate these detectors into the deliverable position control drop tower demonstration package as the most valuable way of preserving this important technology development. These detectors are described in Section 2.6 and are also referred to in the drop tower package description in Section 3.0.

For monitoring of the specimen temperature during solidification, a miniature two-color pyrometer was designed and breadboarded. The decision

to utilize a two-color optical pyrometer rather than a total radiation pyrometer was dictated by the desire to observe specimen temperature changes in the absence of detailed knowledge of specimen emissivity, particularly during phase transformations at which discontinuities might occur in emissivity. In the Skylab Supercooling and Nucleation experiment it was planned to incorporate the pyrometer into the same housing as the optical position sensors. A working breadboard miniature two-color pyrometer is being delivered under the terms of Mod 3 of this contract but was not incorporated into the drop tower package, which at present is designed only for position control demonstrations with cold solid specimens.

Because of the absence of laboratory test data on vaporization rates from the molten specimens in the vacuum provided by the existing Skylab facilities (particularly because some experiment specimens were not determined at the time), there was some concern for problems arising from plating of the optical position sensors by metal vapors. This effect was to be minimized by an arrangement by which the solid state optical sensor element viewed the hot specimen in reflection by a front service mirror. Baffles were considered which would shield the detector from vaporization products traveling directly from the molten specimen in vacuum. Because of the possibility of detector contamination by specimens which might be proposed by other investigators to which the detector would be especially susceptible (it was considered that the detector could survive a wide range of specimen experiments), a back-up

position control system was considered utilizing the electromagnetic detection principle originally studied under Contract NAS 8-26157. This work is discussed briefly in Section 2.5.1.

An analysis is given of the possibilities for specimen rotation control using the electromagnetic position control fields. This is important with respect to inhibiting or controlling rotation rates induced by single-phase induction motor action in freely floating conducting liquid masses. In addition, possibilities exist for shape forming masses into oblate spheroids by inducing controlled rotation rates by means of a two-phase induction motor action which can be arranged by proper phasing of the position control coils.

Section 3.0 gives some detailed description of the demonstration drop tower package for electromagnetic position control. This package was designed to be compatible with the MSFC 400 foot drop tower facility. Diagrams are given showing connections for power and telemetry which should be fully compatible with the carriage which was developed at MSFC for use in both the drop tower and the KC135 aircraft.

Listings of the computer programs which were written for the magnetic field and force analyses are given in an appendix.

In the course of performing the work described in this report, numerous drawings were generated. Some of these drawings are included in this document but many were not of a nature to be referenced here. However, a list of all

drawings prepared is included in Volume II. Microfilm copies of all drawings have been provided to the Contracting Officer's Representative and prints may be obtained from him, if desired.

2.0 TECHNOLOGY DEVELOPMENTS

In this section the technology developments are described which are of most general interest for applications to subsequent efforts in the new area of containerless processing of metals and semiconductors.

2.1 FOUR COIL OPTIMIZATION

In this section we will discuss the four-coil tetrahedral arrangement and its optimization.

The function of the four coils in the tetrahedral configuration is to provide the force, within the available power, required for specimen deployment or retrieval, damping, positioning and, after solidification, ejection or stowage. This force is obtained by selective excitation of one or more coils by radio frequency currents controlled by the position sensing subsystem. The theory describing this force is treated in Section 2 of the final report dated June 15, 1971 on Contract NAS 8-26157. It was shown there that force is dependent on the following parameters.

1. current magnitude in driven coil
2. driven coil size and shape
3. specimen size
4. specimen to coil distance
5. skin depth of specimen.

Efforts were made to optimize the force capability of the coils under the following constraints.

A. Mechanical

- M512 vacuum chamber size
- Specimen size
- Electron Beam Clearance
- Specimen, Specimen Wheel and Indexing Motor Clearance
- Specimen Stowage Path.

B. Optical

- Position Sensor Field of View
- Temperature Sensor Field of View
- Camera Field of View
- Visual Field of View

C. Electrical

- Input R.F. Power (Thermal)
- Coil Interactions
- High Voltage

A four-coil facility was identified that was compatible with these constraints and which could handle specimens up to 1 cm in diameter. The coils were 2 cm inside diameter, spaced tangent to an inscribed sphere of 4 cm diameter. These coils were each wound with 3 turns and had a cross section

approximately 0.4 cm. The coil and its leads are cut from one piece of copper strip about 0.08 cm thick and is self-supporting.

Referring to the expression* for the total force exerted on the sphere by the applied field (Equation 2-4 of the referenced final report):

$$F = -2\pi R_2^3 \mu H \frac{dH}{dZ} G(X) \text{ where}$$

R_2 = Sphere Radius,

G(X) = Body Force Function, discussed in more detail below,

Z = Axial Distance from Coil to Sphere,

we can describe how each parameter can be varied to optimize force.

2.1.1 Sphere Radius (R_2)

The force of a given field and field gradient varies as the cube of R_2. For maximum force we see that R_2 must be kept as large as possible. We will see later where G(X) also requires a large R_2 for appreciable forces. For free

* In the formulae in this section, the MKS system of units is used, i.e. meters kilograms and seconds. The field intensity is expressed in Maxwells. In some later sections cgs units are used, i.e. centimeters, grams and seconds, because of their greater convenience for apparatus of the dimensions considered here and because of the convention of expressing surface tensions and viscosities in these units. Because of the non-triviality of conversion between these sets of units when one is considering magnetic field strengths and induction, a short discussion of units and their inter-conversions is given in Appendix C. We will encounter mixed units and the necessity for conversion in Section 2.7.

body acceleration forces (g forces) the mass varies as the cube of R_2 so R_2 is not significant for acceleration except, as noted above, in G(X). In the event there is wetting of the pedestal holding the molten specimen it is important to provide adequate electromagnetic faces to overcome surface tension forces binding the specimen to the sting on which is is melted, as was the arrangement using the M553 specimen wheel. The sphere radius R_2 then must be kept as large as practical and the coil system must have a free volume sufficient to handle a sphere of this size.

2.1.2 Magnetic Field (H)

For a single turn coil of radius a, the field on axis at a distance r from the coil winding is given by

$$H = \frac{\pi i a^2}{2\mu_o r^3}$$

where r is the slant distance to the winding and i is the current in amperes. The force exerted on the specimen is proportional to H and therefore varies as the square of the coil radius, the inverse cube of the coil-specimen distance, and directly with current i. Immediately we have contradictory requirement because increasing a makes the coil assembly larger and that makes r larger for a specimen located at the center of the coil assembly. Because H is more sensitive to r than to a, some advantage is gained by keeping the coil assembly compact.

2.1.3 Magnetic Field Gradient $\left(\frac{dH}{dZ}\right)$

In the center of the coil the field H is greatest but the change in field, $\frac{dH}{dZ}$, is zero. At a far distance along the axis, the field and field gradient are small. As we move away from the coil the field starts to reduce and the gradient increases rapidly. The force, which is proportional to the product of the field and the field gradient, must therefore increase as we proceed away from the coil plane, but vanishes at large distances. It is thus obvious a maximum force exists somewhere. This maximum is found to occur at a distance from the coil of approximately one-third the coil diameter.

2.1.4 Body Force Function, G(X)

Figure 2.2-1 is a plot of the function G(X). $X = \frac{R_2}{\delta}$ where R_2 is the specimen radius as before and δ is the conducting skin depth. Nothing can be done to the coil to optimize G(X). The specimen size R_2 can be maximized as mentioned previously but will affect the volume of the coil assembly. Because X needs to be at least 3, so that $G(X) \rightarrow 1$, the skin depth must be kept shallow. Therefore, for any specimen size and resistivity, there is a minimum frequency which must be exceeded in order to yield a G(X) near unity.

2.1.5 Selection of an Operating Frequency

The frequency of operation is significant because it must be above that required to make $G(X) \approx 1$ for the highest resistivity material being considered for the specimen. For $R_2 = 0.5$ cm, $\delta \leq 0.17$ cm, and a specimen material

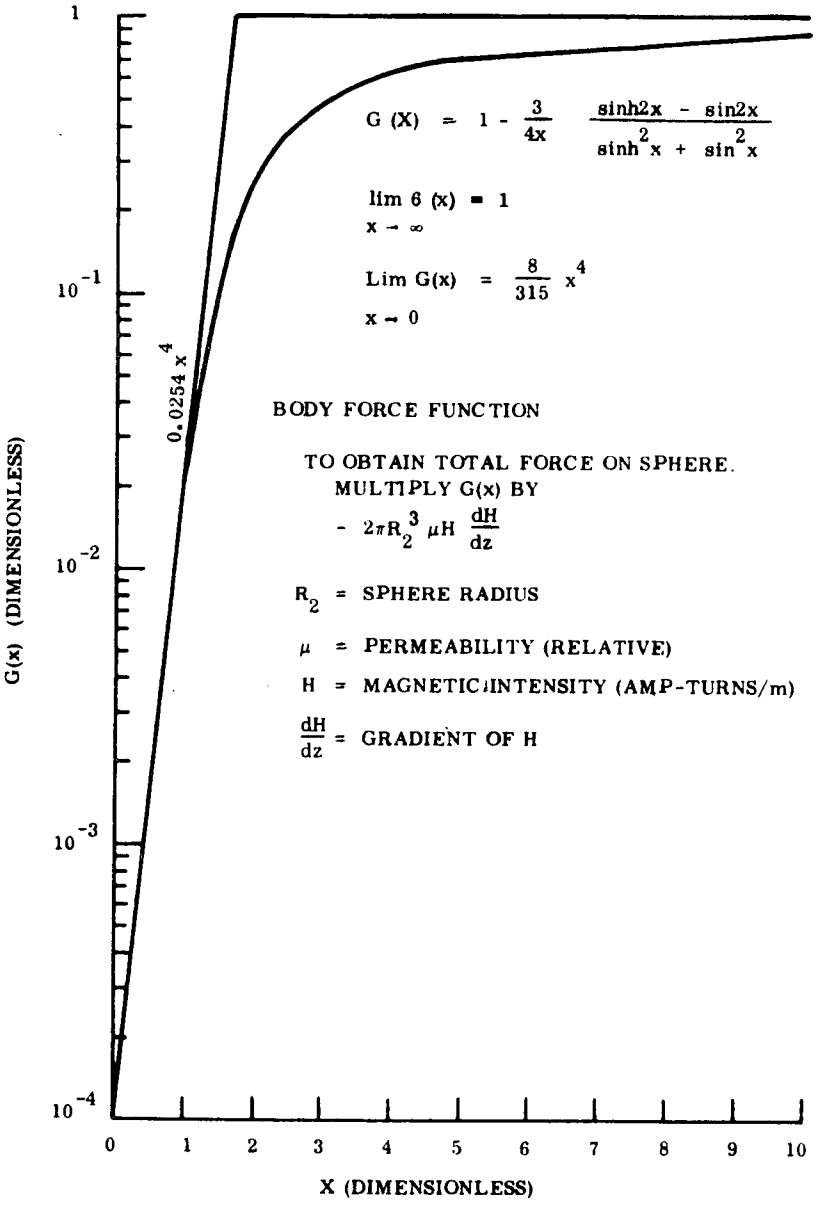

Figure 2.1-1. Body Force Function

with a resistivity of 100 $\mu\Omega$-cm, this requirement dictates a minimum frequency of 900 kHz.

We have described how parametric variation affects force and now must consider the constraint of available power. Changing parameters to maximize force alone is insufficient; maximum force per unit power input is the desired criteria. The major R.F. power loss of the system occurs in the coils. In our consideration of the magnetic field we saw that the field is proportional to the current, the coil radius squared and the inverse cube of the specimen distance. The coil loss is proportional to the resistance and therefore to the coil radius, a, and the field is proportional to a^2. We gain in force per unit power by using the largest a practical. The need for clearances, however, puts a very definite limit on the coil radius, a. The coil loss is proportional to coil resistance so we find that the higher the frequency the greater the loss due to the decrease in conducting skin depth of the coil material. As a minimum, the frequency should not go above that which produces a skin depth of half the coil conductor thickness. For copper at 90 kHz, the skin depth, δ, is 0.022 cm. With a coil conductor thickness of 0.08 cm, δ should be in the order of 0.04 cm or larger. This condition would occur at 27 kHz. Above this frequency, the coil loss increases by the square root of the frequency. However, we have found that a minimum operating frequency approaching 90 kHz must be used because G(X) drops off below much faster rate than the square root of the frequency below 90 kHz. Therefore the optimum frequency for a 100 μ r-cm specimen is in the neighborhood of 90 kHz.

From this discussion, we can conclude that the maximum force per unit power is always lower for the higher resistivity materials in any given coil configuration.

The previous analysis indicates that the copper conductors can be thinner and the number of turns increased. Such a coil is feasible for this application if the temperature rise in the coils for full power input is within the limitations of any insulators needed to survive grazing contacts with the hot specimen.

2.1.6 Impedance Matching Transformer

Another item which entered into the optimization of the coils was the impedance matching transformer. This unit had a one turn secondary which for the available core being used could drive a coil of at most three turns. For a four turn positioning coil, a second secondary turn was needed at the power level used. This would double the turns in primary winding. Overall, the additional loss in the impedance matching transformer with the larger number of turns would offset the gain in going to four turns in the positioning coil. A four turn coil is feasible if a special (non-standard size) core is specified for the impedance matching transformer, a procedure that could be used on any flight program.

2.1.7 Mechanical Configuration

In the simplest geometric arrangement of the four-coil system, each coil would be oriented to be in the face of a simple tetrahedron as shown in

Figure 2.1-2. This initial arrangement permitted the specimens to enter the coil system along path A, the electron beam to enter via path B (which also includes a continuing clear exit path in case the beam is ever permitted to progress that far) and the ejected specimens to leave via C (or in the direction opposite to that of C for "on-the-wheel" stowage). This initial concept was considered to be unsatisfactory primarily for the following two reasons.

A. If a specimen should stick to its support on the wheel after having been melted, the forces which may be created at the location of the support may be too small to push the specimen off the support.

B. If the specimen should readily free itself from the support and push itself away from it - as a consequence of it assuming a spherical shape and of non-wetting of the support - the forces on the opposite side of the coil system, midway between two coils may be insufficient to prevent the specimen from leaving the coil system prematurely. Analysis of this situation is included in Section 2.3 below.

It was essential to the success of the experiment that the specimen come free of its support and then remain within the coil system without touching the coils until it again becomes solid. Since no useful data on the release of typical molten specimens from supports in a freely falling experiment were available during design of the coil system, it was decided that the set of coils, and possibly the specimen with its support, must be rotated to place the specimen at a location at which the forces were known to be larger. This resulted in a tetrahedronal coil configuration and wheel modification shown in Figure 2.1-3.

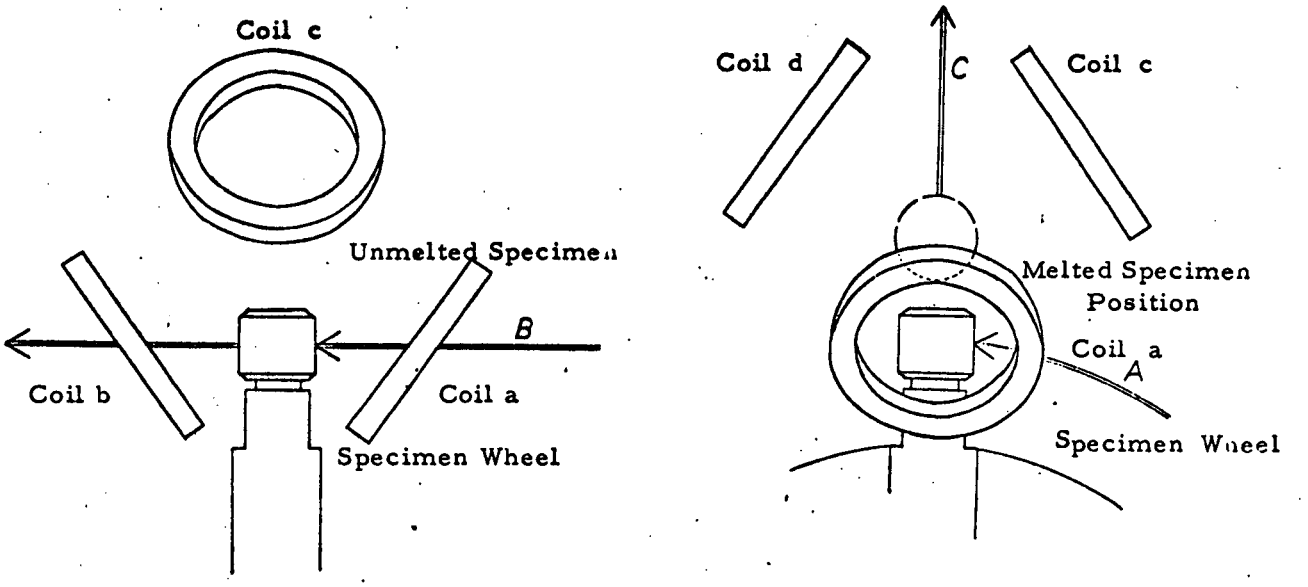

Figure 2.1-2. Tetrahedronal Coil Arrangement

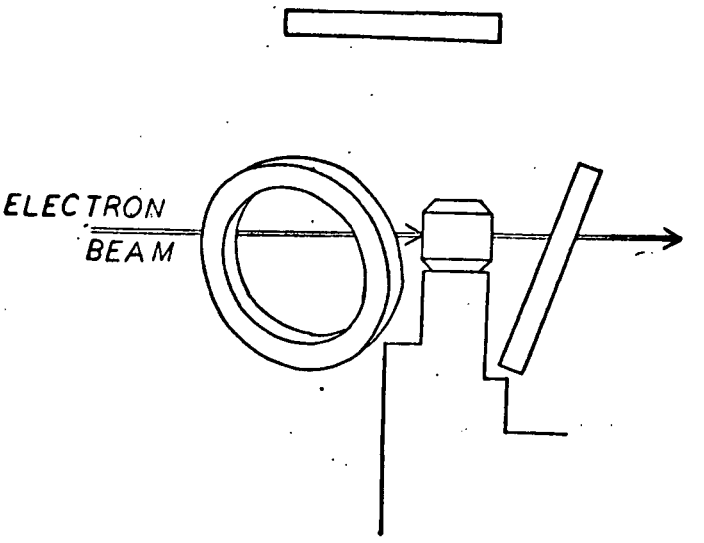

Figure 2.1-3 Modified Tetrahedronal Coil Arrangement

2.2 FOUR-COIL VERSUS SIX-COIL CONFIGURATION COMPARISON

2.2.1 Size

For three dimensional control the four-coil configuration requires only two thirds the number of high power components of a comparable six-coil configuration. Because the power components are the largest parts used, it follows that the four coil system had the best chance to fit within the small space available for this experiment.

The small signal parts count however will rise significantly. These parts are used to perform the coordinate conversion and the servo force vector resolution. This results from the four-fold symmetry of the tetrahedral configuration as compared to the existence of only three independent coordinates for the position errors. The position sensors are on three corresponding orthogonal axes. In general, output from three coils is needed to generate force vectors that are parallel to these axes. A further discussion of the tetragonal coordinate system, coordinate converter and the servo is found in Section 2.3.

In the six-coil system, no coordinate converter is required. In this configuration, axes of the coils define three orthogonal position measurement axes, and the force vectors can easily be derived as proportional to the negative of the position error vectors. Each of the three sensing systems controls only the two coils along that coordinate axis and has no coupling affect into the other coil systems. In total piece part count the six-coil system has fewer parts than the four-coil system. The size and weight of the six-coil system is greater by

about twenty percent than those of the four-coil system because of the larger count of high power components.

2.2.2 Force Considerations

When the force vector created is along a coil axis and directed away from that coil, relatively high force levels are achieved. When the force is directed at a significant angle off-axis, we find the force greatly reduced. In fact, if the specimen is near a coil and on-axis (in a system as defined in Section 2.3.2.3), it could experience over 50 dynes of force. On the other hand, if the specimen is approaching a corner of the four coil system (the part of the tetrahedron on a coil axis but beyond the center of the coil assembly) the force could not exceed about 5 dynes at the very modest total power available from existing M512 circuitry. Further, if the specimen moves 1 cm or more from the center toward a corner of the four-coil system, the force is zero or negative and the specimen can be lost by being ejected from the enclosure. The difficulty presented to the servo by this gross non-symmetry of available forces in the four coil system was being resolted at the termination of work on this contract as reported in Section 2.3.3 below. In view of the forces resulting from the specimen either wetting the substrate or being repelled by it as the molten specimen assumes a spherical shape, and the lack of experimental data in this area, considerable uncertainties remained.

The forces from a given coil in the six-coil system are no greater than those from an identical coil in a four-coil system. The six-coil system, however, can contain a specimen so long as the specimen is within 2 cm of the

enclosure center. Further, if the specimen were near a coil and directed toward a corner (where the force in a six-coil system is no greater than in a four-coil system), it must pass near two coils both of which will direct it toward the center thereby preventing the specimen from approaching the corner and reducing the probability of it being ejected out of the enclosure.

A further operational advantage of the six-coil system is that for any force vector directed to the center region of the enclosure, an equal and opposite vector can be generated after the specimen passes the center. Where there was gross non-symmetry in the four-coil system, we find symmetry in the six-coil system and the servo difficulty noted previously in the four-coil system does not exist.

2.2.3 Interface Effects

Because the EMLS wheel was to have been attached to the M553 Sphere Forming Experiment's motor shaft and because the distance between this shaft and the electron beam had been determined, the diameter of the specimen wheel was required to remain unchanged from that for the M553 experiment. The specimen size was selected to be the same as that used in M553, that is, a one centimeter diameter sphere when molten, with consideration for some to be of a smaller size to accommodate metallurgists whose experimental techniques require the use of small quantities of material. The use of a smaller specimen in a system designed to process larger specimens poses a possible

problem to the position control system because as the ratio of sphere size to coil size decreases, the forces which can be exerted upon the sphere decrease as discussed earlier in Section 2.1.1.

Because of concern of the dynamics of a specimen within the coil system and the possibility that a specimen might be lost through a weak corner (i.e., a region in which the force the coils can exert upon a specimen is relatively small) as discussed in Section 2.3.3, a six-coil system with nearly square coils was considered as shown in Figure 2.2-1. Note that one of these coils had to be distorted somewhat to provide a clear entry for the incoming specimens. For comparable volumes of specimen confinement within the coils the two coil systems were found to produce forces of comparable sizes. It had been found from previous contract work that the six-coil system gave suitable position control and damping from experimental tests and analyses. No work was done, however, under the present contract to analyze specimen wetting to the sting except for initial conceptual theory.

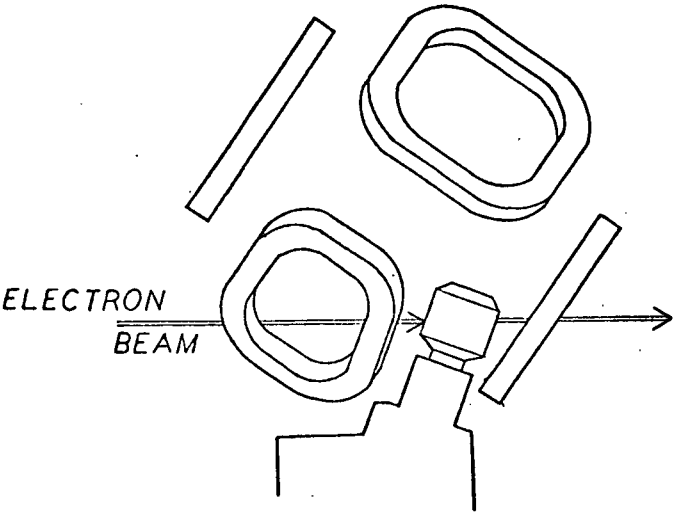

Figure 2.2-1. Possible Six Coil Configuration

2.3 FOUR-COIL POSITION CONTROL SERVO

2.3.1 Introduction

The four-coil tetrahedral configuration was examined with respect to specimen control. Mathematical equations defining the ideal control process were derived. These equations were then integrated with and modified by the results of theoretical and laboratory performance analysis of the actual coils.

On one hand, the defining control equations had to be kept as simple as possible in anticipation of their ultimate implementation via the servo electronics. On the other hand, the actual field forces produced by one coil or by two or three coils acting simultaneously are quite complex and are discussed in Section 2.3.2.4. The exact solution of the system of resulting differential equations is however formidable and implementation of the solution in a servo control requires approximations.

The approach taken was minimization of the servo electronics by simplifying assumptions while maintaining control over a specimen contained in the complex coil force field. This objective was met. The details of the computations and simulations that have been performed are presented below.

2.3.2 Derivation of Servo Control Equations

2.3.2.1 Field Approximation and Comparison to Measurements

The sequence of events as they appeared in the servo control operation is as follows:

1. Specimen position is sensed and velocity calculated by the position sensors.

2. A coordinate transformation is made to the defined axes.

3. Based on the spring-mass-dashpot equations of motion, a vector force is calculated which, if applied to the specimens, would drive it toward the tetrahedron origin (0, 0, 0).

4. The calculated vector force of step 3, $\overline{F}_T$, is resolved into vector components for each of the four coils.

5. An equation is solved, applicable to each coil, which relates the force desired from that coil and the input current required to produce that force.

6. The current of step 5, is delivered to the coils and the coils respond by exerting a total vector force on the specimen, $\overline{F}'_T$.

7. After some Δt, say, 0.01 sec., 1. begins again. As the specimen nears (0, 0, 0) damping is accomplished and the specimen eventually comes to rest at (0, 0, 0).

In the highly idealized system the command force, $\overline{F}_T$, is equal to the delivered force, $\overline{F}'_T$. If the model assumed to compute the equations of Step 3. posses a stable solution, then with $\overline{F}_T = \overline{F}'_T$, the specimen will be precisely controlled and be brought directly to (0, 0, 0). In practice, however, taking into account all the field interactions would require a very complicated control system.

With some reflection, it is clear that the equation of motion assumed in step 3. above is somewhat arbitrary. All that is required is that these equations generate commands for $\overline{F}_T$ appropriate to the desired system operation; strong forces on the specimen, directed toward the origin, when the specimen is far

(~ 1 cm) from the origin; forces directed opposite to velocity and proportional to velocity (damping); and zero force when the specimen is at (0, 0, 0) and at rest with respect to the control volume.

A tractable equation of motion is provided by a spring-mass-dash pot analogue. The solution of these equations can be implemented by the four-coil system for suitably chosen values of the spring constant, k. The controlling equations are of the form

$$\bar{F}_T = m \frac{d^2\bar{p}}{dt^2} = -k\bar{p} + b \frac{d\bar{p}}{dt} \qquad (1)$$

Where: $\bar{F}_T$ is the force applied to the specimen and whose mathematically derived direction is toward the origin of the tetrahedral system (0, 0, 0); $\bar{p}$ is the displacement vector of the specimen from (0, 0, 0); k and b are the 'spring constant' and damping term, respectively; $b = (4\ m\ k)^{1/2}$ for critical damping; and m the mass of the specimen.

For a specified value of k, the controlling equations are defined for critical damping. The value of k selected depends primarily on the capability of the individual coils, the resultant field and the specimen material.

The value of k must be judicially chosen. Too high a value would result in the coils operating near or at maximum current until the specimen gets very near (0, 0, 0). Too low a value of k would result in the neglect of the system's full capability. Ideally, a unique value for k would be use with a given coil geometry for each specimen.

2.3.2.2 Current to the Coils

Equation (1) specifies the command force $\bar{F}_T$, i.e., the force to be applied to the specimen. Whether or not the specimen actually experiences the $\bar{F}_T$ depends upon the equation used to relate the command force to the current to be delivered to the coils and even more so upon the actual field behavior of the forces generated.

The solution of Equation (1) assumes that the forces generated off-axis of the coil are identically equal to the force that would be calculated, for the same distance from the coil, on the center line. That is, Equation (1) contains no provisions for variation of the field over the radius of the coil. There is no simple procedure by which the off-axis effects can be handled mathematically, save by a solution of the equation of motion with these effects included. This would lead, however, to a complex servo electronics and, as will be shown, such complications are necessary.

The block diagram of Figure 2.3-1 outlines the ideal operation of the system and the approximate approach for which the electronic design has been completed.

As noted on Figure 2.3-1, the ideal servo analysis would include the electromagnetic field and force expressions derived by Fromm and Jehn*.

* Fromm, E. and Jehn, H., "Electromagnetic Forces and Power Absorption in Levitation Melting," Brit. J. Appl. Phys., 1965, 16, 653.

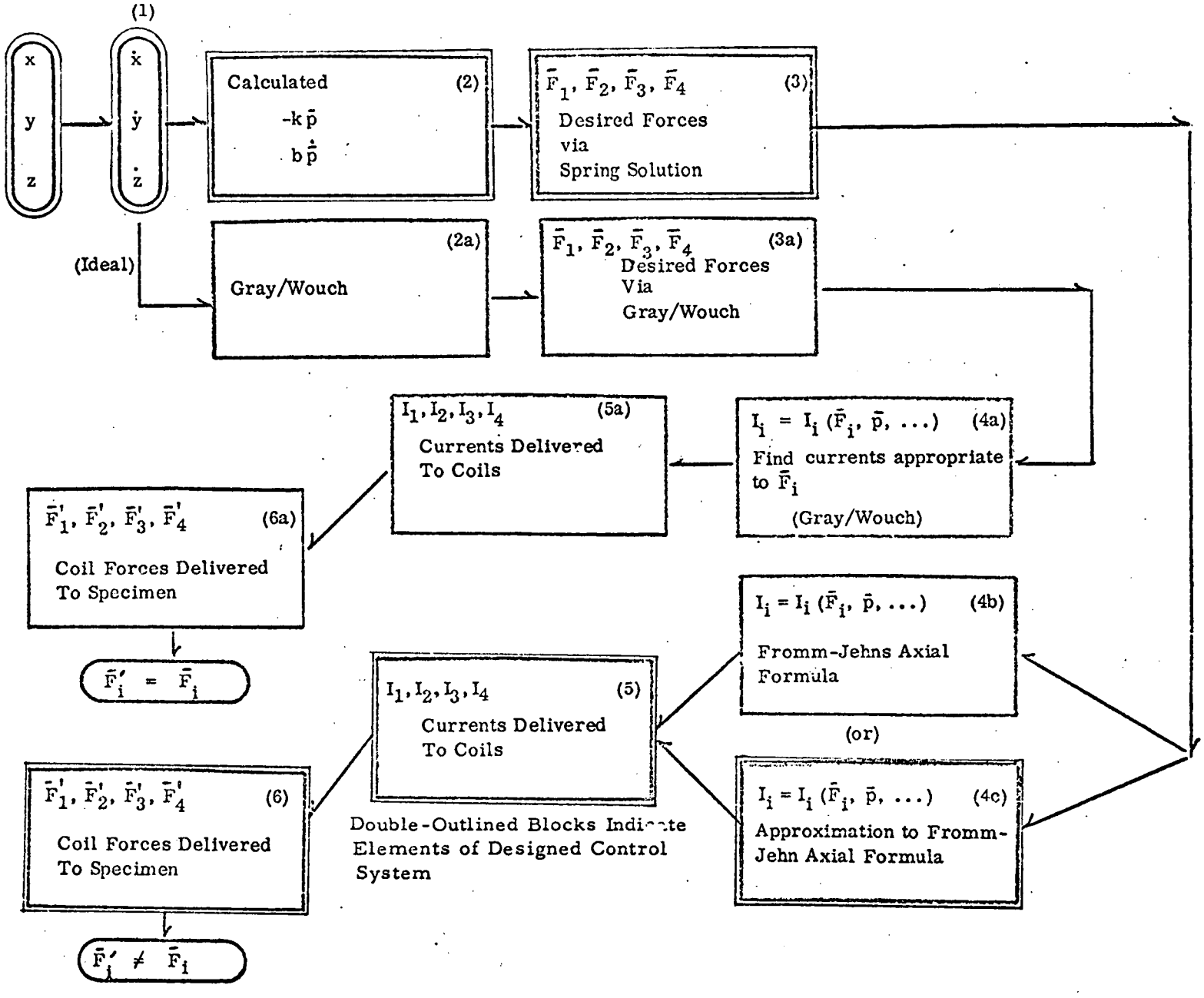

FIGURE 2.3-1 Block Diagram of Idealized and Actual Control System

Here the command forces are equal to those delivered, $\bar{F}'_T = \bar{F}_i$, where the i subscript denotes the acting coil.

Equation (1) yields the desired electronically implemented command forces. Employing the approximations to the electromagnetic force equations at 4b of Figure 2.3-1 yields currents that, by definition, yield the command forces. However, if the specimen is off-axis of the acting coil(s), the force experienced (i.e., delivered) is not equal to that desired, i.e., $\bar{F}'_i \neq \bar{F}_i$. The specimen then does not experience the precise magnitude nor direction of the force required by Equation (1) and errors evolve. The magnitude of these errors and their effect on specimen motion have been simulated when we apply the command current to coil i, but the force delivered was computed on the basis of the off-axial forces due to the four-coil system, described in an appendix.

2.3.2.3 Analysis of Postulated System

In terms of the block diagram (Figure 2.3-1), when currents are calculated at 4b or 4c, these currents must be used as input for electromagnetic field and force equations and the true resulting forces examined. Thus, the actual dynamics of the specimen via the spring equation and either the Fromm-Jehn equations (4b) or an approximation (4c) are studied relative to what is actually taking place.

It will be shown that a workable, rather than an exact, solution is provided by the spring-on-axis approach.

The electromagnetic force acting on a sphere of radius R_2 on the axis of a coil carrying I amperes in N windings has been discussed previously* and is repeated here for convenience.

$$F = \frac{3}{50} \pi^2 (NI)^2 A(y) G(x) \left(\frac{R_2}{R_1}\right)^3$$

y is the specimen-coil distance in units of the coil radius R_1, x is the ratio of sphere radius to RF skin depth. The function G(x) has been discussed in Section 2.1.5 above.

It has been found that an excellent approximation to the force near the center of the tetrahedron is $F = (NI)^2 C_1 \exp(C_2 z)$ as shown graphically in Figure 2.3-2 for the parameters:

Coil Current	45 amp (maximum acceptable)
Diameter of Sphere	1.0 cm
Material	Al at 20°C
Distance between Coil Centers	3.05 cm
Distance between Center of Coil and Center of Tetrahedron	1.87 cm
Coil Diameter	2.3 cm

The constants C_1 and C_2 were determined by fitting the exact expression plotted in Figure 2.3-2 over the control region near z = 1.87.

* Frost, R. T., et al , Field Management for Positioning and Processing of Free Suspended Liquid Materials. General Electric Co., Contract NAS 8-24683, Modification No. 2, Task IV, Final Report, May 15, 1970.

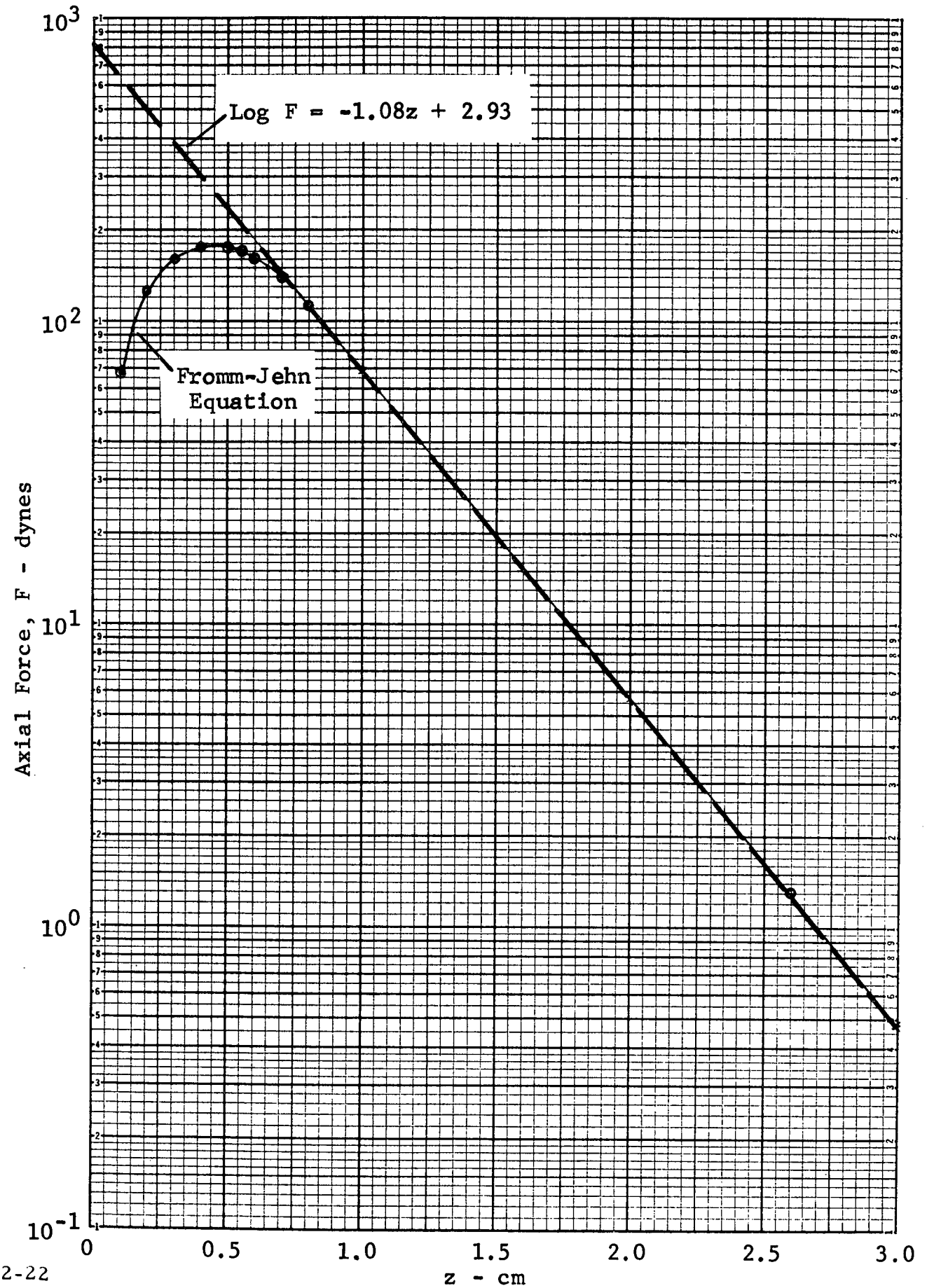

Figure 2.3-2. Fromm-Jehn Force Equation and Approximation

These conditions reproduce those for which more elaborate field calculations are available as well as laboratory measurements (see appendix for computer program).

As indicated in Figure 2.3-2, the approximation can be written:

$$\text{Log } F = -1.08z + 2.93 \tag{2}$$

dividing out $(NI)^2$:

$$\text{Log } F/(NI)^2 = -1.08z - 1.33 \tag{3}$$

or in terms of ℓ ($z = \ell + 1.87$):

$$\text{Log } F/(NI)^2 = -1.08\ell - 3.36 \tag{4}$$

where ℓ is referenced to the center of the tetrahedron.

Consider the case of a single coil, given that a force $\bar{F}_i$ is desired along the axis. From Equation (4) with N = 3, I is easily calculated (and easily implemented electronically). Equation (4) agrees quite well over the control volume near z = 0 with the more exact solution for the single coil as shown in Figure 2.3-3.

Extending the approximation to include off-coil axis positions for two and three coils yields the comparison of Figures 2.3-4 and 2.3-5. The approximation to the left of zero (0) (toward the acting coils) fails completely. This is expected as it is in this region that the coil field superposition effects are most significant. On the positive side of zero (0), the approximation tends to agree rather well with the experimental data.

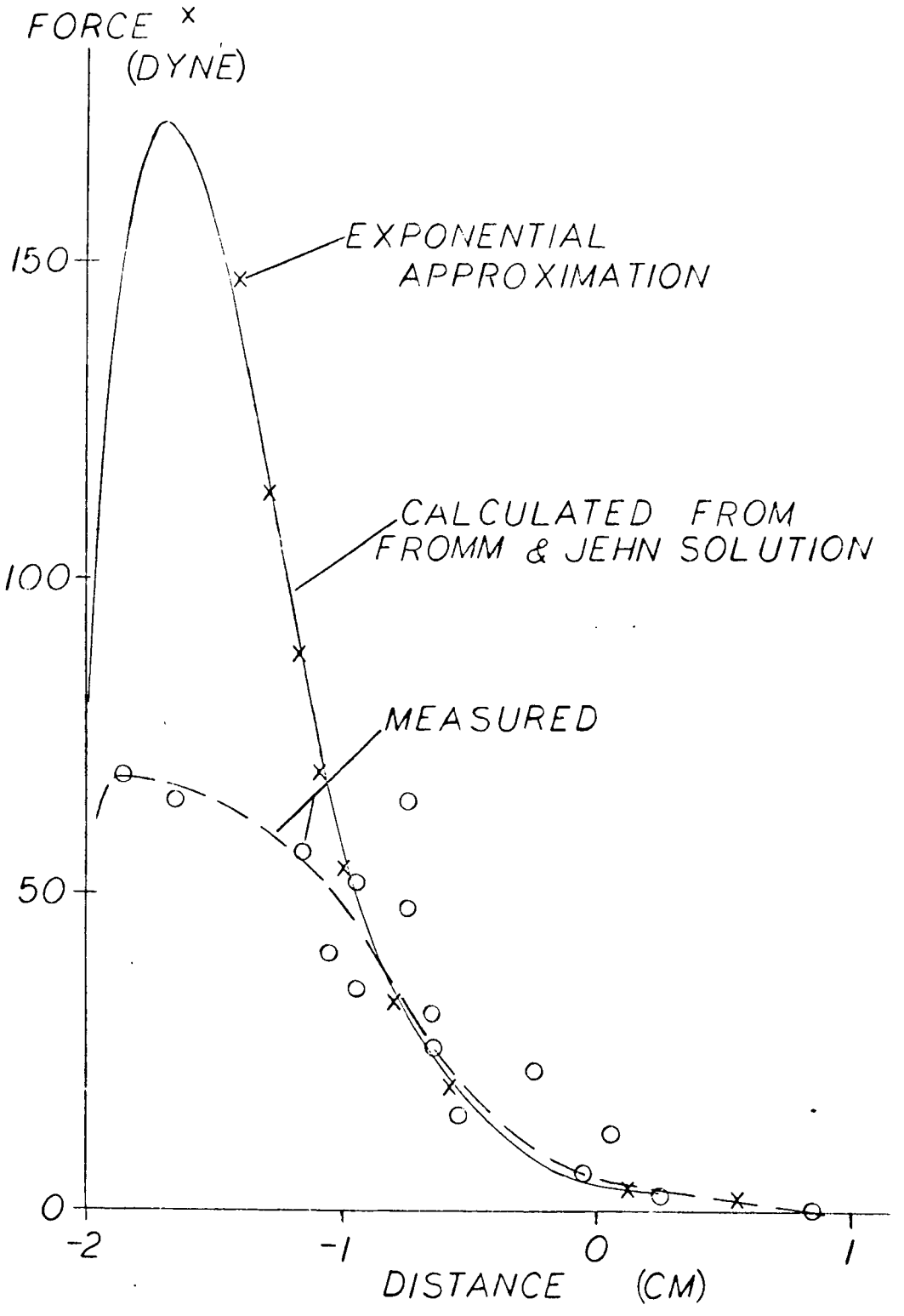

FIGURE 2.3-3 Force Along Axis of Symmetry of One Coil

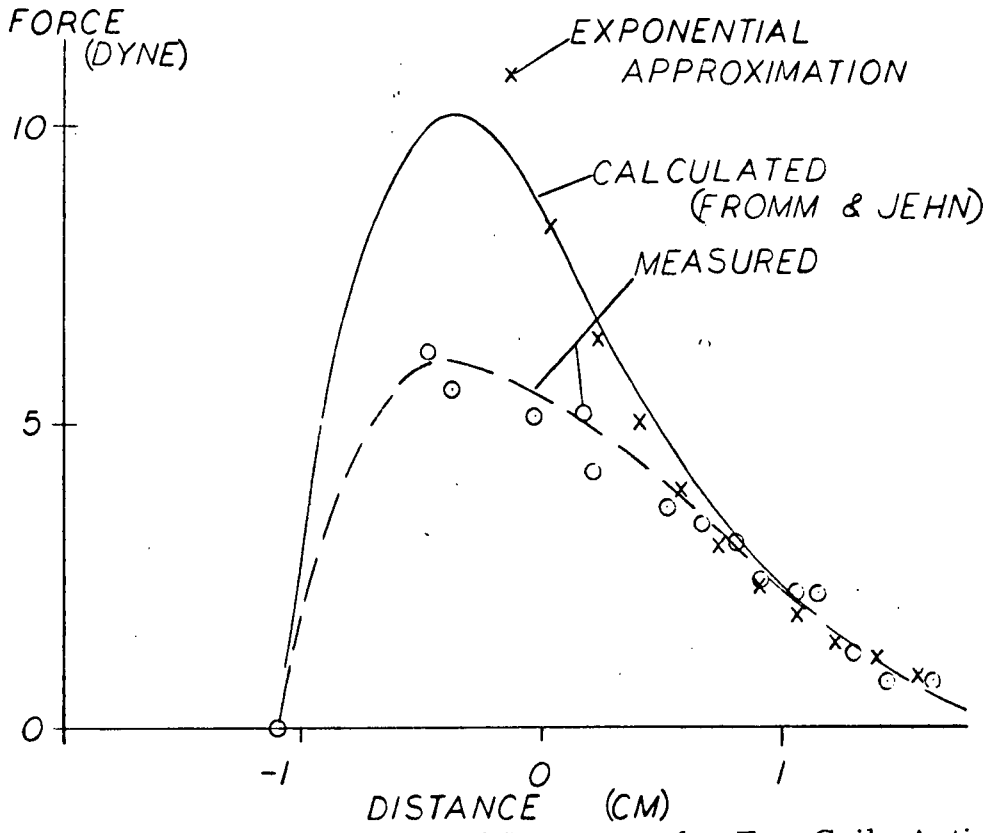

FIGURE 2.3-4 Force Along Axis of Symmetry for Two Coils Acting Simultaneously[x]

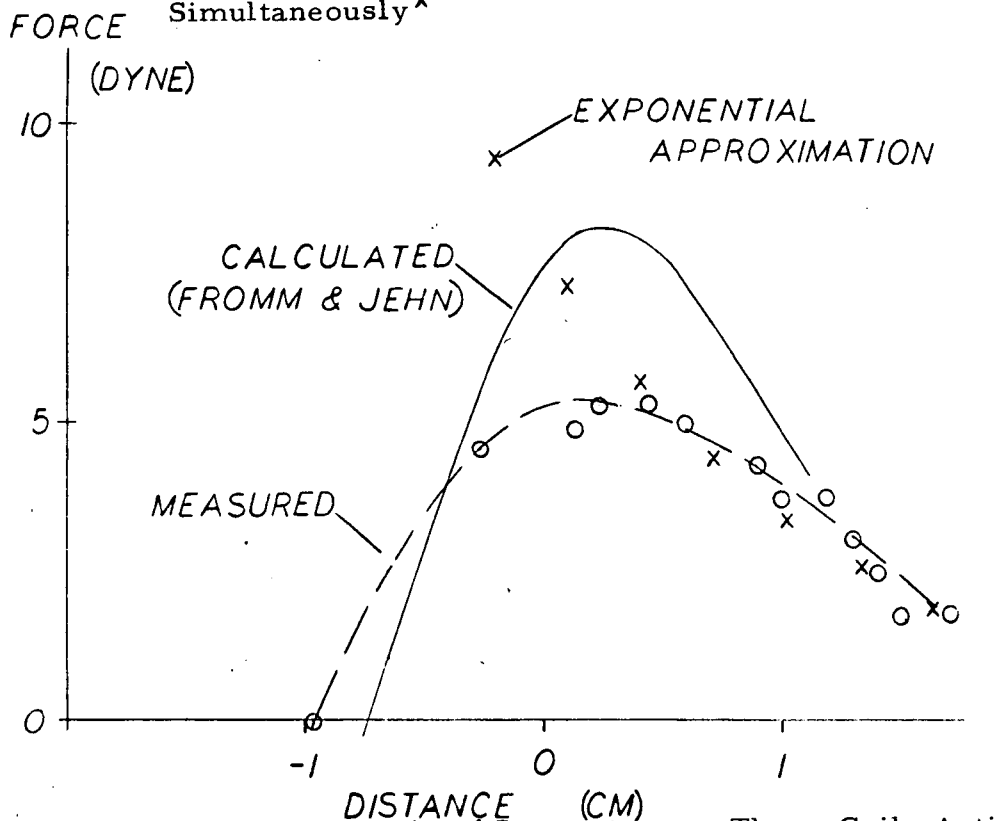

FIGURE 2.3-5 Force Along Axis of Symmetry for Three Coils Acting Simultaneously

Note that although Equation (4) over-predicts forces to the left, forces are produced out to a distance of -1 cm, as in Figures 2.3-4 and 2.3-5. This is the basis of the 'workable' solution. Even though the precisely desired command forces are not delivered, the specimen does experience forces which tend to move it toward the origin.

2.3.2.4 Coil Vectors

A symmetric orientation of the tetrahedron is shown in Figure 2.3-6.

Let the edge length, A to B, be 2L. From the geometric properties of the regular tetrahedron, the unit vectors directed normally from the coils are:

$$\bar{L}_1 = 0\,\vec{i} - \sqrt{2/3}\,\vec{j} + \sqrt{1/3}\,\vec{k}$$

$$\bar{L}_2 = -\sqrt{2/3}\,\vec{i} + o\,\vec{j} - \sqrt{1/3}\,\vec{k}$$

$$\bar{L}_3 = \sqrt{2/3}\,\vec{i} + o\,\vec{j} - \sqrt{1/3}\,\vec{k}$$

$$\bar{L}_4 = 0\,\vec{i} + \sqrt{2/3}\,\vec{j} + \sqrt{1/3}\,\vec{k}$$

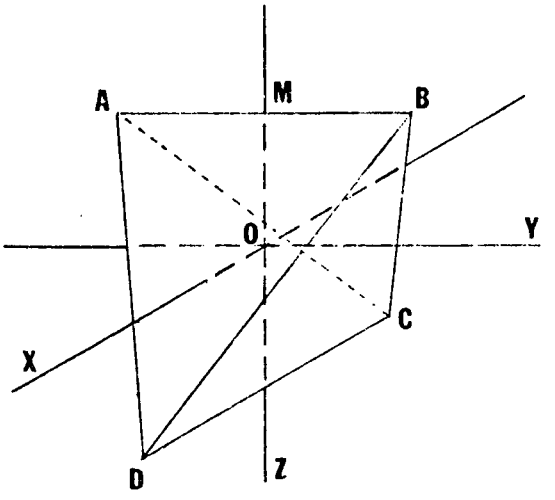

Edge AB || to Y
DC || to X

Face 1 = BDC = Coil 1
Face 2 = ADB = Coil 2
Face 3 = ABC = Coil 3
Face 4 = ACD = Coil 4

Figure 2.3-6. Tetrahedron Orientation

Assume each coil is capable of producing force F_i on a particle, at rest, at vector position $\bar{p}(x, y, z)$. It is desired to determine the force F_i, which each coil must produce so as to achieve a net force in the desired direction, i.e., in the direction opposite to the position error $\bar{p}$. The physical problem is to return the particle to the origin (0, 0, 0) by manipulation of the coil forces. The direction taken by the particle is determined by the ratio of the coil forces.

If we define a unit vector oppositely directly to the position error, $\bar{p}' = \frac{\bar{p}}{p}$, the vector problem is then to solve for F_i from the set of equations

$$\bar{p}' = \sum_i F_i \bar{L}_i , \quad i = 1, \ldots, 4 \tag{5}$$

The direction cosines of the unit vector $\bar{p}'$ are $\cos\alpha$, $\cos\beta$, $\cos\gamma$. We require then that the coefficients of $\bar{i}$, $\bar{j}$, $\bar{k}$ in $\bar{p}'$ be equal to the sum of the $\bar{i}$, $\bar{j}$, $\bar{k}$, coefficients of the $\bar{L}$'s.

Let $\quad a = \sqrt{2/3}$, $\quad b = \sqrt{1/3}$

Then

$$\cos\alpha\ \bar{i} = \left((F_1\ (0)) + (-a\ F_2) + (a\ F_3) + (0\ F_4)\right)\bar{i} \tag{6}$$

$$\cos\beta\ \bar{j} = \left((-a\ F_1) + (0\ F_2) + (0\ F_3) + (a\ F_4)\right)\bar{j} \tag{7}$$

$$\cos\gamma\ \bar{k} = \left((b\ F_1) + (-b\ F_2) + (-b\ F_3) + (b\ F_4)\right)\bar{k} \tag{8}$$

The vectors $\bar{L}_i$ are linearly dependent, but any combination of three of them are linearly independent. Consider an arbitrary value for $\bar{p}'$. In the

physical geometry, $\bar{p}'$ can be represented uniquely by selecting the three appropriate coils of the four. That is, a maximum of three of the pushing (positive F_i) coils will return the particle to the origin. The fourth coil is not employed. Equations (6), (7) and (8) will form a 3 x 3 system of equations if one of the F_i's is set to zero.

The system in Equations (6), (7) and (8) are written in standard matrix form as

$$\underbrace{\begin{bmatrix} o & -a & a & o \\ -a & o & o & a \\ b & -b & -b & b \end{bmatrix}}_{(A')} \underbrace{\begin{bmatrix} F_1 \\ F_2 \\ F_3 \end{bmatrix}}_{F_4} = \begin{bmatrix} \cos\alpha \\ \cos\beta \\ \cos\gamma \end{bmatrix} \qquad (9)$$

Since these three equations do not yet determine the four force components F_i, one more relation involving the F's is required. We may excite the coils in such a manner as to give a fixed arithmetic sum for the four force components:

$$\sum_i F_i = C \text{ , a constant} \qquad (10)$$

Then

$$F_1 + F_2 + F_3 + F_4 = C \qquad (11)$$

Set C to 1. Then

$$\underbrace{\begin{bmatrix} o & -a & a & o \\ -a & o & o & a \\ b & -b & -b & a \\ 1 & 1 & 1 & 1 \end{bmatrix}}_{A} \underbrace{\begin{bmatrix} F_1 \\ F_2 \\ F_3 \\ F_4 \end{bmatrix}}_{F} = \underbrace{\begin{bmatrix} \cos\alpha \\ \cos\beta \\ \cos\gamma \\ 1 \end{bmatrix}}_{p'} \tag{12}$$

So that

$$F = A^{-1} p' \tag{13}$$

Substituting a and b in A and inverting yields

$$A^{-1} = \begin{bmatrix} o & -c & d & e \\ -c & o & -d & e \\ c & o & -d & e \\ o & c & d & e \end{bmatrix} \tag{14}$$

Where

$$\begin{aligned} c &= 0.61237273 \\ d &= 0.43301290 \\ e &= 0.25000000 \end{aligned} \tag{15}$$

Thus, given $\bar{p}'(x, y, z)$, F_i is determined from Equation (13).

A number of solutions to equation (12) have been obtained and can be summarized as follows:

Case	For $\bar{p}'$	General Result
(1)	Not in the plane of two coils	one - F force, three + F forces
(2)	In the plane of two coils	two equal - F forces, two + F forces
(3)	Along one coil axis	three zero forces, one + F force

The negative F forces occurring in Cases (1) and (2) are due to the fact that system of Equation (13) is dependent and there is no way to mathematically restrict the signs of F_i. The negative forces are very easily handled. Since any one of the F_i's can be resolved into components on the other three, the negative F of Case (1) can be resolved onto the three positive F_i's. It can be shown that this resolution is accomplished by simply adding directly the absolute magnitude of the negative F to the magnitudes of the other forces. Note than when this manipulation of the negatives is performed, the constraint Equation (11) is broken; i.e., $\Sigma F_i \neq C$ or 1 as for Equation (12). This is unimportant as it is the F ratios that are desired at this stage.

The above analysis is the "coil solution" to the equation $\frac{\bar{F}}{F} = -k \frac{\bar{P}}{P}$, where k = 1. The second term (damping term) of the equation $\left(\bar{F}_{\text{velocity}} = b \frac{d\bar{p}}{dt}\right)$ is handled in an analogous manner. The velocity data provided by the position sensor electronics, x, y, z is resolved onto the coil-origin axis and the vector sum of the position term and velocity term is taken along each axes,

i.e., $\bar{F}_i = \bar{F}_{i(\text{position})} + \bar{F}_{i(\text{velocity})}$

Again, any negative forces arising are resolved onto the positive (pushing) forces.

2.3.2.5 Resulting Control Equations

The control equations define the current, I_i, to be delivered to each coil. To perform this calculation we must first calculate the negative of the position vector $\bar{p}$ resolved on each coil vector, ℓ_i. These are given below for the tetrahedral geometry.

$$\ell_1 = +\sqrt{2/3}\ y - \sqrt{1/3}\ z$$
$$\ell_2 = \sqrt{2/3}\ x + \sqrt{1/3}\ z$$
$$\ell_3 = -\sqrt{2/3}\ x + \sqrt{1/3}\ z$$
$$\ell_4 = -\sqrt{2/3}\ y - \sqrt{1/3}\ z$$

These functions are differentiated to obtain $\dot{\ell}_i$, for the damping term. The force required of each coil is now calculated from the above using the spring-mass-dashpot form of solution

$$F_i = +K\ \ell_i + b\ \dot{\ell}_i$$

As discussed previously, the magnitude of negative forces are added to each of the other three forces so that a positive (pushing) solution is obtained. The

force required is at this point to be considered a constant and the current for each coil is given by the approximation to the Fromm-Jehn solution by

$$I_i = F_i \; e^{(m \ell_1 + n)}$$

where m and n are scaling constants. These constants are chosen so that maximum current is delivered before a specimen approaches the minimum force position among three coils.

2.3.2.6 Mechanizing Electronics

A complete electronic block diagram and schematic is contained in Appendix A. The implementing electronics of the coordinate conversion equations is depicted in Zones B10-D10 to B8-D8 in GE Drawing ER 47J225305, Sheet 1 in that appendix. The Force/Current Computation electronics are shown in Zones A8-D8 through A3-D3 on the same drawing. As noted in that appendix, the design effort on these circuits had not been completed nor test circuits built at the time of contract termination.

2.3.3 Analysis of Motion of Aluminum Specimen in Four-Coil System

A limited number of computer simulations were made to study the capture capability of the four-coil system. Each coil was limited to a maximum 45 amps. The analytic field solution was employed in the analysis. Although differences exist between these solutions and the experimental measurements, the two agree well enough (see Figures 2.3-3, 2.3-4, 2.3-5 to warrant use of the field solution.

The specimen material chosen was an aluminum sphere of 1 cm diameter. An arbitrary temperature of 700°C was assigned and the skin depth calculated at this temperature is $0.04 < \delta < 0.05$ cm depending on coil frequency. The frequencies assigned were 10^5, 1.16×10^5, 0.78×10^5, and 0.84×10^5 Hz.

2.3.3.1 Sting Position 1

The specimen position selected for the first runs was that shown in Figure 2.3-7 with the coil number designations as indicated in Figure 2.3-6 This was one postulated position in effect when work on the contract was terminated. However, this position is unacceptable since the action of the postulated control is to eject the specimen completely from the control volume

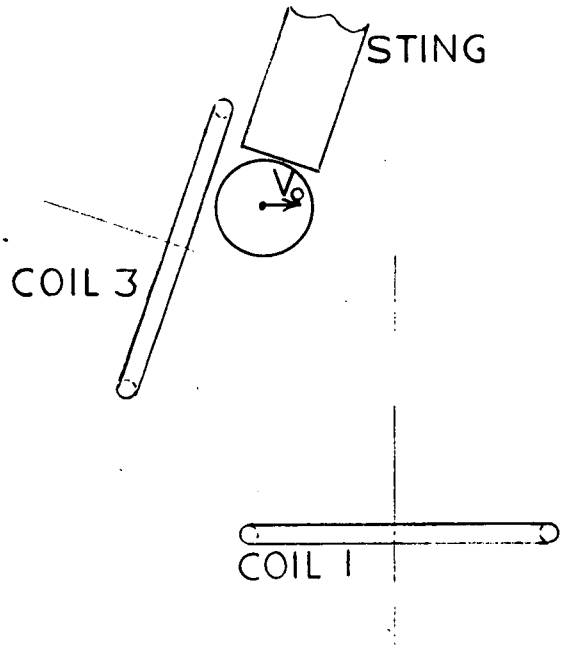

Figure 2.3-7. Sting Position 1

At the position location of the specimen as given above, off-axis effects of Coil 3 are significant. Presuming that the direction of first motion of the specimen is in the direction of the total force vector given by Gray/Wouch, the specimen was ejected from the system for initial velocities of 0.0 and 0.5 cm/sec.

This result was due primarily to the force component perpendicular to the Coil 3 center line. The initial motion is indicated by V_o in Figure 2.3-7. Note that Coil 1 cannot aid in establishing motion toward the origin (0, 0, 0). The specimen is thus moving in the volume defined by Coils 3, 2 and 4 (Coil 2 and Coil 4 are not shown). This combination puts the specimen in the weakest position of the system, i.e., approaching the three coil symmetry line where "negative" (expulsive) forces exist beyond about 0.65 cm (Gray/Wouch results) or 1 cm (lab results). The specimen eventually enters the "negative" force volume and is expelled.

2.3.3.2 Sting Position 2

A second specimen position was chosen so that the axis of the sting lay along the Coil 3 center line and was 1 cm from the origin (0.87 from Coil 3). The initial motion here is along the center line.

Results of several runs from this position are shown in Figure 2.3-8. Up to 3 cm/sec. initial velocities are managed by the system such that critical damping is achieved. Between 3 and 3.5 cm/sec, the specimen overshoots the

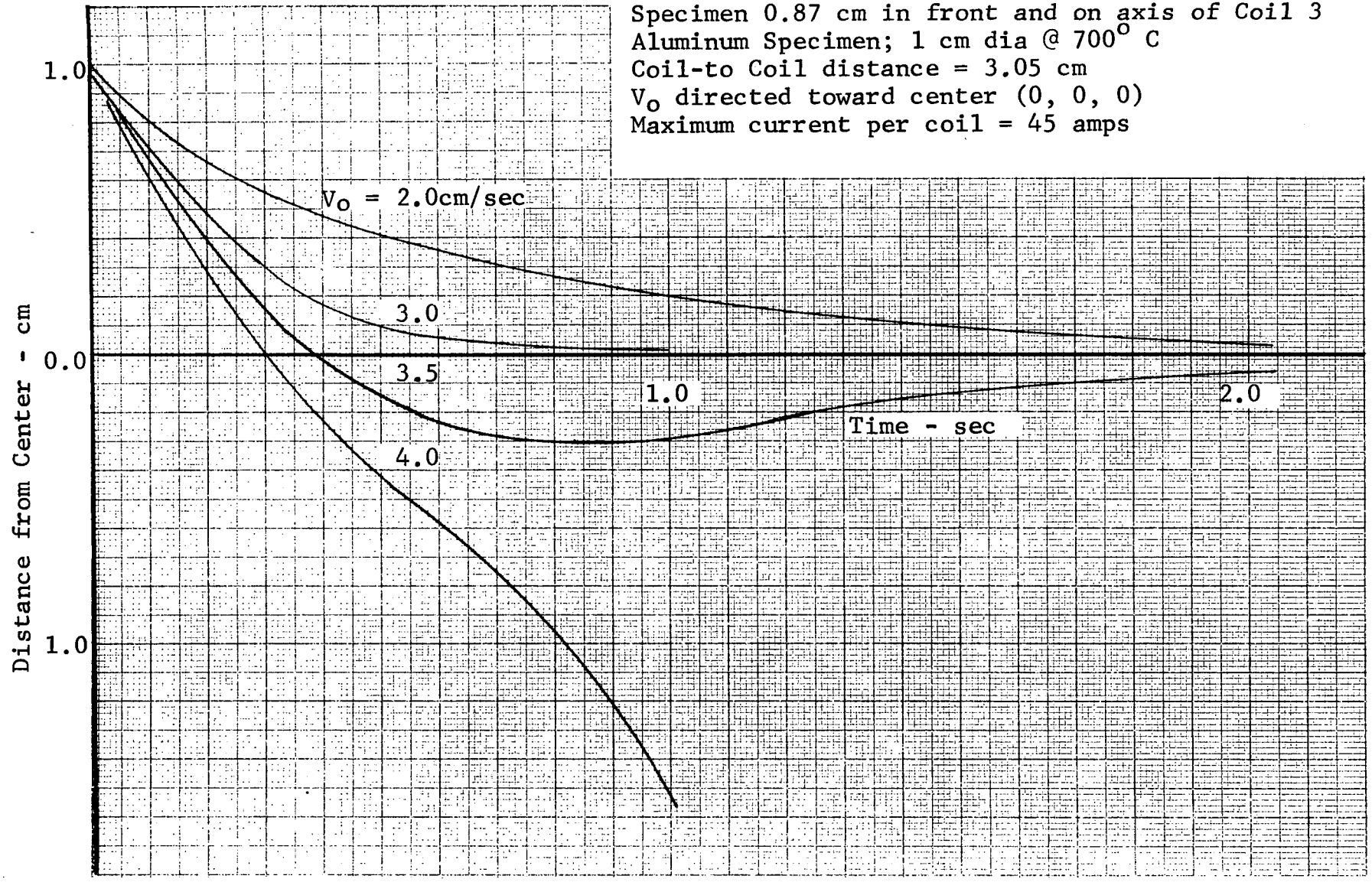

Figure 2.3-8. Motion from Sting Position 2

origin but is eventually turned around and damped. Between 3.5 and 4.0 cm/sec, a velocity exists such that the three damping coils (Coils 1, 2 and 4) cannot handle the initial velocity if limited to 45 amps/coil. The result is ejection of the specimen.

2.3.3.3 Sting Position 3

The unacceptability of Sting Position 1 indicated that a change in the sting location and orientation was necessary. Sting position 2 yielded well controlled specimen motions for reasonable initial velocities. No hard data were available on "wetting" properties of various candidate materials and therefore initial expected velocities could not be accurately predicted. The sting position chosen for this simulation is sketched in Figure 2.3-9 and represents a mechanically feasible configuration as compared to Sting position 2. The sting enters the control volume between Coils 2 and 4 (not shown in Figure 2.3-10). This location would permit a relatively strong force to be developed by Coils 2 and 4 working in concert to lift the material from the sting in case it "sticks" due to some partial wetting of the sting platform by the molten specimen. The initial velocity is, in effect, aimed toward the center of the control volume to permit effective utilization of Coils 1 and 3 as retarders.

2.3.3.4 Ejection Geometry and Constraints for Sting Position 3

1. Coil to coil separation: 3.05 cm

2. Sphere radius: 0.5 cm
   Coil radius: 1.15 cm

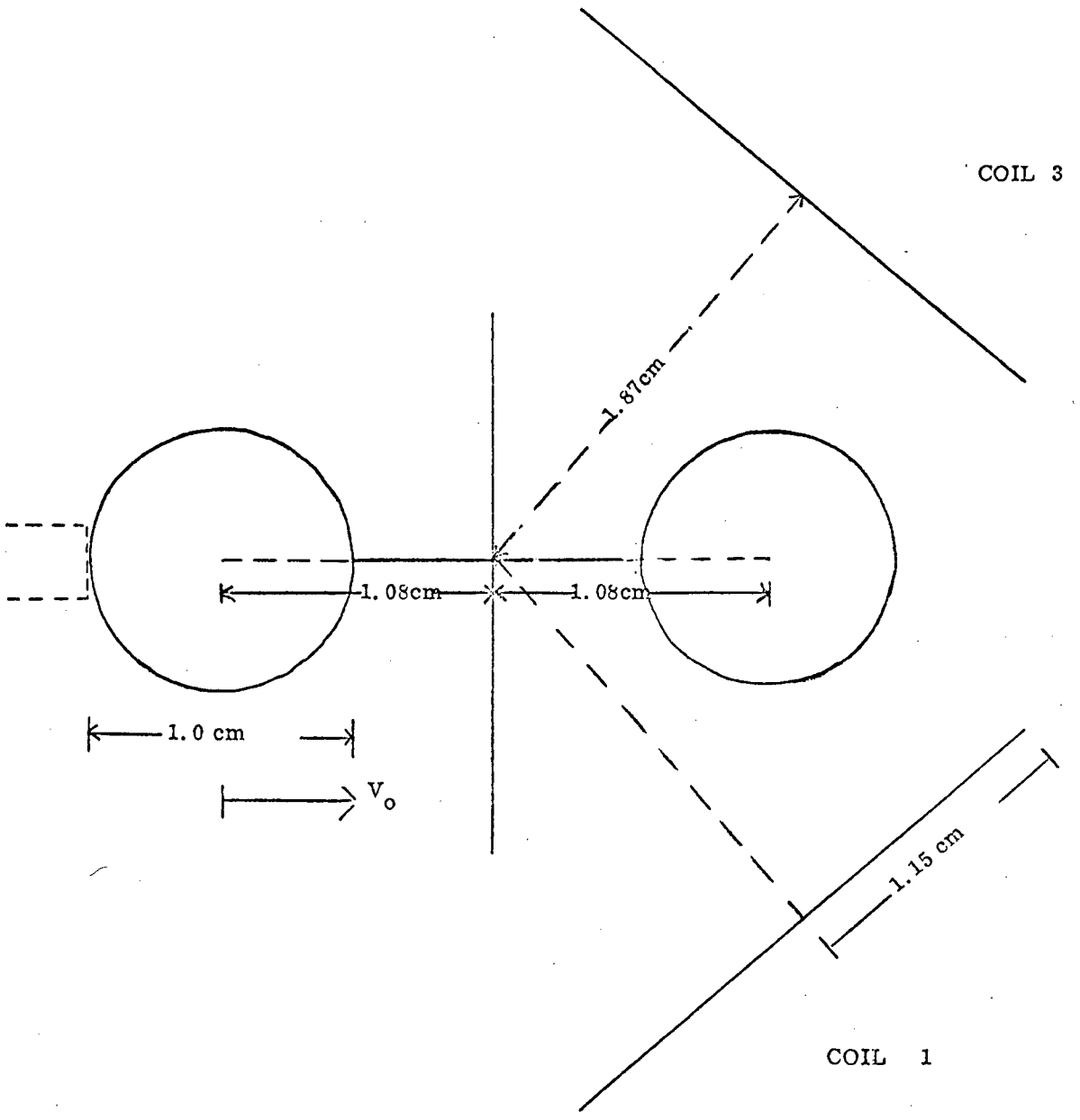

Figure 2.3-9. Geometry for Sting Position 3

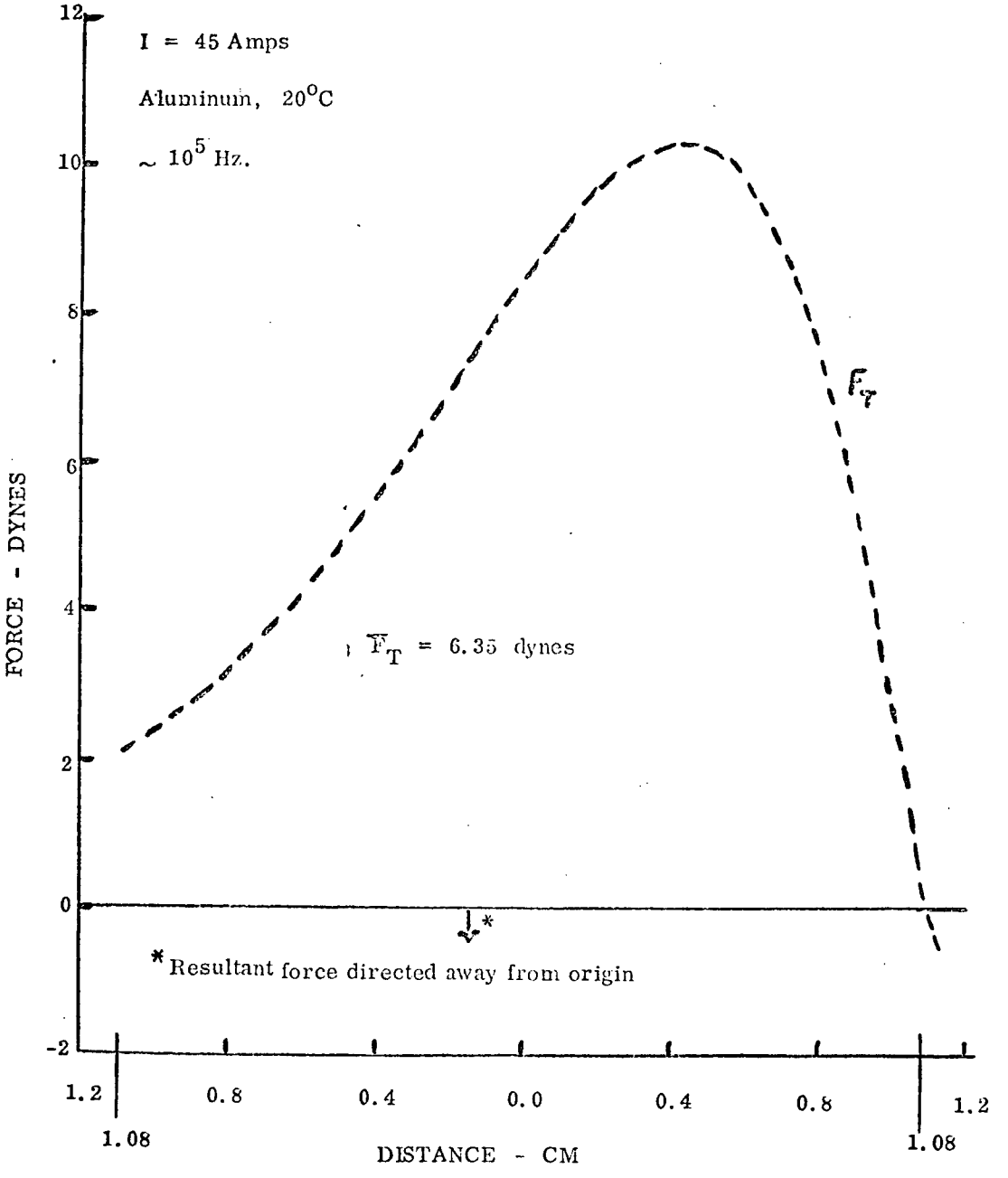

Figure 2.3-10. Force Function for Sting Position 2

3. Release: sphere off parallel to longitudinal axis of sting and toward origin.

4. Coil forces: Data are shown in Figure 2.3-10 for two coils with I = 45 amps, N = 3.

5. Problem geometry: Figure 2.3-9.

6. Material properties (molten):

	δ, Skin Depth, cm at 10^5 Hz.	Mass, gm (1cm dia. spheres)	G (x) *
Silver (Ag)	0.066	4.97	0.802
Copper (Cu)	0.073	4.29	0.781
Aluminum (Al)	0.078	1.24	0.901
Iron (Fe)	0.188	3.58	0.428
Nickel (Ni)	0.147	4.48	0.555

*See Section 2.1.4

2.3.3.5 Procedure

From Figure 2.3-9, the kinetic energy imparted to the sphere at the sting, namely, $1/2\ mv^2$, must be removed by the force experienced by the sphere over the distance 2(1.08). This is equal to the average force over the distance times the total distance, $\Delta 1$.

$$0.5\ mv^2 = \left[\int_{-\ell}^{\ell} F(1)\, dl \Big/ \int_{-\ell}^{\ell} dl \right] \Delta 1 \qquad (16)$$

$$= \left[G(x)\, I^2 \int_{-\ell}^{\ell} C(1)\, dl \Big/ \int_{-\ell}^{\ell} dl \right] \Delta 1 \qquad (17)$$

The bracketed term on the right can be evaluated from Figure 2.3-10 by numerical integration of F_T (from -1.08 to 1.08) and then dividing out G(x) and I^2. The average force exerted is

$$F_T(1) = G(x)\, I^2\, 3.48 \times 10^{-3} \qquad (18)$$

Here mixed units are used, the force in dynes and the current in amperes.

In Figure 2.3-10, $F_T \simeq 6.4$ dynes. Equation (18) is used instead of the more familiar*:

$$F = 3/50\ (NI)^2\ A(y)\ G(x)(R2/R1)^3 \text{ in MKS units.} \qquad (19)$$

Figure 2.3-10 is presumed to be the more accurate description of the force function due to the two "stopping" coils, 1 and 3.

From Equations (16) and (17)

$$V_o = \left[2. * 3.48 \times 10^{-3} * 2.16 * \frac{G(x)}{m} \right]^{1/2} I \qquad (20)$$

and

$$I = 8.16\ (m/G(x))^{1/2}\ V_o \qquad (21)$$

* Frost, R. T., et al, Investigation of the Preparation of Materials in Space, Task IV, Field Management for Positioning and Processing of Free Suspended Liquid Materials. Final Report (U), GE-SSL for NASA, Contract No. DCN1-9-54-20055, 52, 15 May 1970, Pg. VII-5.

2.3.3.6 Results

Figure 2.3-11 shows the application of Equation (21) for the five molten materials examined.

As may have been expected, aluminum, because of its light weight and small skin depth, is the least current demanding. At any ejection velocity V_o, the other four materials (Cu, Ag, Fe and Ni) require from 2 to 2-1/2 times the current necessary to stop an Al sphere.

For a maximum coil current of 45 amps, the maximum tolerable ejection velocity for the five materials are

Molten Material (1 cm sphere dia)	Maximum Sting Velocity for Maximum Coil Current 45 amps (cm/sec.)
Al	4.37
Cu	2.36
Ag	2.22
Fe and Ni	1.92

Note that the ejection geometry as postulated confines the sphere to the plane containing the axes of the two stopping coils. Should the sphere have a velocity component out of this plane, Coils 2 or 4 (not seen in Figure 2.3-9) will act (via the servo system) to restore the sphere to the plane. This force will however tend to increase the apparent sphere ejection velocity, "fighting" Coils 1 and 3. If ejection parallel (or nearly so) to the sting longitudinal axis

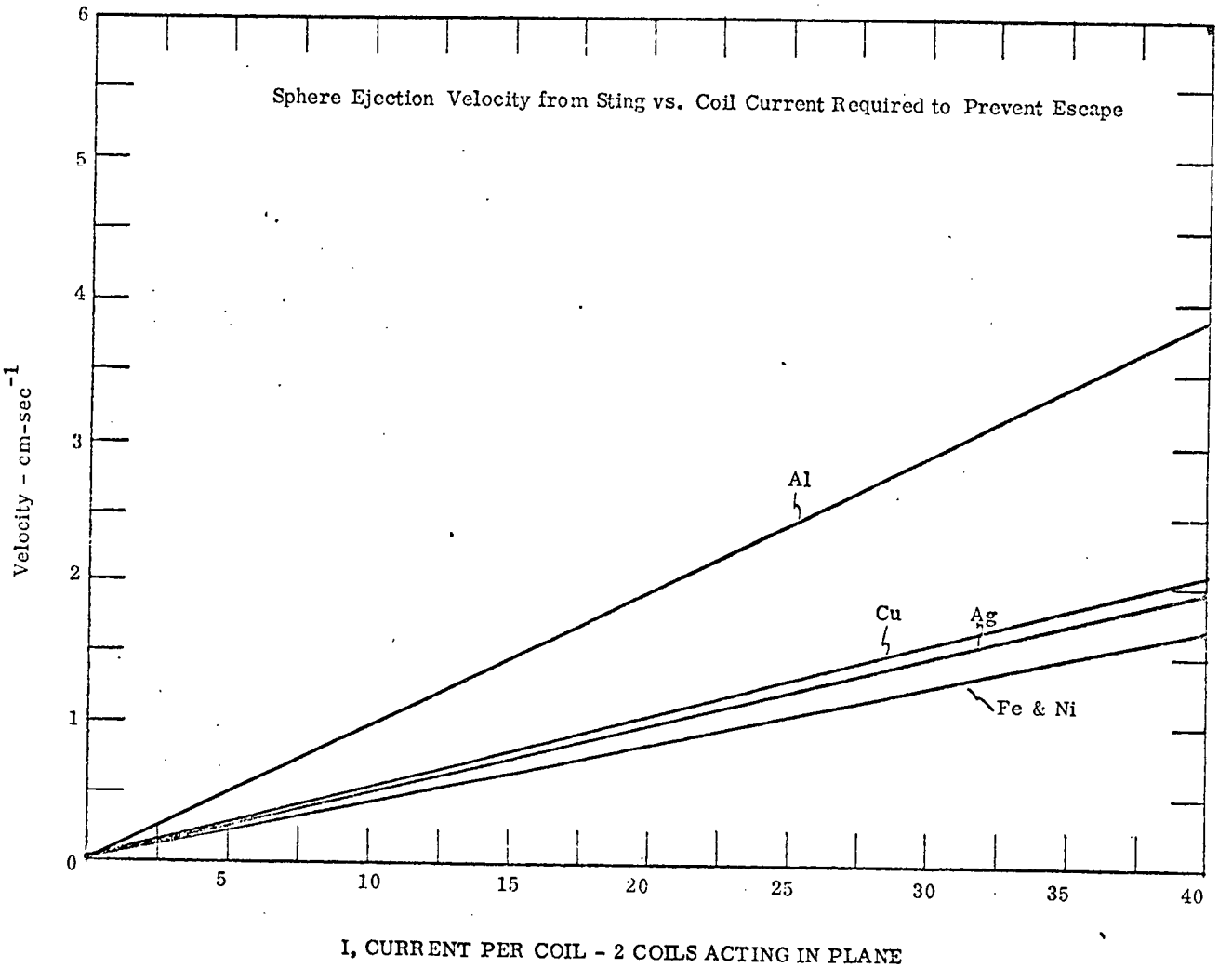

Figure 2.3-11. Sphere Ejection Velocity for Sting Position 3

cannot be assured, the results herein are to be viewed on the optimistic side. That is, the in-plane case represents the best (current conservative) configuration for handling an ejection velocity, v.

2.3.4 Specimen Capture

After each specimen has been melted, and then has again become solid, it must be removed from the positioning coil system to make way for the next specimen to be melted. To do this, the position control system places the specimen to be ejected in a location from which one or more coils acting simultaneously can push the specimen from the interior of the set of coils. Several techniques were considered to prevent ejected specimens from returning to the vicinity of the coils and electron beam once they had been ejected. They are listed below using the words capture or non-capture depending upon the degree of confinement resulting from each technique.

2.3.4.1 Non-capture, Freely Drifting

During the course of the experiment the entire apparatus will experience an acceleration due to the drag of the atmosphere upon the vehicle, due to gravity gradient effects and due to rotation of the vehicle (if any rotation exists). Any acceleration relatively constant in direction will cause freely drifting specimens to drift to one side of the vacuum chamber and to congregate there. If the net acceleration upon the experiment is in a suitable direction for a sufficiently long time the ejected specimens would remain away from the coils and electron beam.

2.3.4.2 Non-capture, Inelastic Rebound

The technique described above could be improved by decreasing the length of time it takes each specimen to attain a relatively motionless state if an energy absorbing surface were placed in the path of the ejected specimens to deflect and reduce their velocity or if an energy absorbing surface were placed somewhere in the vicinity of the region in which they congregate. This latter surface might be a sticky surface of a suitable material, such as a low vapor pressure vacuum grease, to be certain of each remaining in that region. Materials used to decrease the speed of ejected specimens would have to tolerate contact with the hot metal spheres and the degree of outgassing produced by this contact would have to be evaluated to determine to what extent such outgassing would necessitate delaying the melting of subsequent specimens.

2.3.4.3 Capture, Fiber Trap

The use of very fine metallic fibers to construct a valve-like device was considered at length in response to the desire for a simple passive means of capturing processed specimens on or in the wheel to which they were initially attached. In this technique one or more fibers are installed around the mouth of a cavity. If a specimen ejected from the coil system possesses sufficient kinetic energy to deflect and pass the fibers but insufficient energy to rebound out, each specimen could be stored in the wheel in the same order in which they were initially while yet attached to the wheel.

Several tests were performed to assess characteristics of such a technique by using a pendulum-like apparatus which permitted a metal sphere of a size comparable to that used for the specimen wheel study to swing into a "capture port" at several known speeds. The result of these tests indicated that kinetic energy at least of the order of 40 ergs is required to operate such a capture device successfully. This concept is therefore marginal for use with the low forces dictated by the very limited power availability for this experiment from the M512 facility.

In order to carry a greater number of specimens on each wheel the melted specimens might be collected in a separate container thereby allowing the space formerly used for stowage cavities to be used to attach more specimens to the wheel. The fiber trap technique could also be applied to such a container. However, because it does not assure passage through the port in the event that one or more previously captured specimens are in or near the port, thereby blocking the entry of another specimen, it was abandoned for this application in favor of one of the following techniques.

2.3.4.4 Capture, Coil

A desirable technique for operating a port in a collection box is to place a coil about the port and operating it, in a manner similar to that used for the positioning coils, to repel previously captured specimens from the port. The coil could be turned on only as commanded by "specimen-sensors" (e.g., light emitting diodes paired with light detecting diodes) or it could be on continuously

to be turned off by logic circuitry whenever a new specimen is to be sent into the box. Such a coil would have to be placed far enough from the positioning coils to prevent the mutual induction between it and any one of the positioning coils from being large enough to cause a disturbance in the servo-positioning system. The passive techniques, described in Sections 2.3.4.1 and 2.3.4.2, could be applied to the captured specimens to minimize the chance that an incoming specimen could collide with a previously captured specimen in such a manner that it could rebound out through the port before the coil could force it into the container.

2.3.4.5 Capture, Door

An alternative to the preceding capture, coil technique involves the substitution of a door or gate which opens inward to accept new specimens at the same time pushing previously captured specimens away from the port.

2.4 FOUR-COIL ENGINEERING DEVELOPMENT BREADBOARD

In order to perform functional tests of the four-coil configuration involving forces, coil interactions, position sensing (electromagnetic, infrared and optical), impedance matching circuits and general servo behavior, a breadboard was constructed. The construction was done simultaneously with other studies such as position sensing, coil optimization, mechanical considerations, etc. The most important contribution made by this breadboard was a full three-axis control demonstration of a free and neutrally buoyant hollow aluminum sphere. Demonstrations were performed and a movie was taken (included as a part of this effort) of this sphere immersed in a mixture of silicone oils or in a brine solution. The set-up can be seen in the photograph, Figure 2.4-1, where the white ball (representing the levitated specimen) is visible centered in the liquid filled glass sphere.

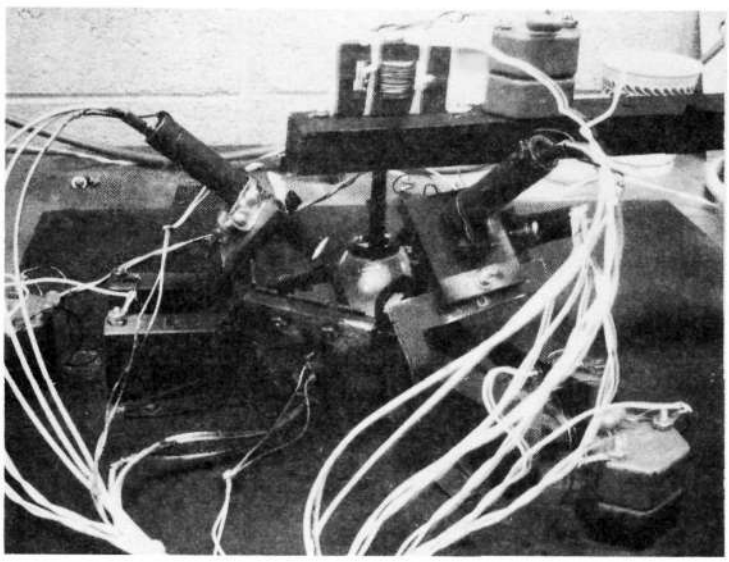

Figure 2.4-1. Engineering Breadboard Coil and Specimen Arrangement

2.4.1 Electronic Circuitry

The electronics conformed closely to the circuitry for the proposed system in all respects except for the infrared position sensing and the coordinate converter. These last items were not complete at that time so they were not incorporated. Instead, the ball corresponding to the specimen was painted white and illuminated by several incandescent lamps. Position sensing was accomplished by three single axis sensors which required no coordinate converter. The sensors and incandescent lamps can be seen by careful examination of Figure 2.4-1.

2.4.2 Position Sensing

The single axis sensor looked into the enclosure between two coils at their closest approach (mid-way between vertices) and was aligned so that the position error was sensed along a plane containing the sensor and the centers of the two opposite coils, as shown in Figure 2.4-2.

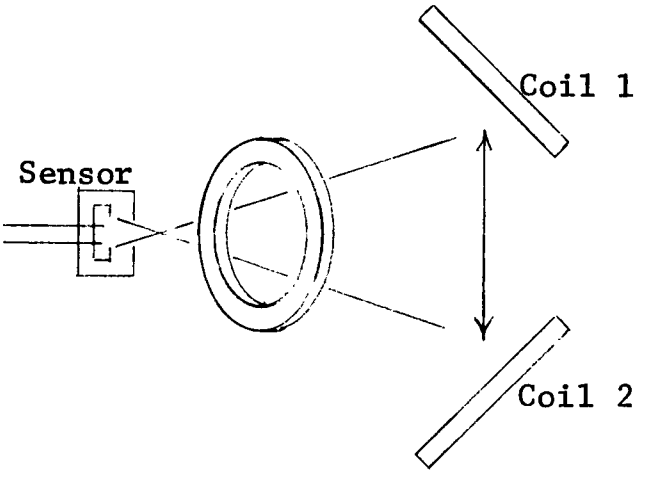

Figure 2.4-2. Direction of Sensed Error on Breadboard

In Figure 2.4-2 the arrow shows the direction of the sensed error. This error drives either Coil 1 or Coil 2 depending on whether the specimen is above or below the center of the facility.

There are two other sensors similarly placed between other pairs of coils so that position information is available on the specimen throughout the coil volume for a two centimeter radial displacement of the specimen from the center of the coil facility.

If the preamp design for infrared position sensing had been completed, the four-coil breadboard could have been reworked to use it with the single axis sensors, both the single axis and dual axis (4 quadrant) sensors being silicon junction devices. To use infrared position sensors, a stainless steel bob was to have been suspended on a long pendulum and heated in an induction heater. The hot pendulum bob would then be transferred to the four-coil facility for tests.

2.4.3 Test Procedures

All test runs using the four-coil breadboard were with the neutrally buoyant sphere. Four switches were added to the position sensing circuits to displace the ball in the facility which can be seen at the upper right hand corner of Figure 2.4-3. Actuating a switch caused the sphere to move in an arbitrary direction. Releasing the switch enabled the servo to re-center the sphere in the coil facility. Four switches provided four directions for sphere

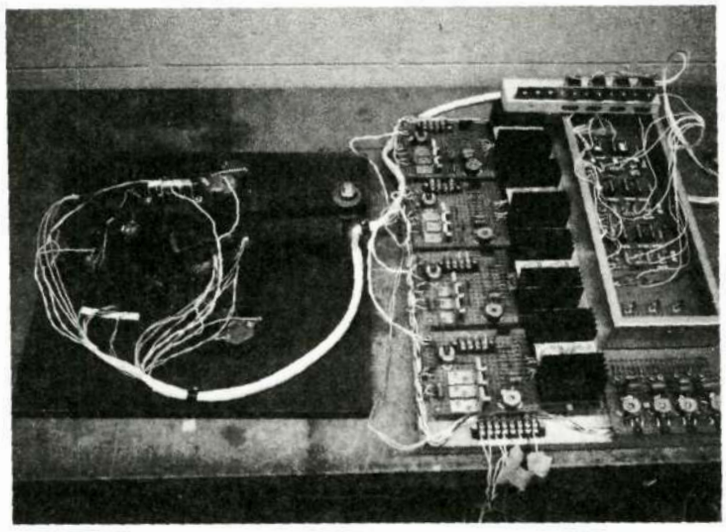

Figure 2.4-3. Complete Four-Coil Engineering Breadboard

displacement. This displacement was accomplished by introducing a position voltage in one of the position sensor amplifiers for the servo to null out by moving the sphere away from center. Simultaneously, the other position sensor amplifiers are disabled.

2.4.4 Schematic

A full schematic is given in GE Drawing ER 47E225310 included as Figure 2.4-4 in this report. Figure 2.4-5 depicts the wiring for the positioning switches and is used with Figure 2.4-4.

FOLDOUT FRAME 1

FOLDOUT FRAME 2

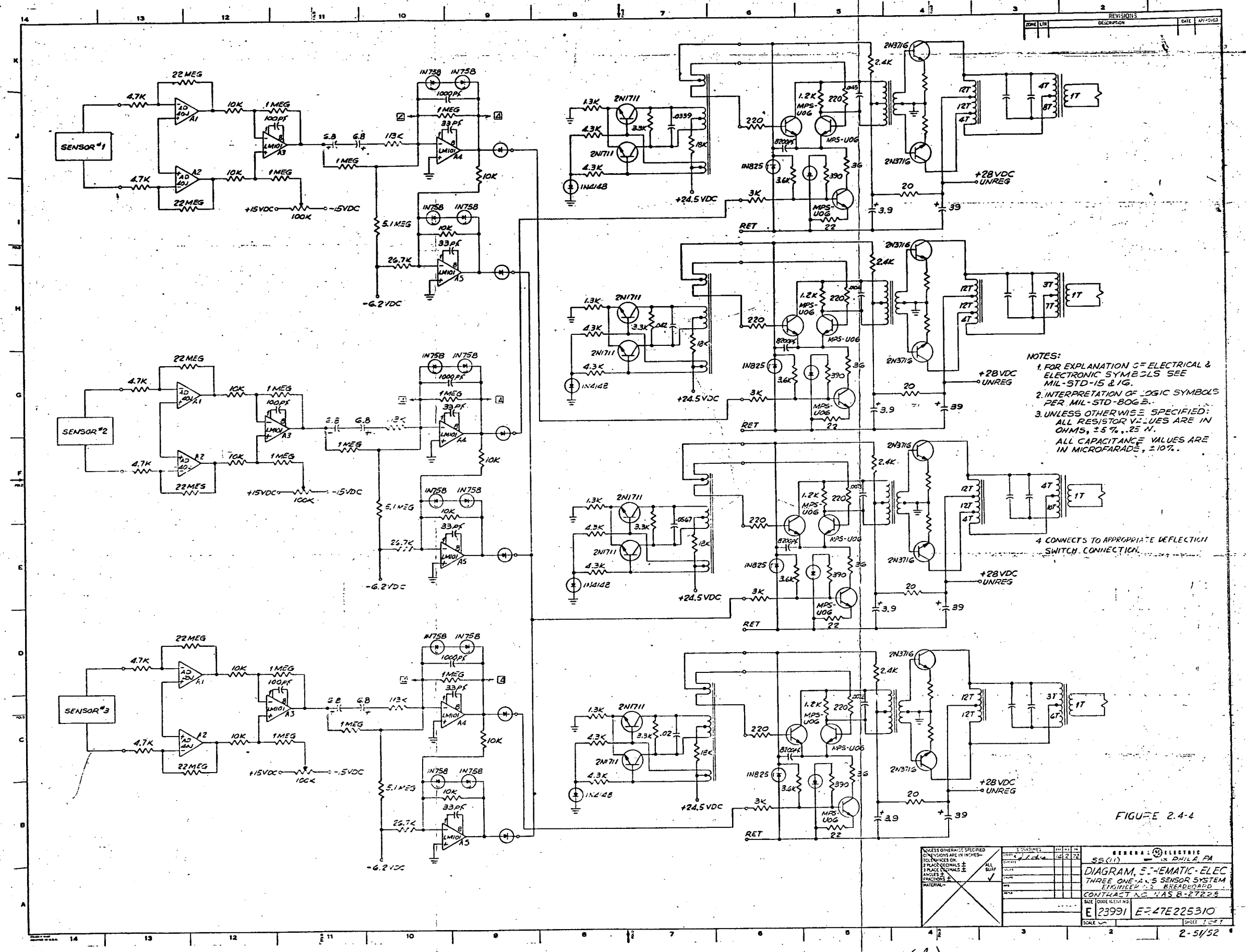

FIGURE 2.4-4

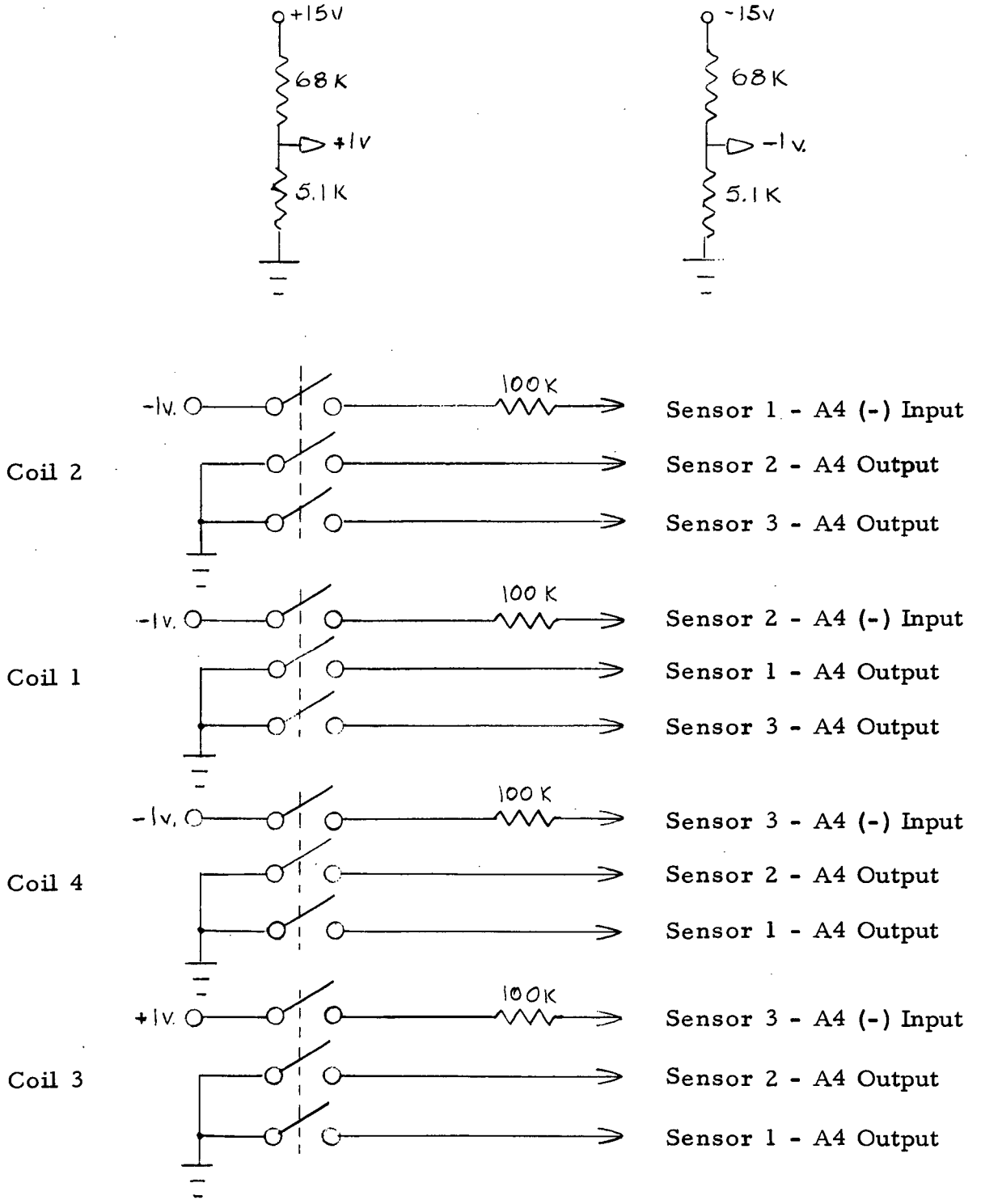

Figure 2.4-5. Sensor Coil Deflection Test Switches

Preceding page blank

2.5 POSITION SENSING AND SERVO SYSTEM

2.5.1 Optical Position Sensing

The location of the hot specimen inside the coil system was determined, in the reference design, by a four quadrant sensor in a suitable optical arrangement that detected energy radiated by the specimen in the near-infrared spectrum. Electronic preamplifiers and a divider, to normalize the amplitude variation of the cooling ball, provided signals to the coordinate converter proportional to errors along three orthogonal planes.

2.5.1.1 Molecular Environment

The position sensing system was to operate in a vacuum chamber. Since the experiment consisted of melting metal spheres, metal vapor would be the most significant contaminent during the experimental period. Calculations were made to determine the thickness and optical properties of the metal films deposited on surfaces in such an environment. For aluminum spheres, a metal film of between 10 angstroms and 100 angstroms thickness would be deposited on exposed hardware surfaces during a period of approximately one second at a radial distance of two centimeters from the source. The melting phase of the experiment was expected to last for perhaps two seconds for each specimen, and since metal films of 10 angstroms to 100 angstroms thickness are opaque to the visible and near infrared radiation, it was evident that transmissive optical components, if used, could not be directly exposed to the metal vapors.

2.5.1.2 Thermal Environment

The electron beam used to melt specimens would be operated at a power of about 1.6 kilowatts for between two and four seconds per specimen. During this period of time, between 4000 and 8000 joules of energy would be deposited in the specimens and the attached sting. This energy must be either radiated or conducted away by equilibrating physical processes. The nearness of the optical system and its associated housing to the target specimen would influence the portion of the total energy that would be absorbed by these components. A large portion of the energy absorbed in the specimen would be conducted away through the sting to the relatively massive support wheel and associated support mechanisms (see Figure 1.1-1). The remaining mode of energy transfer would be through a radiative process. Fortunately, the thin layer of metal vapor deposited on the optical system and associated housing will effectively reflect the incident thermal radiation falling on the sensor subsystem. Since, however, all the other parts of the chamber undergo similar vapor treatments, the amount of radiation which would be received by the optical subsystem was difficult to evaluate exactly.

Calculations were made in which it was assumed that all the energy radiated from the hot spheres into a solid angle subtended by the proposed optical systems were absorbed. The optical subsystems were in good thermal contact with a large heat sink. The calculation showed that we could expect only a few degrees centigrade rise in temperature within the optical housing.

Therefore as long as reasonable precautions were taken to ensure a good heat sink for the housing of the optical components and that the housing itself be made of highly conductive material there would be little problem with thermal conditions in the optical positioning devices.

2.5.1.3 Thermal Gradients

Both the positioning sensors and the temperature measuring sensors (Section 2.6) would be affected by thermal gradients within the specimen. In a NASA film showing the melting of a 0.5 cm diameter sphere, temperature gradients within the sphere were clearly visible. This could result in a false interpretation of the position of a specimen. A one centimeter diameter specimen would perhaps increase the magnitude and spatial extent of the thermal gradients owing to the eight-fold increase in its mass and a decrease in the ratio of its area to volume. The control system as presently conceived would force the specimen into a position which corresponds to the centroid of the energy emitted from the specimen.

2.5.1.4 Optical Line-of-Sight

A constraint on the optical line-of-sight for the position sensing system was that within the tetrahedral geometry of the coils there be a spherical control volume of four centimeters diameter. If the specimen was anywhere within this control volume the position sensor must not have an ambiguity in its control function output. Stated simply this means that the specimen must be controlled back to the midpoint of the volume and not ejected if it was

contained within this volume. A second condition which must be taken into account was that the housing for the optical system should not be closer than approximately two coil diameters from any particular coil so as not to influence the field about this coil. In addition we desired the fewest required number of sensors so as to minimize the number of components of the system.

Figure 2.5-1 shows the schematic configuration of the location of the two optical positioning sensors. Each sensor consisted of a pinhole lens system, a folding mirror, a detector, and optical filter. These sensors were placed at two of the corners of a tetrahedron configuration; the control coils of which were on the faces of the tetrahedron. The size of the detector and the "focal length" of the pinhole lens was chosen so that an inscribed sphere of four centimeters is completely within the optical field-of-view of the sensor and there are no areas which vignette within this field-of-view. The two sensors were used to define a three-axis cartesian coordinate system. The detector within each sensor was a four quadrant PIN-Si photodiode. A four quadrant detector can be used to define a two-axis coordinate system within the plane of the detector by judiciously summing the outputs in the proper fashion from each quadrant of the detector. When the image of a sphere is exactly on the center the outputs from all four quadrants are equal and a null signal can be obtained. By employing two such sensors we can define the three-axis coordinate system within the tetrahedral geometry as follows.

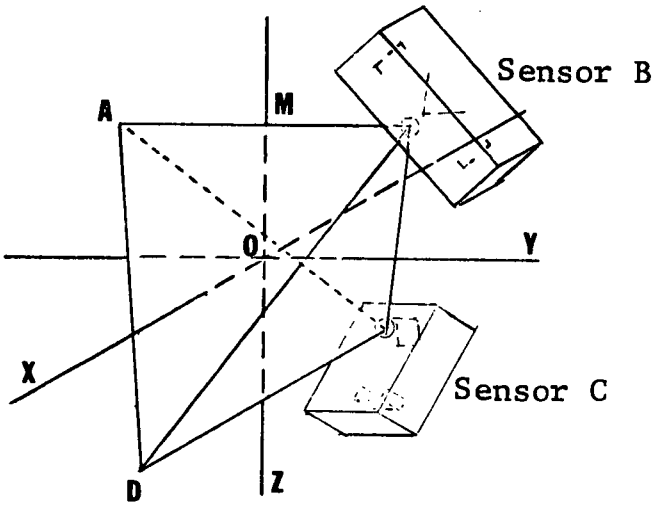

Figure 2.5-1. Optical Sensor Orientation

Figure 2.5-2 is the same as Figure 2.3-6 but is repeated here to simplify the explanation of the relation of the optical sensors to the coordinate system utilized.

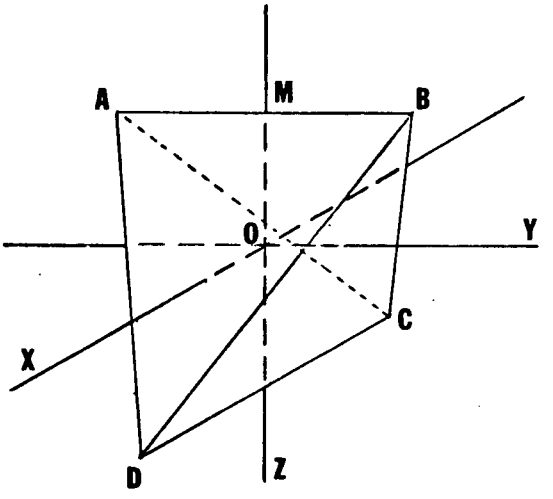

Edge Length = 2L = S
Edge AB || Y
DC || X
Face 1 = BDC = Coil 1
Face 2 = ADB = Coil 2
Face 3 = ABC = Coil 3
Face 4 = ACD = Coil 4

Figure 2.5-2. Tetrahedron Orientation

Locating an optical sensor at point B (O, L, L′) we can rotate the detector so that the X_B axis, that is a local coordinate axis within the detector, is parallel to the X axis within the tetrahedron. Any motion of the specimen along the X axis within the system results in movement of the specimen image along the axis of the detector in accordance with the following equation:

$$X = (M/f)X_B.$$

Where M is the distance from the pinhole lens to the center of the coordinate system; f is the "focal length" of the pinhole lens and equals the distance from that pinhole to the detector; and X_B is the position along the axis in the detector plane parallel to the tetrahedron X axis. Another detector located at point C can be oriented so that its axis is parallel to the Y axis within the tetrahedral geometry. A similar equation is derived for the motion of the image on this detector in terms of motion within the tetrahedron; i.e.,

$$Y = (M/f)Y_C.$$

Motion of the specimen along the Z axis within the tetrahedron is given by a combination of the motion of the image on the detector at point B and the perpendicular axis (which axis lies in the plane defined by the system X and Z axes) within the detector at point C, and the following equation is derived.

$$Z = \left[Z_c\,(M/f)/\sin 54^\circ 44' - \frac{Z_c}{f}\cos 54^\circ 44'\right] - \left[\frac{\cos 54^\circ 44' + \frac{Z_c}{f}\sin 54^\circ 44'}{\sin 54^\circ 44' - \frac{Z_c}{f}\cos 54^\circ 44'}\right]\left[\frac{M}{f}\,X_B\right]$$

The electrical signal for each axis of motion is determined by the responsivity of the detector to motion of the image on the sensitive element.

Figure 2.5-3 shows the relative output from the detector packages versus displacement of a specimen from the center of the tetrahedron. This function is single valued for all points within the control volume for a given specimen temperature. Since the temperature of the specimens would vary, we must normalize the output as a function of the absolute output from the detectors as will be discussed in Section 2.5.1.7 below.

2.5.1.5 Signal-to-Noise Ratio for Position Sensors

Since multi-element arrays were necessary to define the coordinate system within the field-of-view and, in the early considerations of detectors we were also attempting to measure temperatures of the specimens with the same detectors, several different detector types were considered. A multi-element array of detectors of perhaps PbS and PbSe were found to be both expensive and long lead-time items. The temperature sensing element was therefore separated from the position sensing element employing the relatively low cost off-the-shelf silicon multi-element arrays for position sensing. Temperature sensing development is discussed in Section 2.6 below.

The signal from a silicon detector placed at the foregoing positions in the tetrahedral geometry is controlled by the absolute temperature of the specimen, the specimen emissivity, the aperture of the pinhole lens, and the responsivity

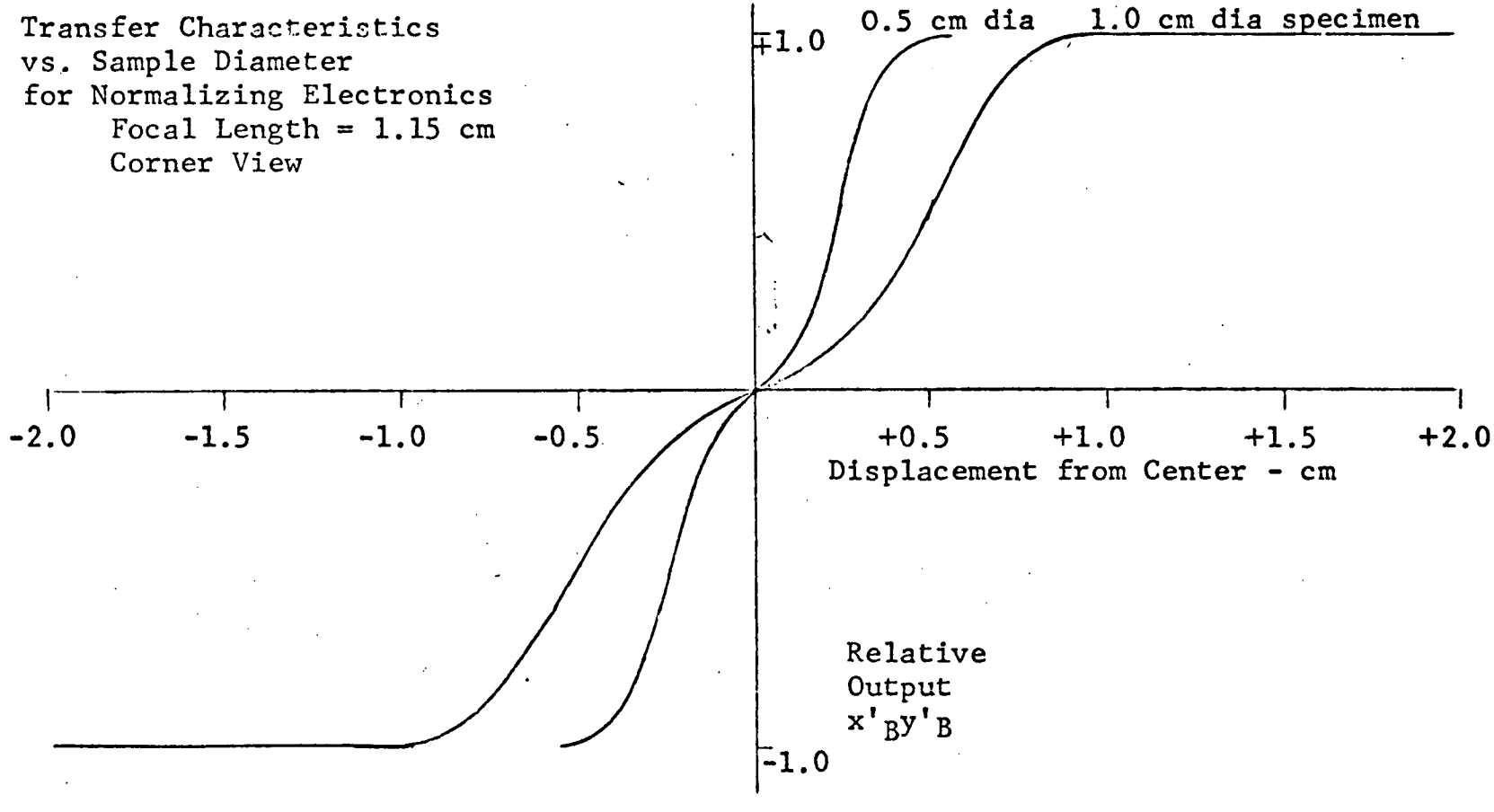

Figure 2.5-3. Transfer Characteristics of Detector

of the detector element. For the purpose of calculation, the average emissivity from typical candidate specimens was assumed to be approximately 0.1. The size of each of the specimens was to be one centimeter in diameter. The aperture of the lens was assumed to be two millimeters and the responsivity of each of the detectors from published data by United Detector Technology is 0.5 amps per watt. All of the candidate specimens were estimated to solidify by about $800^{o}K$ and this defined the lower temperature limit for the control system. Conversely all candidate specimens would melt below a temperature of $1773^{o}K$ defining the upper temperature limit and demarcating the dynamic range requirements of the position and temperature sensors. The calculations were performed for a specimen at the null position in which the sum of two detectors each seeing one quarter of the specimen were added together. A minimum output current was calculated to be 3.3×10^{-10} amps.

The noise associated with each of the detectors is controlled by the electrical bandpass of the system and the leakage current at the silicon junction. A safety factor of ten from the published data was incorporated into the design figures. The output electrical noise in a 100 Hz bandpass is on the order of 8×10^{-11} amps. An additional contribution to noise would be false signals from elements within the field-of-view not associated with the specimen. For calculation of these signals it was assumed that the background consisted of a blackbody at $300^{o}K$ with an emissivity of unity. The output resulting from this assumed background would be 4×10^{-19} amp and therefore could be

totally neglected. Figure 2.5-4 shows the signal-to-noise ratio for two cells versus the temperature of candidate specimens for the null position. It is worth noting that at a temperature of 800°K, a signal-to-noise of approximately ten was expected. Since in this application the detectors were operating in a differential mode, the accuracy of the null position would be controlled by the noise output from the detector elements. Attention must be called to the very low current levels expected and to the extreme precautions required in the design of the electronic shields.

A definite improvement in signal-to-noise ratio could be achieved through the use of a mechanical chopper, such as the Bullova Tuning Fork Choppers. However, questions of reliability in the functioning of a chopper in this metallic environment led us to attempt to operate in a dc fashion. The design however does not preclude the use of such a chopping system and if actual testing of the breadboard equipment would demonstrate the necessity of improving signal-to-noise ratio then such a chopper could be added at a later time.

2.5.1.6 Mechanical Design

An engineering model of a combined position and temperature sensor was constructed and housed in an aluminum case which is 1.15 by 4.5 inches long (exclusive of connectors) by 1.2 inches high. Figure 2.5-5 is an outline drawing of the prototype assembly and Figure 2.5-6 is a photograph of the unit fabricated together with the temperature sensor electronics in breadboard

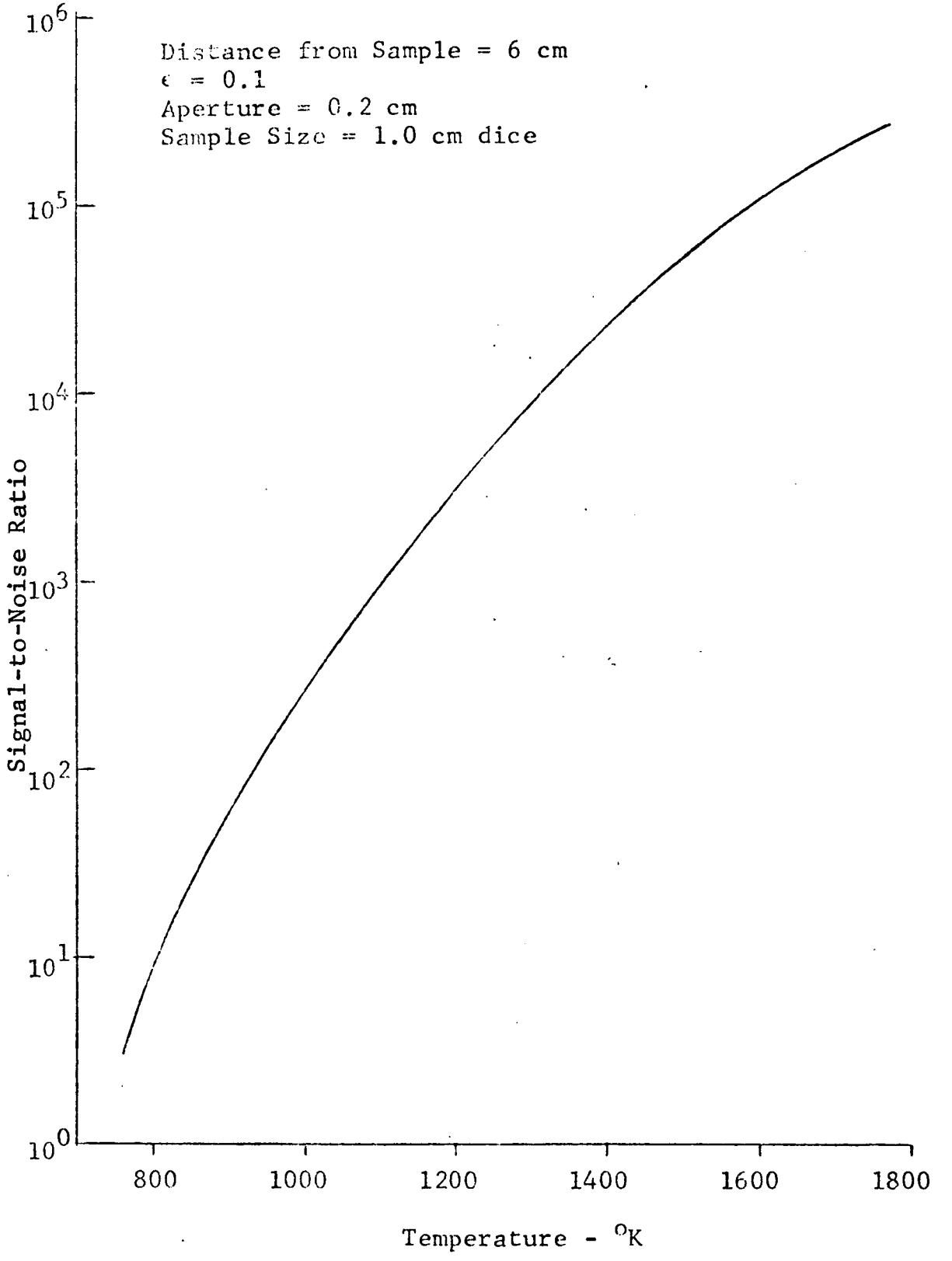

Figure 2.5-4. Signal-to-Noise Ratio of Silicon Detector Elements

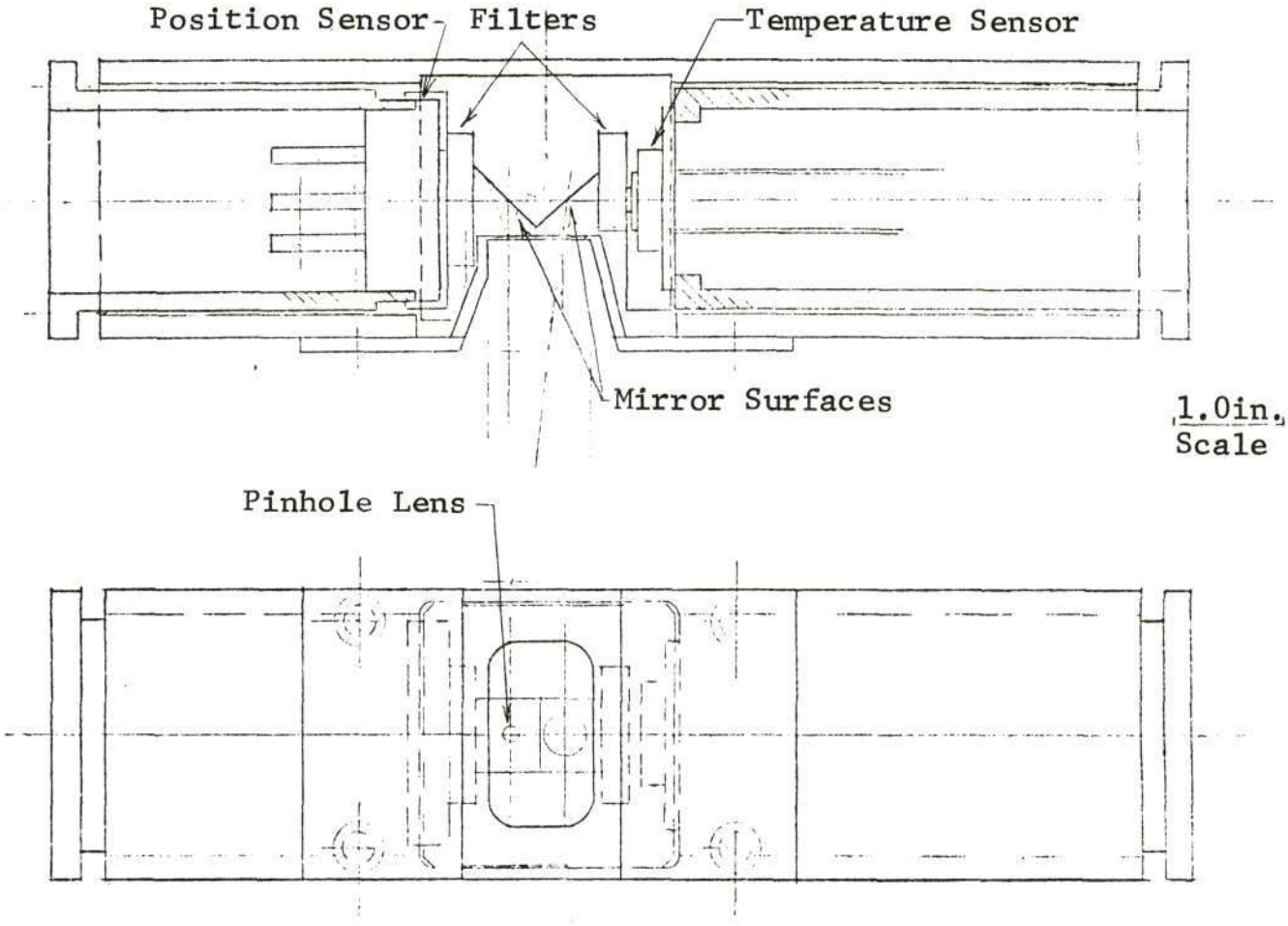

Figure 2.5-5. Position and Temperature Sensor Housing

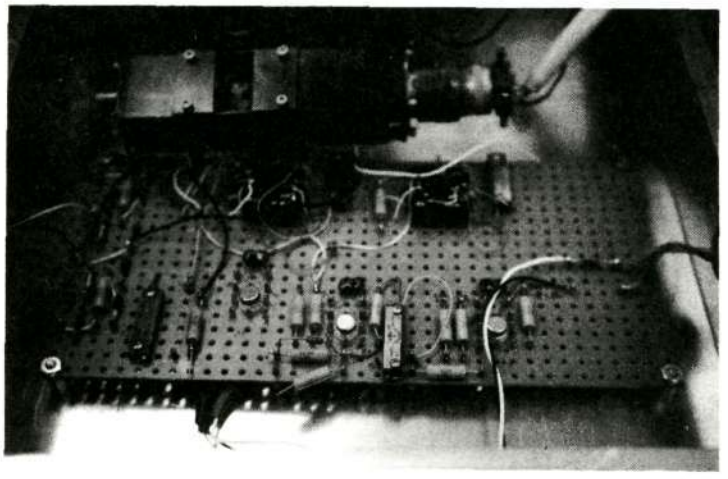

Figure 2.5-6. Prototype Sensor and Electronics Breadboard

form. Each sensor, that is the position and temperature sensor, sees the entire control volume by means of a pyramidal mirror structure and though its own aperture. The mirrors are utilized to fold the optical path and permit both sensors to view the control volume. They also serve to introduce a reflective optical element in the optical path from the hot, potentially evaporating specimen. Any vaporization deposits will have a negligible effect upon the performance of the front-surface mirrors and because of the folded optical paths, they would not reduce the transmittance of the refractive optics. One aperture serves as the pinhole lens for the position sensor, the second aperture simply limits the total field of the temperature sensor to be somewhat larger than the control volume. An optical filter in each path rejects the visual portion of the optical spectrum. This filter is used to prevent spurious signals from entering the detectors due to the photo floodlamp used in conjunction with the motion pictures that were to be taken during the melting experiments. At each end of the case is a connector which connects the respective detectors to the appropriate electronic circuitry. The mechanical design serves as almost a continuous electro-magnetic shield to prevent spurious radiated signals from entering the signal channels.

Only one of the sensor elements would contain both temperature and position sensing elements. The second sensor would contain the position sensing element alone. As noted in Section 2.5.1.4 above, the other sensor is required to supply the third axis of positioning information.

2.5.1.7 Electronic Circuitry Design

An optical schematic of the quadrant detector and aperture, without the flat mirror, is included in Figure 2.5-7.

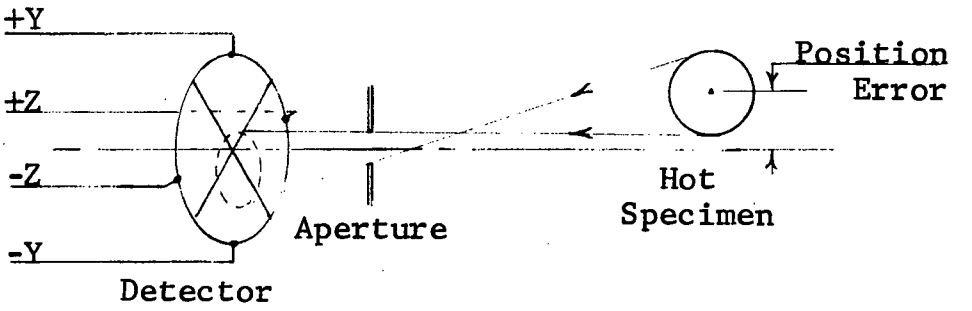

Figure 2.5-7. Optical Schematic for Y and Z Axes

The specimen is shown displaced in "Y" so that detector quadrant -Y is illuminated more than +Y. The photo-generated current in -Y exceeds that in +Y by the amount of the error. Note that all the radiation passing through the aperture falls on the four quadrants. This requirement must be met in order to normalize the amplitude variation due to the cooling specimen. Normalizing for changes in temperature and emissivity is done by dividing the differential output of opposite quadrants by the sum of all four quadrant outputs. This scheme is depicted schematically in Figure 2.5-8 and the proposed implementation is shown in Zones B10-D10 to B12-D12 on Drawing ER 47J225305 of Appendix A. As noted in the preface to that appendix, these circuits had not been completely developed.

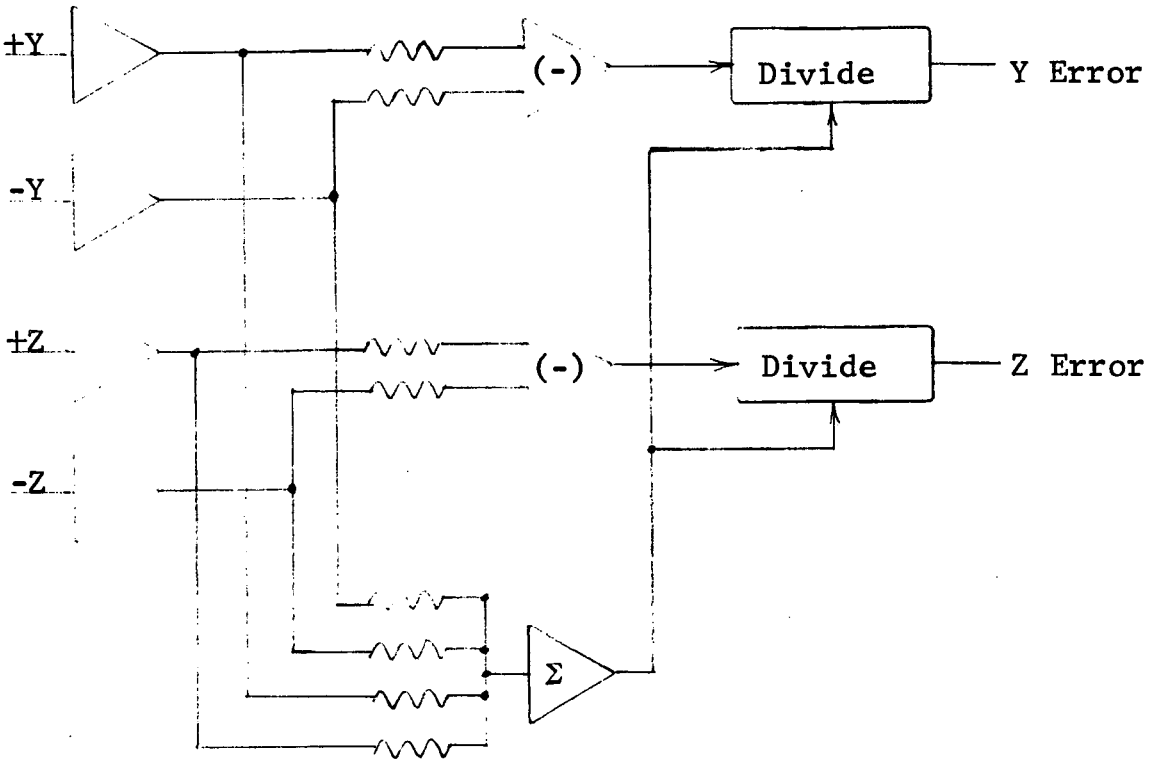

Figure 2.5-8. Conceptual Schematic of Normalizing Circuits

The output of the dividers is accurately proportional to the specimen displacement so long as the specimen temperature is high enough to produce a workable signal, and all radiation through the aperture falls on the detector.

The arrangement for the X axis is different in that two quadrants are parallel as shown in Figure 2.5-9 so that +X is from these quadrants and -X is from the opposite two quadrants. Implementation of these circuits is included in the Appendix A in the same area as mentioned immediately above.

Laboratory measurements using a blackbody source (IR Industries Model 406) produced a preamp output of 10 volts at a source temperature of 1000°C and 0.035 volts at 590°C.

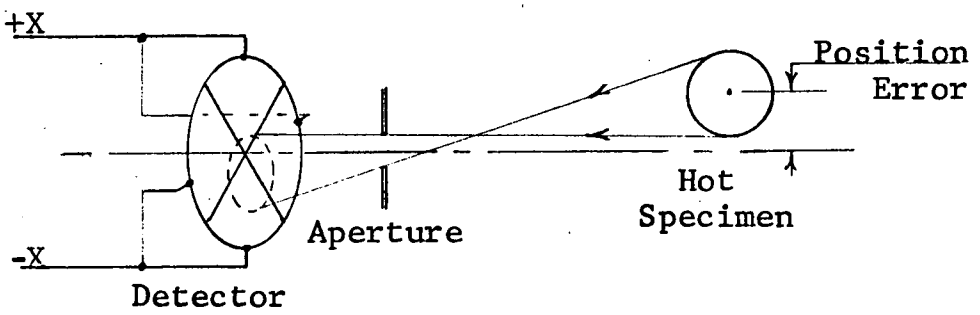

Figure 2.5-9. Optical Schematic for X Axis

2.5.2 Electromagnetic Position Sensing

2.5.2.1 Basic Concept

The presence of the specimen in the alternating magnetic field gives rise to two changes in the coil's properties. The specimen will absorb power from the field and, due to the induced magnetic dipole, it will decrease the inductance of the coil. Examination of Figure 2.5-10 shows that both these factors tend to reduce the power factor angle θ of the coil. Both the above effects are increased as the field amplitude increases. Consequently, if the specimen approaches a coil the power factor of that coil will be reduced. The power factor angle then could be used, under the proper conditions, to determine relative ball position within the coil system.

The electromagnetic position sensing system developed under this contract sensed the power factor angle of one coil and compared it to the

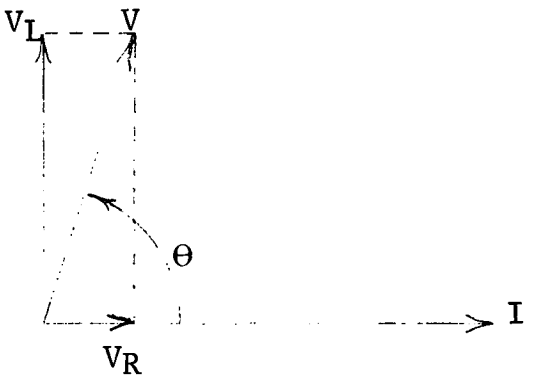

Figure 2.5-10. Phase Relationships in Coil

average of the other three coils to define the specimen position relative to the coil system. The block diagram of this system is shown in Figure 2.5-11.

Figure 2.5-12 depicts the waveforms and the reference pulse which represents θ. The dotted curves show the waveforms when the specimen is close to the coil.

2.5.2.3 Operation

The voltage and current waveforms are normalized by using a zero cross-over circuit providing from that point on the bipolar switching signals, preserving only the phase of the two waveforms. V and I are defined as the positive half-cycles of the waveforms and $\overline{V}$ and $\overline{I}$ are the negative half-cycles of the waveforms. The logic provides a reference pulse only when the two waveforms are of opposite polarity. All reference pulses from all coils are of the same height and are exactly proportional to the respective phase angles

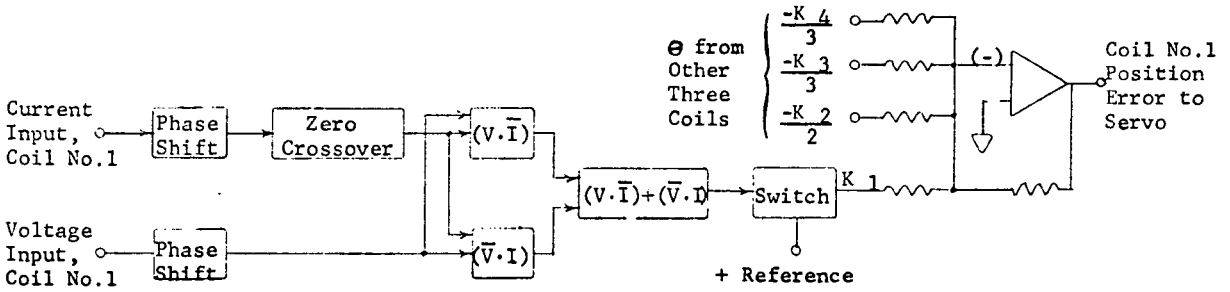

Figure 2.5-11. Block Diagram - Electromagnetic Position Sensing

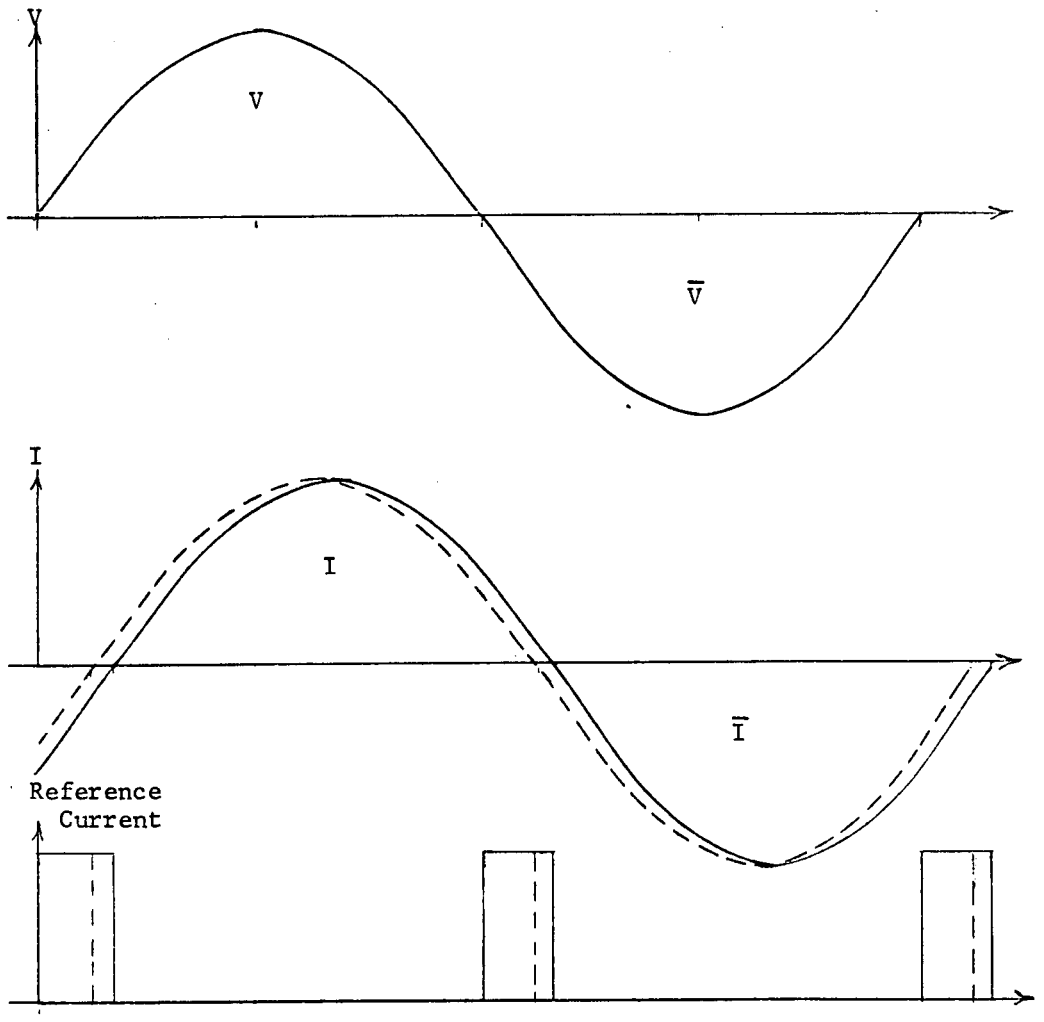

Figure 2.5-12. Waveforms - Electromagnetic Position Sensing

in width. If all pulses have the same average value, then all coils have the same power factor angle and the specimen is centered. Under this condition, the position error to the servo of each coil is zero because

$$K\theta_1 - \left[\frac{K\theta_2}{3} + \frac{K\theta_3}{3} + \frac{K\theta_4}{3}\right] = 0 = \text{error of coil \#1.}$$

If the specimen moves toward coil #1, then $K\theta_1$ is reduced and $K\theta_2$, $K\theta_3$ and $K\theta_4$ are increased and

$$K\theta_1 - \left[\frac{K\theta_2}{3} + \frac{K\theta_3}{3} + \frac{K\theta_4}{3}\right] < 0,$$

so coil #1 has a negative position error. At the same time coils 2, 3 and 4 have a positive position error. In the servo, a negative error increases the power amplifier drive so as to repel the specimen from that coil.

2.5.2.2 Electronic Circuitry

The basic scheme of electromagnetic position sensing had been devised and demonstrated under Contract NAS 8-24683. Under the aegis of the present contract, the concept had been developed for use with the tetrahedral coil configuration. The schematic of a single channel the circuit developed is depicted on Figure 2.5-13. A breadboard incorporating electromagnetic sensing channels for all four of the tetrahedral coils was fabricated and is shown in Figure 2.5-14. Check-out was completed for the channels associated with the three coils in the breadboard which had upward directed force

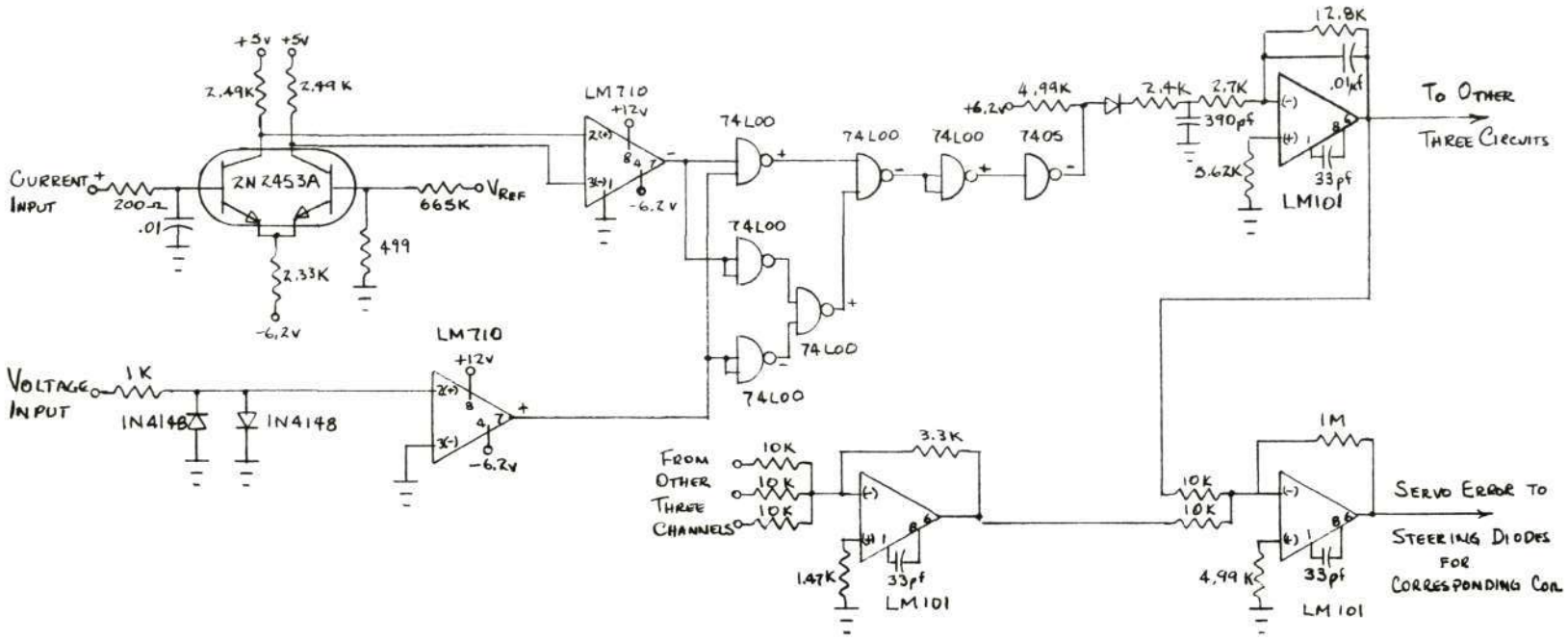

Figure 2.5-13. Schematic of One Axis of Electromagnetic Position Sensing

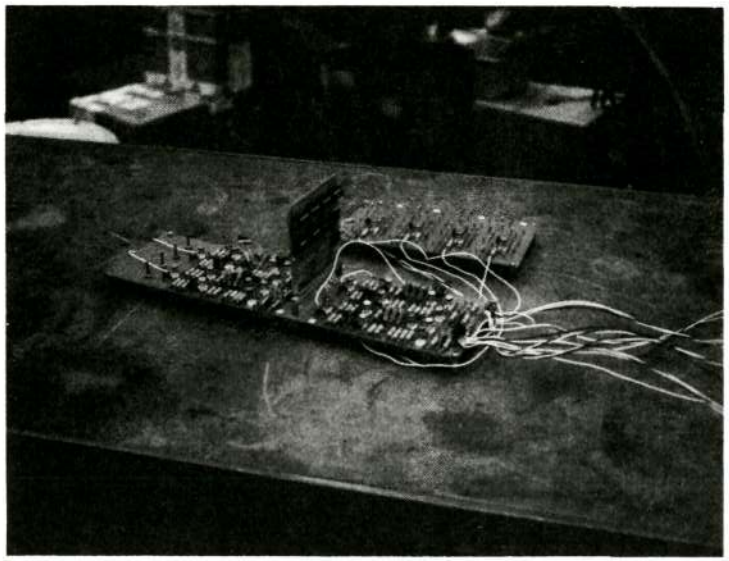

Figure 2.5-14 Breadboard of Electromagnetic Position Sensing Circuits

components before contract termination. With these three channels operating, the capability of the system was demonstrated to move a simulated specimen suspended from a fine wire. No effort was exerted on the fourth channel since it was not utilizing in controlling a specimen suspended as a pendulum in the laboratory.

2.6 TWO-COLOR PYROMETER

2.6.1 Overall System Description

Calculations were performed to show the feasibility of using a dual detector system consisting of a silicon detector with a lead sulphide cell immediately behind it. This detector system was purchased from Electro Nuclear Laboratories (ENL), Menlo Park, California, and made into a sensor head package that included a small circular aperture, deflecting mirror and IR filter as sketched in Figure 2.6-1.

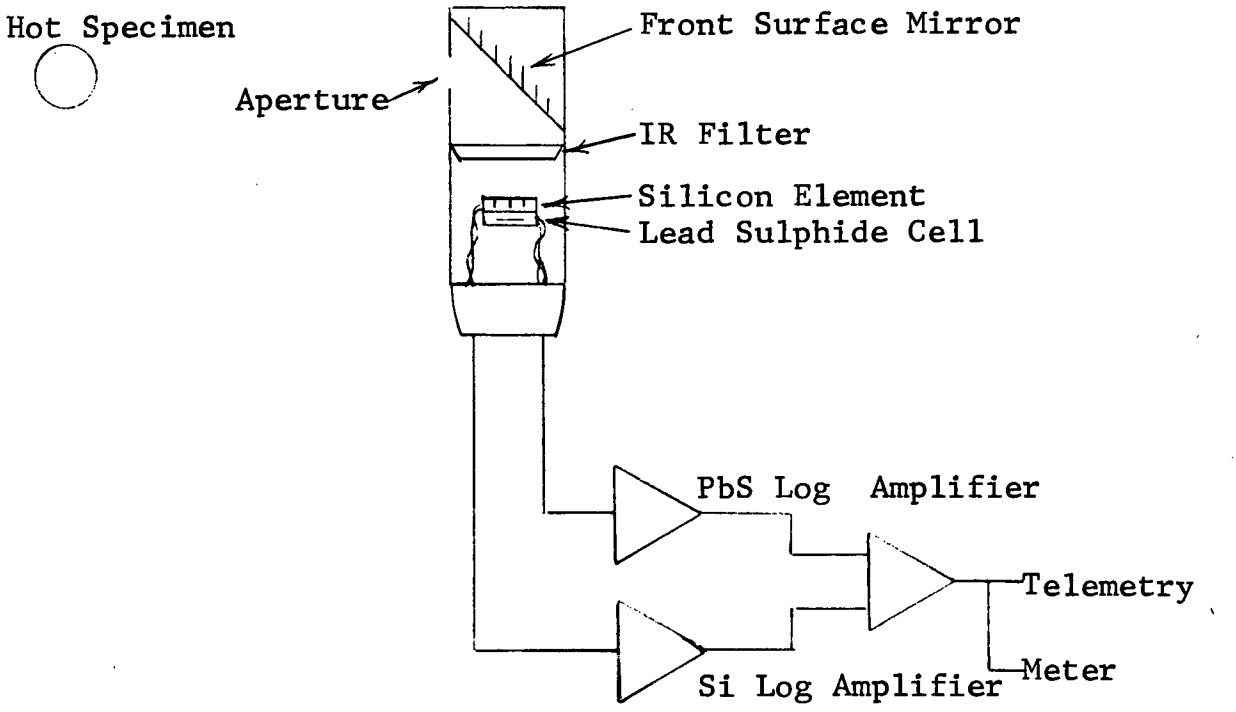

Figure 2.6-1. Two-Color Pyrometer Block Diagram

The radiant power from the hot spherical specimen passes through the aperture and is reflected by the mirror, through the IR filter, and then onto

the sensor head. The emitted radiation in the wavelength range up to 1.1 μ is absorbed by the silicon cell which generates an e.m.f. that is proportional to the radiation absorbed. The longer wavelengths are transmitted through the silicon cell so that they fall onto the underlying Lead Sulphide cell where they are absorbed to produce an increase in conductivity.

Over the temperature range of interest ($800^{\circ}K$-$1700^{\circ}K$) the signal dynamic range produced by the silicon cell is 10^5:1 and that of the Lead Sulphide is 10^2:1. The parameter produced by the cells that can be uniquely related to temperature (for a black or gray body) is the ratio of the two outputs; i.e.,

$$\frac{V_{PbS}}{V_{Si}} = F(T).$$

Since the ratio of V_{PbS}/V_{Si} itself covers a wide dynamic range the signals from the two cells are amplified by log amplifiers and the ratio of the two cell outputs are fed into a differential output, so that the output signal is then a function of the ratio of the two outputs. Thus

$$\frac{V_{PbS}}{V_{Si}} = F(T)$$

$$\Delta V_{out} = \log (V_{PbS}) - \log (V_{Si}) = \log F(T).$$

The sensing system should be independent of the amount of energy received (i.e., the size or emissivity of the hot sphere), and only dependent on the

amplifier. Differing time constants and thermal capacities of the PbS cell cell and thermistors cause an imperfect balance to exist in practice but the magnitude of the error introduced is not large enough to cause very serious inaccuracies. The cell output passes through a follower of high input impedance and then into a divide-by-four circuit before being amplified by the logarithmic amplifier. The latter has an FET, 2N3823, as the logarithmic element.

The silicon cell drives current into what is essentially a short circuit load; i.e., the virtual ground of the 40J operational amplifier with the FET feedback providing the logarithmic response. The silicon cell drive current covers the range from 10^{-10} amps to 10^{-5} amps.

The outputs from the two logarithmic stages feed directly into a 40J operational amplifier operating in a linear mode.

2.6.3 Circuit Setup and Tests

The amplifying circuitry for the lead sulphide cell and silicon cell were tested as separate entities. Test input circuit configurations were set up and the logarithmic responses checked over the expected input signal dynamic range; the output point monitored was at the output of the logarithmic stage.

2.6.3.1 Electronic Current Tests

The input test circuit was as shown on Figure 2.6-2. In the initial state the voltage at A was set to the smallest achievable positive voltage. The trimming resistance on the logarithmic amplifier was then adjusted so that the

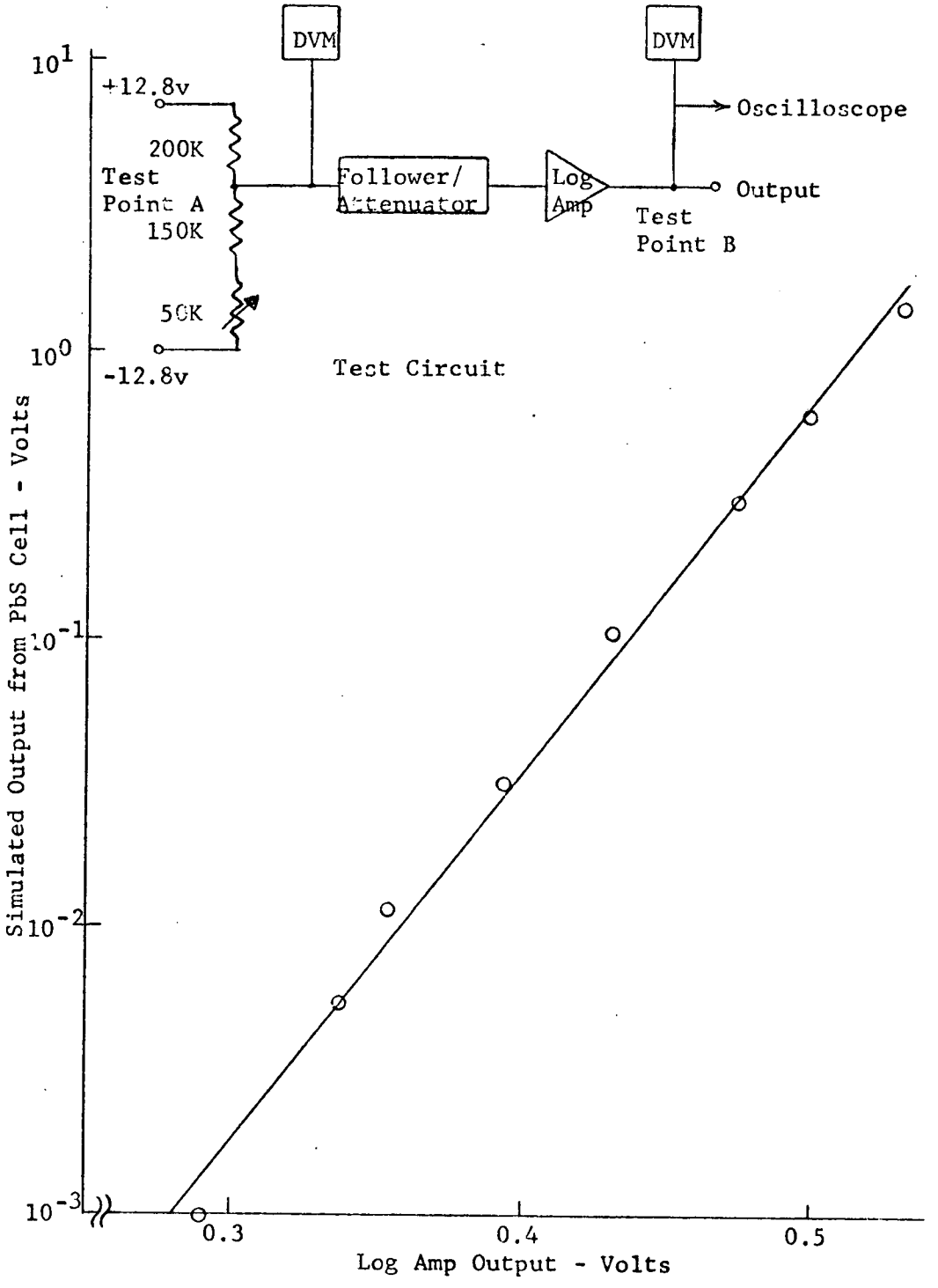

Figure 2.6-2 Lead Sulphide Cell Test

ratio of the signals developed by the two detectors. The output of the amplifying electronics, in the experimental configuration, is monitored by a digital voltmeter.

2.6.2 Circuit Description

The complete circuitry up to the input of the telemetered or recorded signal is shown in zones A8-A10 on Drawing ER 47J225305, Sheet 1 in Appendix A. The lead sulphide cell is biased with a total voltage of 25.4 volts; its series load is not optimum in terms of signal sensing efficiency but is optimized for stability in the d.c. output at the cell load-cell junction. The load consists of two thermistors, type FA425 made by Fenwal Electronics, each of which has a nominal resistance of 20 KΩ at 22°C. In series with the thermistors is a 1% tolerance resistor of value 66 KΩ and a trim potentiometer of 10 KΩ. The thermistors are bonded to the periphery of the PbS-Si detector combination; their function is to offset the changing resistance of the PbS cell as a function of temperature. A theoretical analysis of the circuit showed that if

$$\frac{\Delta R_D}{\Delta R_T} = \frac{R_D}{R_T + R_L}$$

where ΔR_D, ΔR_T are the temperature coefficients of resistance of the PbS cell and the thermistor respectively; R_D, R_T and R_L are the resistances of the PbS cell, thermistors and resistive load, then thermal changes around the sensor package should not affect the voltage applied to the input of the

log amplifier output was in its most stable condition with the output voltage at a minimum. Under these conditions the input voltage (pt A) was +1 mv and the output (pt B) was 0.297 volts.

The input voltage at A was varied from 1 mv to 1.44 volts by means of the variable 50 KΩ potentiometer. The relationship between input voltage and output voltage was plotted. The output voltage was also monitored by an oscilloscope to ensure that there was not an excessive amount of 60 Hz noise. The results of the test are shown also on Figure 2.6-2.

The silicon cell test circuit was as shown in Figure 2.6-3. A variable voltage was derived from a small battery and variable resistance, and this voltage was fed through a 10 MΩ resistance into the input terminal of the logarithmic amplifier. The initial conditions were similar to that of the lead sulphide cell with the exception that the input voltage was negative. The initial voltages were 0.5 mv input and 0.280 volts output respectively; they were measured with the same DVM's as in the lead sulphide cell test circuitry. In order to cover the total range of input current, the 10 MΩ resistor (measured value = 9.945 MΩ) was replaced by one of 1 MΩ (measured value = 1.172 MΩ). The results of the test are shown on Figure 2.6-3.

2.6.3.2 Optical Checkout

The final test consisted of irradiating the optical sensor with black body radiation from a 1 cm aperture of an IR Industries radiation source with a

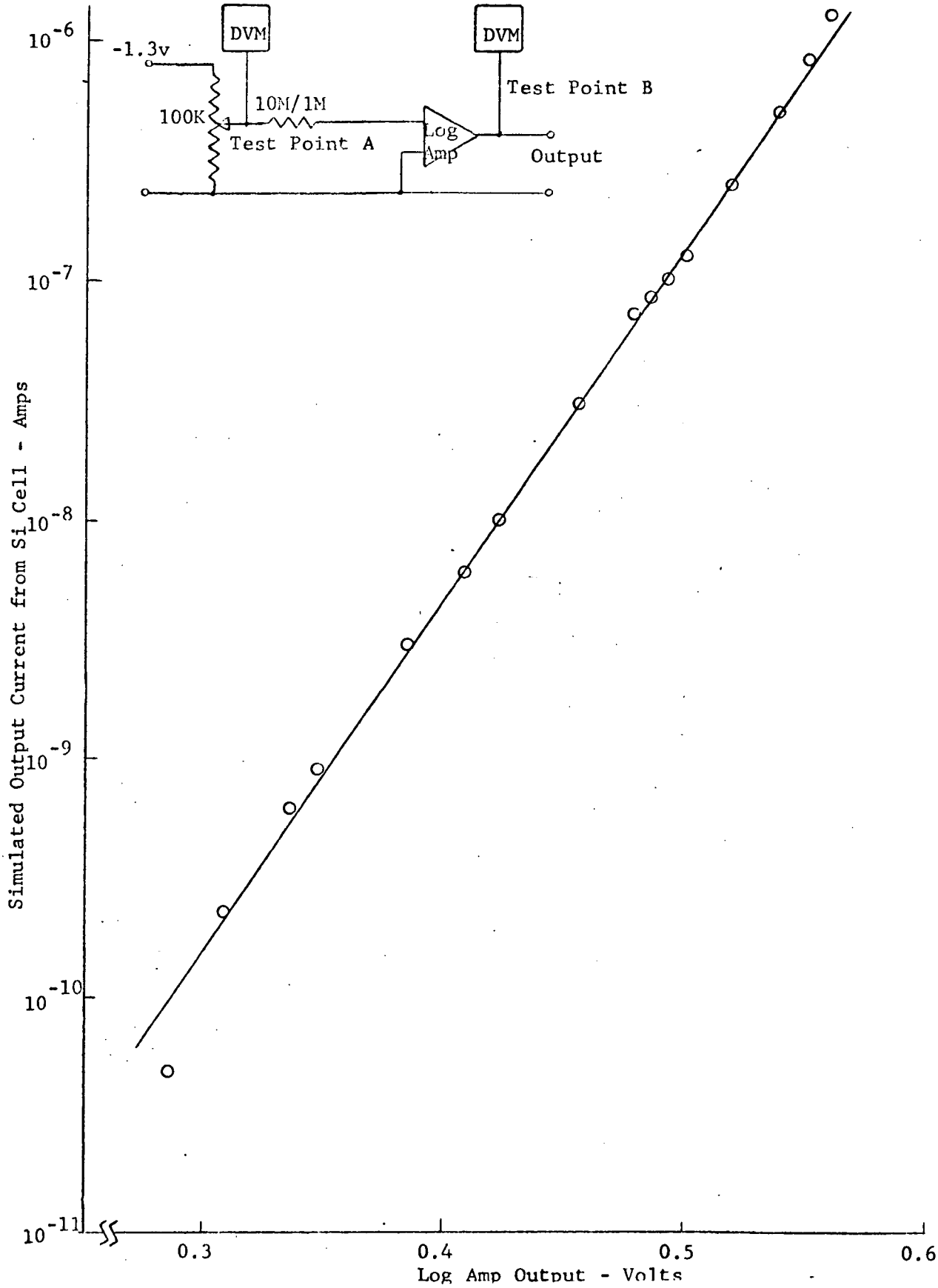

Figure 2.6-3. Silicon Cell Test

C-2

set-up as sketched in Figure 2.6-4. The source was controllable in temperature over a range that extended from room temperature to about 1200°K.

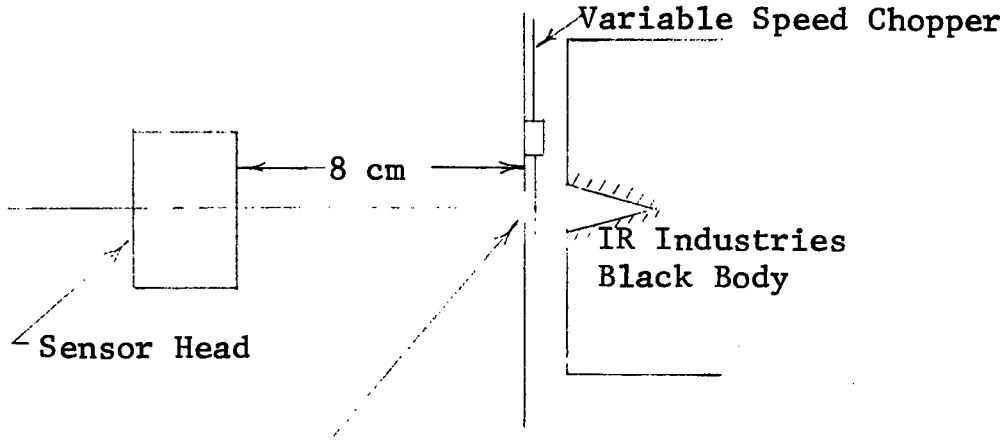

Figure 2.6-4. Optical Test Set-up

Measurements were initiated at a temperature of approximately 950°K and were made at 50°K intervals from this temperature up to 1200°K. In addition to the output of the sensing circuitry other circuit parameters were monitored for each measurement made.

The circuit was designed to make dc measurements only but because a simple chopper system was an integral part of the black body source, additional measurements were made with the input radiating chopped. The results are tabulated in Table 1. Plotted on Figure 2.6-5 is the output from the electronics with the sensor illuminated by a steady radiation. An inconsistency was observed in the data for a chopped input and time limitations did not permit further analysis. These data were not plotted.

TABLE 1

Source Temperature ^{o}K	Output Volts Steady Input	Output Volts Chopped Input
974	0.157	0.14
1026	0.117	0.080
1081	0.114	0.070
1131	0.065	0.26
1180	0.060	0.32

2.6.4 Discussion of the Results

The sensor circuit cannot be used in its present form because the change in impedance of the Lead Sulphide cell resulted in changing voltages being applied to the logarithmic amplifier that amplifies its signal output. Apparently the change in impedance was caused by cell temperature changes resulting from the proximity of the cell to the heated specimen and in spite of the interposition of the IR filter. The thermistors appeared to compensate adequately for ambient changes. The change may have been a consequence of hysteresis since after irradiation the output voltage of the Lead Sulphide log amplifier was observed to have changed 120 mv at the highest temperature while at the lower temperature ($\sim$ 1000^{o}K) the change was of the order of 20 mv. There was insufficient time available to determine the exact cause of the impedance change.

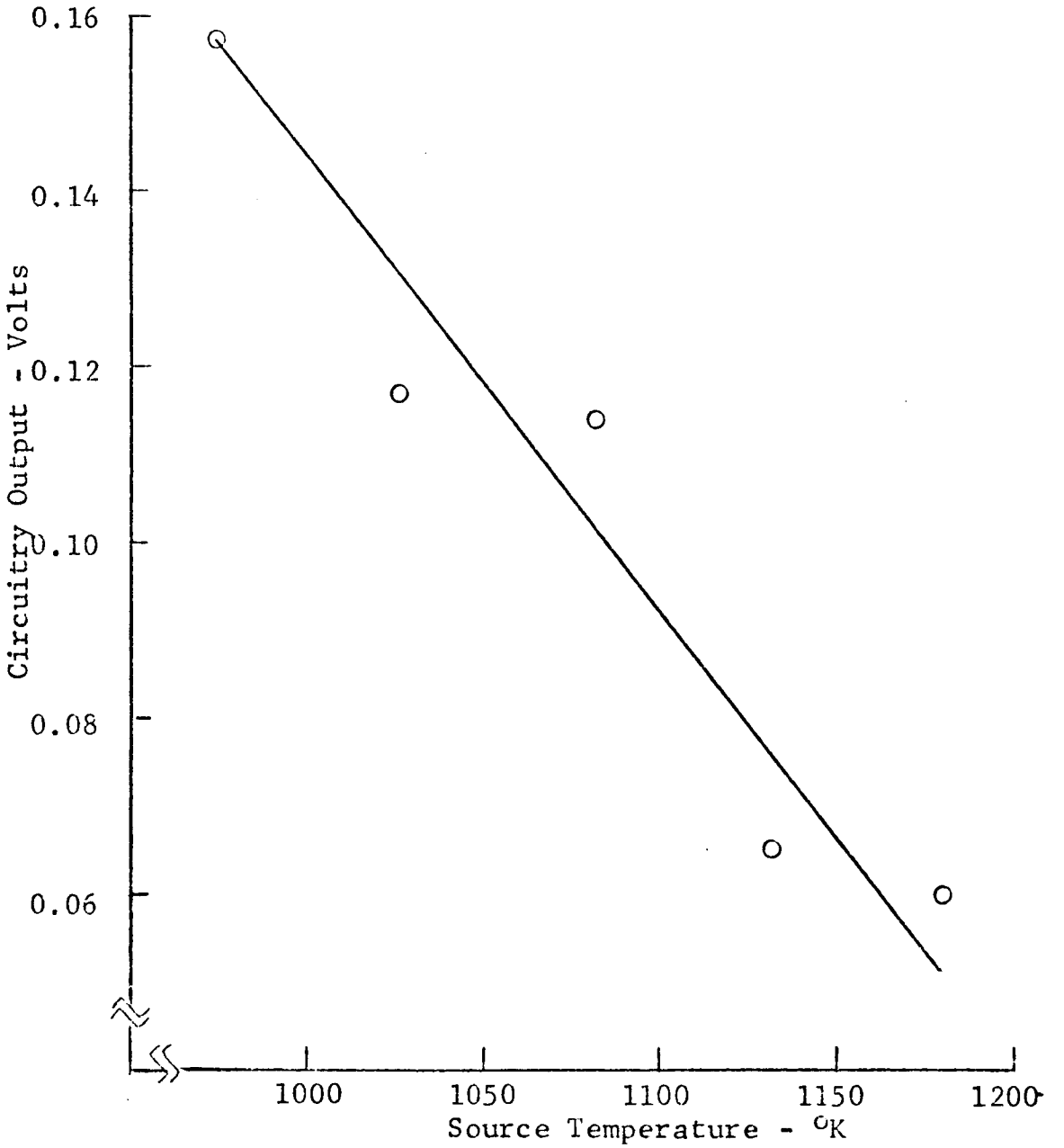

Figure 2.6-5. Temperature Sensor Test Results

The silicon cell circuitry was extremely stable, varying by only 1 mv over a period of about one hour.

2.6.5 Recommendations

There are two possible alternatives to the present system. The first is to use silicon cells separately filtered between 0.7 μ and 1.1 μ followed by a dc amplifying system. This arrangement could be used if the temperature range of interest lies above 1000°K. This approach would require two separate silicon cells in conjunction with a split-beam optical system.

The second alternative is to use the current detector system of Silicon and Lead Sulphide but the radiation must be mechanically chopped so that an ac amplifying system can be used with the Lead Sulphide Cell. The electronics for this application would require a dc restoring system so that the logarithmic amplifier is not subjected to negative-going signals.

With either of these two versions a reliable instrument can be made.

2.7 SPECIMEN ROTATION MODE ANALYSIS

2.7.1 Shape Forming By Rotation of Containerless Melts

Because of the possible importance for zero gravity shape forming by exploiting the equilibrium rotational forms of liquid masses acted upon only by surface tension and centrifugal forces, we here give a brief discussion of the application of electromagnetic fields for rotation mode control. The formation of spherodial glass, metal or other material objects by solidification while rotating in an equilibrium ellipsoidal form has been proposed by Deeg and others[1, 2].

For materials with reasonable electrical conductivity, including metals, semiconductors and high conductivity glasses in the molten state, controlled rotation can be imparted by causing the magnetic field used for position control to rotate at the desired rate. The levitated object will then spin up as a rotor of an induction motor and the rate of spin can be adjusted by suitable adjustment of the rate of rotation of the magnetic field. This would be implemented by proper phasing of the excitation to the various positioning coils. For example, in a six-coil system, if two opposing pairs of coils are excited at the same frequency but with a 90^{o} phase shift between them, a rotating magnetic field will be set up at the coil excitation frequency. This type of rotational excitation could be applied in place of the normal excitation utilized for position control by

---

1) Deeg, Dr. E. W., "Glass Preparation in Space," Space Processing and Manufacturing Meeting, MSFC, Huntsville, Ala., Oct. 21-22, 1969.

2) Frost, R. T., "Techniques and Examples for Zero-g Melting and Solidification Processes" (paper presented at the Seventh Space Congress, Cocoa Beach, Florida, April 23, 1970), Figure 1.

a time sharing arrangement in which the rotational field is applied for a small fraction of the total time so that position control is not lost. Alternately, the rotational mode excitation can be superposed upon the position control coil excitation without interfering with the normal position control servo action. The latter arrangement would require a separate winding on the coupling transformers which supply excitation to the position control coils and would also require that the rotational fields not be strong as the control field.

2.7.2 Dependence of Equilibrium Shape Upon Physical Parameters

The relation between the rotational speed ω required to give a desired oblate spheroidal shape to a given mass of liquid (presumed in the molten state prior to solidification) can easily be calculated by considering that the difference in surface tension pressure due to the different curvatures at the pole and equator must be compensated by the centrifugal forces acting on a radial column of liquid in the equatorial plane. If we consider an oblate stable spheroidal shape with major and minor semiaxes a,b (the minor axis lies along the axis of rotation), the curvature at the pole can be shown to be $C_p = -2b/a^2$. The curvature at the equator can be shown to be equal to $C_e = -a/b^2 - 1/a$. Assuming that fluid currents within the spheroid have been dissipated by viscous effects, the resulting difference in static pressures along a radial column of fluid in the equator plane will be given by $\Delta p = \sigma(C_e - C_p)$ where σ is the surface tension. This pressure difference must equal the total accelerating force acting upon the radial column of density ρ (considered of unit cross section). The inertial force due to the centrifugal acceleration of the column of fluid is given by integrating the inertial force $\rho\,\omega^2 r$ along the

radius. ω is the angular speed. We thus obtain $\sigma(C_e - C_p) = \int_0^a \rho\, \omega 2\, r dr = a^2 \rho\, \omega^2/2$. Introducing the difference in surface tension pressure between pole and equator, we finally obtain

$$\frac{\sigma}{a}\left(1 + \frac{1}{\xi^2} - 2\xi\right) = \rho \omega^2 \frac{a^2}{2}.$$

where ξ is the shape parameter b/a. The shape parameter is, of course, unity for a sphere and can approach smaller values limited only by stability considerations for rotating liquid masses.

The equilibrium shape of a revolving liquid under its own capillary forces is derived, for example, in Phil. Mag., Vol. XXVIII, pg. 161, 1914. This derivation shows that the shape will approximate that of an oblate spheroid provided that the deformation is not too great. This restraint may be expressed in terms of a parameter $\Omega = \rho \omega^2 a^3/8\sigma$. The shape will approach an exact prolate ellipsoid when Ω approaches unity. We see from the equation above that $\Omega = 1$ corresponds to that rotational speed ω which gives the shape factor $\xi = 1/2$. Thus it is to be expected that the departure from spheroidal shape will begin to be be apparent for such speeds. For small deformations, $\xi = 1 - \frac{\rho \omega^2 a^3}{8 \sigma}$

For a large mass of molten material with low surface tension, we might consider as an extreme example the following parameters

a = 10 cm

ρ = 10 grams-cm^{-2}

σ = 100 dyne-cm^{-1}

ξ = 1/2 (i.e., minor axis = 1/2 the major axis)

and obtain the corresponding rotation speed 0.3 radian per second. As another extreme example, we may consider a molten aluminum sphere of radius 1/2 cm with the same shape parameter $\xi = 1/2$ and obtain the corresponding rotation speed of 157 radians per second (1500 rpm.)

2.7.3 Two-Phase Induction Motor

When the positioning coils are excited in quadrature so as to produce a rotating magnetic field, the resultant torque due to the magnetic dipole generated by the induced eddy currents can easily be calculated, provided that the skin depth in the conductor for the corresponding rotation frequency is large compared to the radius of the sphere. From the examples of required field rotation speeds corresponding to interesting deformations given above, it can be seen that this condition will normally be met for reasonable size objects. The expression for the torque exerted by a rotating magnetic field upon a conducting sphere can be written * as $\tau = 0.1\ (\omega/\eta) B^2 a^3$ per unit volume in MKS units where η is the electrical resistivity. For example, if we consider an aluminum sphere of diameter 1 cm in a field of 100 gauss (10^{-2} webers $-m^{-2}$), rotating at 100 radians/sec., torque per unit volume will be 4.5×10^{-3} newton-meters-meters$^{-3} = 0.045$ dyne-cm-cm^{-3}. Since the volume is approximately 1 cm^3, the torque will be about 0.045 dyne-cm. The moment of inertia of this sphere is approximately 1/7 gm cm^2. For these parameters we see that the ball would be accelerated

---

* Zijlstra, H., Experimental Methods In Magnetism, Vol. 2: Measurement of Magnetic Quantities. (Amsterdam: North-Holland Publishing Company, 1969), p. 89.

at 0.320 radians sec^{-2} so that a speed of 10^2 sec^{-1} would be reached within about 300 seconds. For larger spheres, the moment of inertia varies at the fifth power of the radius whereas the torque varies as the sixth power. Thus the angular acceleration in a given rotation field will increase directly as the sphere radius. On the other hand, the speeds required to give a given shape deformation vary as $a^{-3/2}$, so that the acceleration time for a given deformation varies as $a^{-5/2}$ This, then, seems a practical way to achieve desire rotational shapes provided that the resistivity η is not too high. Since field strengths of thousands of gauss are quite practical, and since spin-up times on the order of many minutes can probably be allowed, we can consider situations for resistivities 10^4 to 10^6 times higher than that for aluminum and still achieve large deformations within a reasonable time.

2.7.4 Single-Phase Induction Motor

This method of spin-up for a solid sphere appears practical and has been previously studied in the laboratory. Both theory and experimentation done to date, however, indicate that this method is not practical for spinning molten spheres due to the very low torques available and the viscous torque due to the inevitable shape distortions of the liquid mass due to magnetostrictive forces. The fluid must rotate, whereas the prolate deformation of the spheroid lies along the direction of the main single phase field, giving appreciable damping torque which we estimate below.

2.7.5 Theory and Experiments

2.7.5.1 Solid Rotor

The torque versus speed characteristic of a single-phase induction motor without special starting provisions is well known and is represented schematically in the sketch.

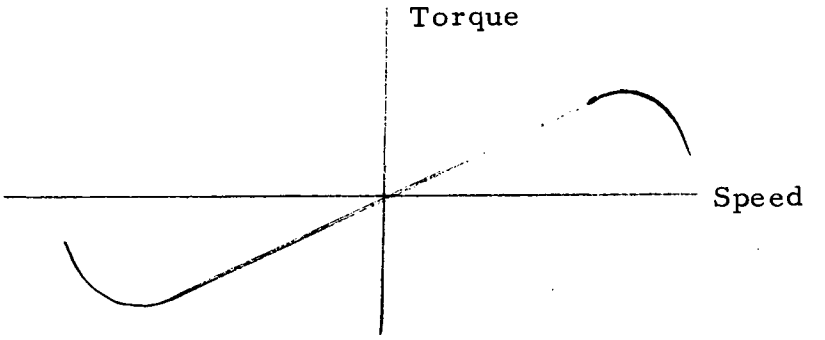

The torque is zero when the rotor is at rest but increases so as to accelerate any rotational motion, in whichever direction it is initially imparted. For field excitation frequencies on the order of tens of kHz which have been utilized for electromagnetic positioning and heating of containerless melts, the torque-speed characteristic can be considered linear up to the highest physically achievable speeds. These limiting speeds were determined in the laboratory to be established by air drag of several thousand rpm for a 1 cm diameter aluminum sphere which was simultaneously levitated and spun-up in the single phase induction mode. In one experiment in which air drag was eliminated by means of a vacuum pump, a 1 cm diameter aluminum sphere was actually burst as it reached its fracture stress limitation at tens of thousands of rpm.

In the presence of air, an angular acceleration rate of 10 radians sec^{-2} was measured and appeared to be reasonably constant over the range up to 3000

rpm. The ultimate rotation speed was 10,000 rpm under conditions corresponding to approximately 150 amperes excitation at 30 kHz into a 2 cm diameter hemispherical coil. The estimated spin-up torque was deduced as approximately 2 dyne-cm. The near constancy of acceleration throughout the lower speed range indicates that the spin-up torque is not due to a torque-speed characteristic such as shown in the sketch above but must be due to a small quadrature component of the alternating field due to coil asymmetries. An auxiliary experiment was done in which a small flat was filed onto one portion of the spherical surface such that a gravitational torque on the order of several dynes-cm would be exerted due to the non-coincidence of the electromagnetic levitation force and the gravitational forces on the sphere. It was found that this asymmetry inhibited rotation and the sphere did not spin-up, thus giving additional confirmation to the order of magnitude of the spin-up torque.

A conclusion of this work is that solid specimens should be sting mounted during melting under zero gravity conditions to prevent rotations where these are not desired. Spin-up to bursting speed of unmounted specimens appears to be inhibited by air drag and this inhibition would remain provided inert gas environments are used at reasonable pressures.

2.7.5.2 Liquid Rotor

In a number of laboratory levitation experiments in which aluminum spheres of 1 cm diameter were melted and superheated, no rotation could be observed. This is attributed to the rather large deformations from spherical shape due to the combination of magnetostrictive and gravitational forces. It

remains to examine whether significant rotational motions can be imparted as a result of single-phase induction motor action when molten spheres are being processed by electromagnetic fields in the weightless condition.

In a zero gravity environment, both the spin-up torque due to single-phase induction motor effects and the asymmetry and consequent viscous damping due to magnetostrictive forces will be proportional to the exciting field strength.

2.7.6 Shape Deformation Due to Magnetostrictive Forces

The asymmetry induced in a conducting liquid sphere due to magnetostrictive forces can be estimated in the following way. Computations of electromagnetic force fields within conducting spheres located in uniform oscillating electromagnetic fields were summarized in the reference * . These show that the magnetostrictive forces act radially inward around the equatorial regions of the sphere and vanish toward the axis of the sphere (assumed in the direction of the magnetic field) as well as diminishing at higher latitudes. Such a force field will result in a circulation of fluid which is radially inward in the equatorial regions and poleward along the axis (see sketch). The resulting flow system consists of two ring vortices between which there will

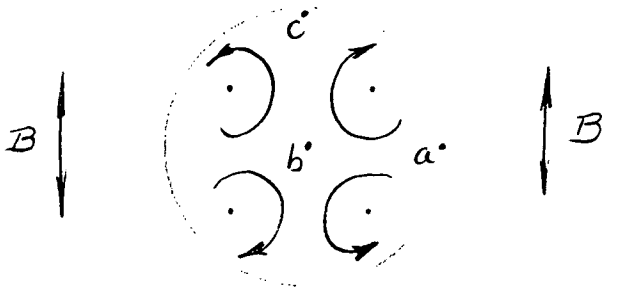

* Frost, R. T., et al, Field Management for Positioning and Processing of Free Suspended Liquid Materials. General Electric Company, Contract NAS8-24683, Modification No. 2, Task IV, Final Report, May 15, 1970.

be a repulsive effect, leading to deformation of the sphere into a prolate shape elongated in the magnetic field direction. Although the fluid dynamics problem has not been solved taking account of viscosity and surface tension, an order of magnitude estimate for the deformation can be obtained by applying Bernoulli's theorem between the points a, b and c. Since these three points are stagnation points, the corresponding kinetic energy per unit volume will vanish and we can write $p_a - p_c = W$, where W is the work done by the electromagnetic force in moving a unit volume of fluid radially inward from a to b against the pressure gradient due to the nonuniform curvature of the deformed surface film. Part of the electromagnetic work will go towards the overcoming of viscous forces but this will be neglected in this order of magnitude estimate. In this approximation, the pressure at points b and c will be the same because both are stagnation points and there are no electromagnetic forces acting along the axis of the spheroid. The pressure differential can thus be taken as due to the difference in surface tension pressure at the points a and c as derived earlier in this section to obtain

$$p_b - p_a = \frac{\sigma}{a} \left(1 + \frac{1}{\xi^2} - 2\xi \right)$$

The work done by the electromagnetic forces per unit volume of fluid moving from a to b can be written as

$$W = - \int_o^a (\vec{j} \times \vec{B}) \cdot \vec{dr}$$

where $\vec{j}$ is the current density and $\vec{B}$ is the magnetic flux. Both j and B will die off rapidly as we proceed inward from point a and these variations were plotted in the reference * For our present order of magnitude purposes the effective B can be taken to be the magnetic field at the spheroid surface and the integral $\int_o^a jdr$ can be equated to the total eddy current flowing around the equatorial region of the sphere per unit latitudinal distance.

$$W = B \int_o^a jdr = i_u B$$

The total circulating eddy current induced in the spheroid can be found by equating the magnetic dipole moment derived by Smythe ** to the classical expression for the dipole moment in terms of current times area. This results in the identity

$$\pi a^3 G(x) H = \pi a^2 i$$

or

$$i = aG(x)H$$

For a representative laboratory situation in which a 1 cm diameter aluminum sphere is levitated and melted in a field of the order of 100 gauss @ 30 kHz the resulting current is approximately 50 amperes and is distributed over approximately 1 cm of latitudinal distance. G(x) = 1. In gaussian units the total work W = i. B = 5 emu current 100 gauss = 500 ergs cm^{-3}. Equating this to the difference in surface tension pressures at point a and point c gives for the deformation parameter ξ the relation

$$\frac{\sigma}{a}\left(1 + \frac{1}{\xi^2} - 2\xi\right) = \frac{\sigma}{a} F(\xi) = 500 \text{ ergs - cm}^{-3}$$

* Frost, R. T., et al , Field Management for Positioning and Processing of Free Suspended Liquid Materials. General Electric Company, Contract NAS8-24683, Modification No. 2, Task IV, Final Report, May 15, 1970

** Smythe, W. R., Static and Dynamic Electricity (New York: McGraw-Hill 1950), p. 398.

giving a deformation parameter of about 0.95.

2.7.7 Viscous Damping Torque

The single-phase induction motor torques are perpendicular to the magnetic field direction and hence will tend to spin the spheroid up in a direction normal to its axis of elongation. Since the direction of elongation remains fixed in the direction of the alternating magnetic field, viscous damping effects will occur when rotational motion is imparted to the entire fluid mass as a result of single phase induction to torques. We can estimate the limiting speed for rotation set up in manner by equating the spin-up torque derived for the solid sphere experiments described earlier to the opposing torque due to the viscous dissipation when the fluid mass rotates but maintains its elongation in a fixed direction. $2\pi\tau = E$, where E is the viscous energy dissipated in a single rotation. The viscous energy dissipated in 1/4 rotation can be estimated as approximately twice that due to deformation of this sphere from the prolate into a spherical shape. The viscous decay problem has been studied for the latter case in terms of a viscous damped sphere initially deformed in a prolate fashion *. For this model, the viscous decay time can be written as $t \frac{a^2}{5} \nu$ where ν is the kinematic viscosity. Estimating that the change in surface area of the spheroid deformed with a shape parameter 0.95 is of the order of 0.0015 cm^2 and taking a surface tension of 900 dynes per cm, the additional surface energy of $0.0015 \cdot 900 = 1.4$ ergs would be dissipated in a time t

* Lamb, Sir Horace, Hydrodynamics (New York: Dover Publications, 1945), p. 640.

of the order of one second for spheres of many liquid metals of the size considered here.* Considering that this energy would be dissipated in approximately 1/8 of a total rotation for the analogous problem of the rotating fluid mass constantly deformed in a given direction, the power dissipation due to viscous forces will be 8 x 1.4 ergs/8 seconds corresponding to a rotational period of 8 seconds. Since the viscous power dissipation will increase as the square of the angular velocity ω we can write for the rate of viscous dissipation $\tau\,\omega$ the product

$$\tau\omega = \frac{11.2 \text{ ergs}}{8 \text{ sec}} \times \left(\frac{\omega}{\omega_o}\right)^2 = 2.6 \text{ ergs-sec} \cdot \omega^2, \quad \text{where } \omega_o \text{ is the angular}$$

speed corresponding to a rotational period of 8 seconds. Finally, since the laboratory experiments referred to indicated spin-up torques on the order of 2 dyne-cm, we conclude that the maximum rotational speed which can be imparted to the viscous, deformed spheroid will be approximately 1 radian per second. At lower field strengths such as in the case where the spheroid would be allowed to solidify under the influence of relatively smaller field strengths, both the deformation and spin-up torque would fall off proportionately so that the same argument would apply. Our order of magnitude estimate for the very low angular rates which can be induced by single phase induction action in suspended liquid metal systems is confirmed by the failure to observe any appreciable rotational motion for molten levitated aluminum spheroids in the laboratory.

---

* Frost, R. T., "Techniques and Examples for Zero-g Melting and Solidification Processes," (paper presented at the Seventh Space Congress, Cocoa Beach, Florida, April 23, 1970), Fig. 1.

3.0 MODIFICATION OF SIX-COIL DROP TEST UNIT

3.1 MODIFICATION TO INCORPORATE TECHNICAL DEVELOPMENTS

When the drop test unit was received it was tested and found in good working order, therefore no repairs were necessary. Figure 3.1-1 is an overall photograph of the equipment as modified. The modifications made as a result of technical developments of EMLS were as follows:

- Power Amplifiers (Figure 3.1-2)

  The operating frequencies of all six channels were changed to those near 100 KHz. The multipliers were modified to go from the original heating mode (all amplifiers delivering maximum power with no specimen position error) to one where the amplifiers only deliver power for positioning.

- Pre-Amplifiers

  Six pre-amplifiers were added to utilize the position sensors developed under this contract. These pre-amplifiers were mounted underneath the coil assembly base within a shielded housing.

- Position Sensors

  New position sensor assemblies were built for the drop package using the sensors and approximate optical system (but without mirrors) of the prototype system described in the Sections above.

- Servo Electronics (Figure 3.1-3)

  Modification in gains and break frequencies were made to be compatible with the new coils, frequencies and specimens.

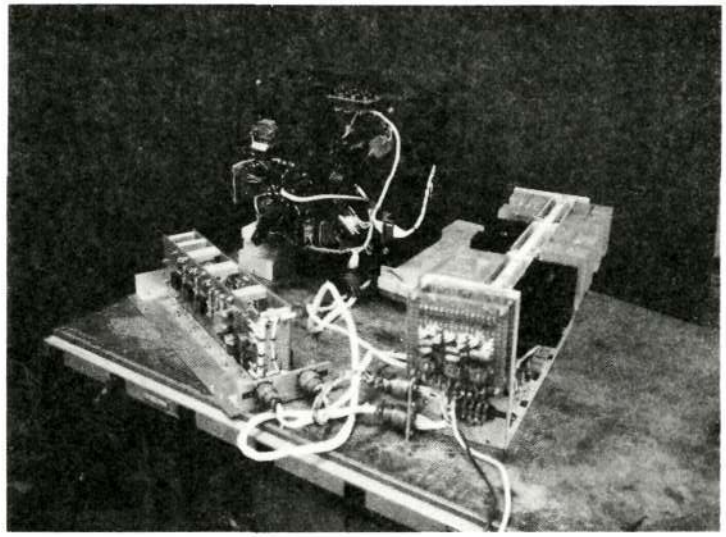

Figure 3.1-1. Modified Drop Test Unit

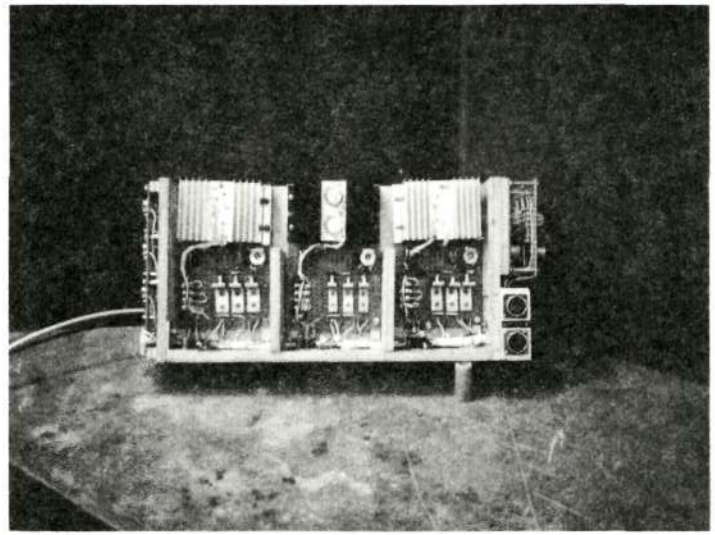

Figure 3.1-2. Power Amplifier Assembly

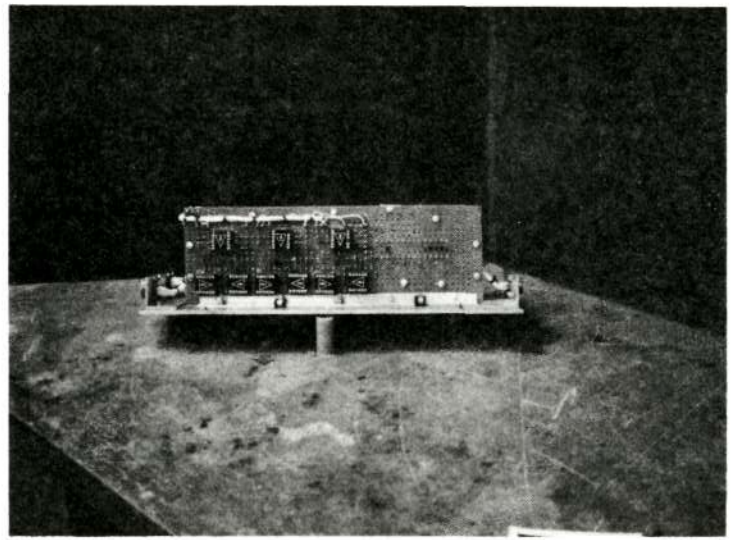

Figure 3.1-3 Differential and Servo Amplifiers Position Sensing

- Coil Assembly (Figure 3.1-4)

  New coils and tank circuits and a new lighting system was built on the original coil assembly base as shown in Figure 3.1-4). Also added were lights, (on the left corner of the assembly pictured in Figure 3.1-4) six of which indicate which power amplifiers is driving and a seventh which indicates an overtemperature kick-out of one or more power amplifiers. A small regulator for the specimen lighting system was added to stabilize the unregulated voltage and maintain a quiet light output. Some interaction with the servo had been found as the light intensity changed according to the servo drive requirement. The regulator eliminated this interaction. The prototype system described in this report defined a sophisticated infrared signal positioning scheme but the drop package uses a painted white ball, the entire coil enclosure being flat back.

3.2 ADDITIONAL CHANGES

The modifications in addition to the technical developments of EMLS were as follows:

- Power Amplifiers

  Over temperature sensors (thermistors) were mounted on each power transistor assembly. A board of electronics (seen on the right hand end of Figure 3.1-5), containing control circuitry and relays in the power lines of each power amplifier, was located on the power amplifier assembly. This board also has inputs from thermistors

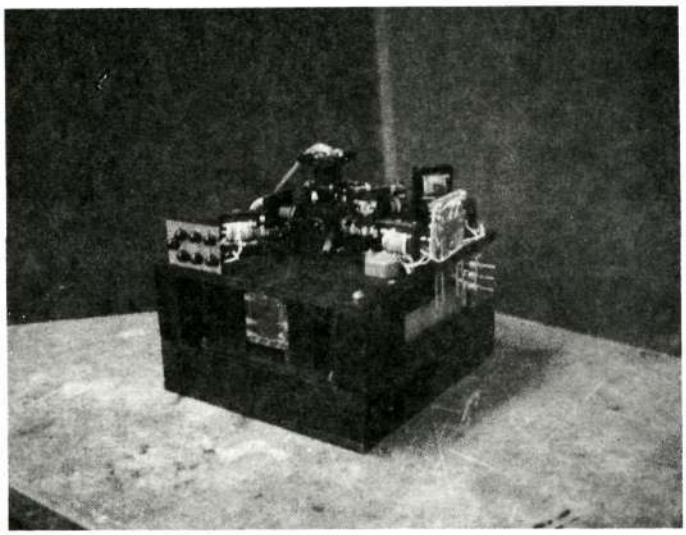

Figure 3.1-4 Positioning Coil Assembly

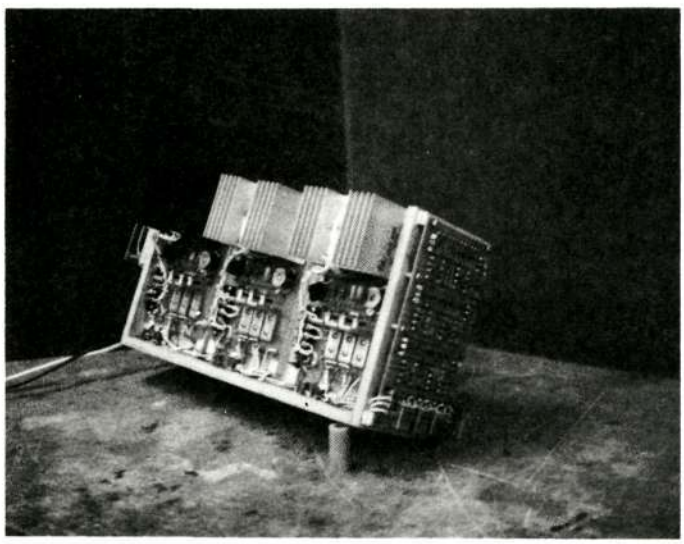

Figure 3.1-5 Power Amplifier Assembly with Overtemperature Protective Circuits

mounted on each coil and so provides protection against over temperature in either the coils or power amplifiers.

A small board containing three additional oscillators was mounted on the power amplifiers assembly and can be seen on the end of the assembly on the right side of Figure 3.1-1.

- Servo Electronics

  A limiter was placed on the position error line, but not the rate line, into the servo amplifier. The purpose of this limiter is to prevent large position errors from driving the power amplifiers at full power. They can be readily removed if full force as a result of a position error is desired. Because full force is available for damping, the time to show convergence from a position saturation condition is shortened. This is important for demonstrating damping in the MSFC drop tower facility where the specimen rests directly over the bottom coil at the instant the drop starts. Without position error limiting this specimen will be accelerated by a force of about 200 dynes for the first centimeter or so, and will overshoot the center with a rather high kinetic energy. The time to damp out this large energy is much longer than that required with position error limiting which limits the coil force to about 50 dynes. Note that with position error limiting there is no rate error limiting so damping has the full 200 dynes available near any coil.

There has been no change in mounting centers, outline dimensions, or cable lengths in the refurbished drop test unit.

Two copies of a technical manual will be delivered with the drop test unit. This document will be the same type as was sent with the original equipment. It will include the following items:

- Description of operation utilizing a block diagram
- Operational and adjustment procedures
- Circuit diagrams (schematics)
- Photographs of circuit board layouts and construction
- Position sensing error curves
- Telemetry calibration data
- Wiring and cabling diagrams.

APPENDIX A

ELECTRONIC BLOCK AND SCHEMATIC DIAGRAMS

Included in this Appendix is the Block Diagram to implement the functions of the Electromagnetic Levitation System (EMLS), General Electric Drawing No. ER 47D225301. The detailed electronic circuits of the blocks enclosed by the broken line in the upper left hand portion of this drawing are depicted on Sheet 1 of General Electric Drawing No. ER 47J225305 which follows the Block Diagram. It should be noted that these circuits represent the first effort to mechanize the design equations for determining drive currents as a function of position errors generated by the position detector and servo system. These circuits include the elements necessary to sense position from information supplied by the IR sensor to accomplish the coordinate conversion, to provide servo lead compensation and to compute the driving currents required. The circuits as shown cannot be considered to be fully designed. No breadboards have been made to permit testing in the laboratory nor have the required analyses been performed. Therefore, these circuits may not represent those which would have been utilized had not the effort been terminated before the design was complete.

The circuits to mechanize the blocks shown on the right hand side of drawing ER 47D225301 are detailed on Sheet 2 of Drawing ER 47J225305. No discussion of these circuits is included in the present report but they were

reviewed in detail in Section 2.4 of the Final Report dated June 15, 1971 for Contract No. NAS 8-26157 entitled, "Free Suspension Processing Systems for Space Manufacturing."

The blocks shown below the broken line on Drawing ER 47D225301 outline the conceptual mechanization for a system to capture the spherical specimen after melting and resolidification was completed. No mechanization of this capture system had been effected at the time of the contract termination and no schematic diagrams are presented.

FOLDOUT FRAME 1 FOLDOUT FRAME 2 FOLDOUT FRAME 3

CIRCUITS ON SH 1 OF ER47J225305

CIRCUITS ON SH 2 OF ER47J225305

IR SENSOR (2)

PRE AMPS (6)

CO-ORD CONV

FORCE/ CURR COMP

POWER AMP #1 MULT & OSC

POWER AMP #2 MULT & OSC

POWER AMP #3 MULT & OSC

POWER AMP #4 MULT & OSC

TANK & COIL

TANK & COIL

TANK & COIL

TANK & COIL

+28 VDC

DC/DC CONV

RATE (U)

TEMP SENSOR & ELECT

TLM

TEMP SIGNAL

MOTOR BEAM SHUT OFF

CONTROL LOGIC

POWER AMP #5 MULT & OSC

TANK & COIL

CAPT ELECT

THESE CIRCUITS NOT DESIGNED NOR BUILT

FIGURE A-1

REVISIONS				
ZONE	LTR	DESCRIPTION	DATE	APPROVED

UNLESS OTHERWISE SPECIFIED DIMENSIONS ARE IN INCHES— TOLERANCES ON: 2-PLACE DECIMALS ± 3-PLACE DECIMALS ± ANGLES ± FRACTIONS ± ALL SURF ✓ MATERIAL—

SIGNATURES	DAY	MO	YR
DRAWN Robert O Hinkle	8	2	72
CHECKED			
ISSUED			
ENGRG			
MFG			
MATLS			

GENERAL ELECTRIC SS (11) DEPT LOC PHILA. PA

BLOCK DIAGRAM ELECTRONIC SYSTEM EMLS

SIZE D | CODE IDENT NO. 23991 | ER-7D225301

SCALE — | SHEET 1 OF 1

A-3/4

Page intentionally left blank

FOLDOUT FRAME 1

FOLDOUT FRAME 2

FOLDOUT FRAME 3

MULTIPLIERS, OSCILLATORS & POWER AMPLIFIERS

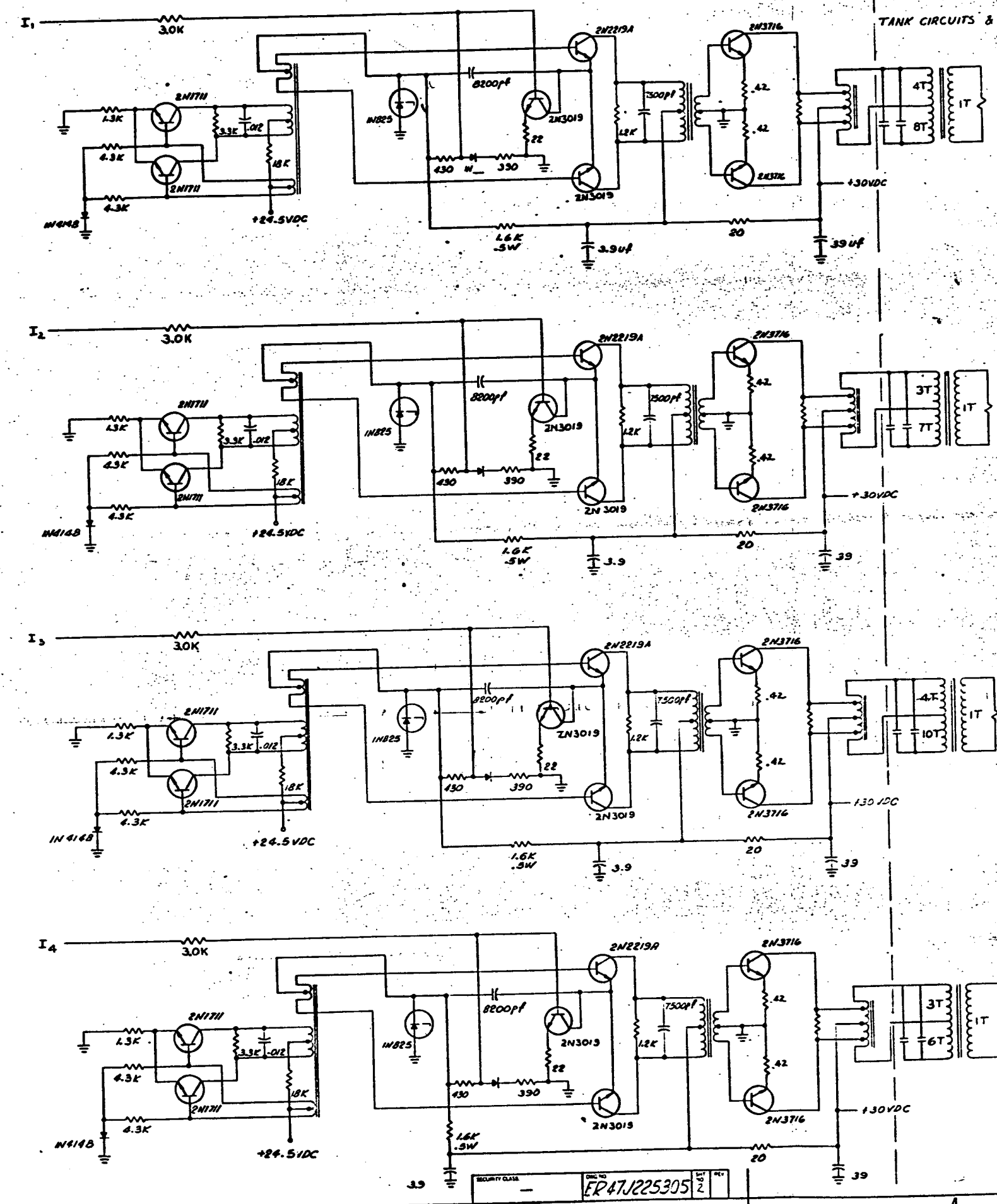

TANK CIRCUITS & LEVITATION COILS

REGULATED POWER SUPPLY

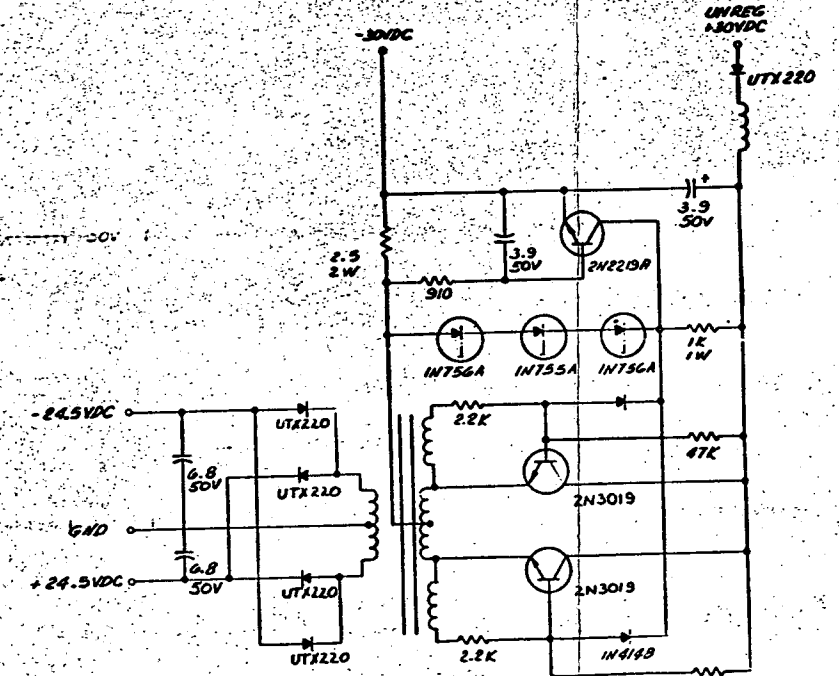

FIGURE A-3

REVISIONS			
ZONE	LTR	DESCRIPTION	DATE

SECURITY CLASS	DWG NO ER47J225305	REV
	SCALE	SHEET

UNLESS OTHERWISE SPECIFIED DIMENSIONS ARE IN INCHES — TOLERANCES ON: 2 PLACE DECIMALS ± 3 PLACE DECIMALS ± FRACTIONS ± — MATERIAL —

GENERAL ELECTRIC — 35 (11) — 2-A FD.

DIAGRAM, SCHEMATIC-ELEC
EMLS

CONTRACT NO NAS 5-2[illegible]8

SIZE J | CODE IDENT NO 23391 | ER47J225305

SCALE — | SHEET 1

A-7/8

J 47J225305 REF

J 47J225305 REF

COMPUTER PROGRAM ABSTRACT

DATE OF ABSTRACT:	PROGRAM NUMBER:	TITLE:
1/26/72	NAS8-27228 Task 2	Optical Position Sensor and Related Programs

SYMBOLIC NAME:	LANGUAGE:	SHARING	STATUS	MAN MONTHS:	COMPUTER TYPE:
OPS CURRENT CNVRTX TETMFO MAG CONURTF	FORTRAN IV	[X] YES [ ] NO	[ ] UNDER DEVELOPMENT [X] OPERATIONAL [ ] COMPLETED	1.00 MACHINE HOURS: 8	GE 605

ABSTRACT

The cited programs have been developed to study the fundamental relationships governing the control system (4 quadrant detector, coordinate converter and servo). Calculations with these programs have provided direction for the implementation of the control system.

Program OPS follows the position and dynamic motion of the specimen as it floats and is manipulated in zero gravity. The force from each coil in the four coil system required (by the spring-dashpot analogue) to position the specimen at the geometric center of the tetrahedral control volume is calculated. Specimen position and velocity, as indicated by the four quadrant detectors and the coordinate converter, is fed to the servo. The appropriate action (i.e., the forces) to be delivered by each coil is calculated.

When the forces required from each coil has been calculated in OPS, a series of subprograms is entered in which the currents to each coil are calculated, coordinate transformations are applied, an estimate of the actual forces produced on the specimens is made, and another coordinate transformation is made.

Subprogram CURENT employs a theoretical coil current/force delivered relationship which computes the coil currents required to produce the desired coil forces at the specimen position. The available coil current is limited according to engineering estimates of the maximum.

Subprogram CNVRTX transforms the coordinate of the specimen in OPS to the system used in the TETMFO subprogram.

Subprograms TETMFO and MAG take the coordinates of the specimen from CNVRTX and the coil currents from CURENT and computes an approximation of the actual forces delivered to the specimen (TETMFO is a slightly modified version of TETRA, a program which together with CUBE is included at the end of this appendix).

These force vectors are then transformed back to OPS coordinate via subprogram CNVRTF. In program OPS, there (presumed) actual forces are allowed to effect the specimen and the simulation proceeds.

Explanatory Notes on Program OPS

Lines 00070	LLi, statement functions for the four unit vectors originating at
100	(0, 0, 0) and directed toward the center of the coils.
110	FFi, statement functions for the solution of the unit force
150	vectors.
170	K = 17. Spring constant - set to allow maximum current at point in field.
260	Output description
360	
400	Position of point specimen on end of string.
420	
430	IVEL, VMAG: pick the velocity unit vector off string and the
530	magnitude.
570	Start up and solution for first set of forces desired
1200	
1210	Find the current at each coil to deliver the desired forces; find
1340	the delivered force components.
1370	Let specimen move according to delivered forces and continue.
2000	

```
READY
$LIST OPS,CURENT,CNVRTX,TETMFO,MAGMFO,CNVRTF

02/15/72  09.002



00010 * OPS PROGRAM  MFO  12/28/71
00020 *
00030     REAL LL1,LL2,LL3,LL4,L1,L2,L3,L4,L11,L21,L31,L41,
00040    &          MAGP,MAGV,MAGF,K
00050    &          I1,I2,I3,I4,MAGFF
00060 *   L IS DIRECTED TOWARD COILS
00070     LL1(X,Y,Z)=                +0.816492*Y     -0.57735*Z
00080     LL2(X,Y,Z)=+0.816492*X                     +0.57735*Z
00090     LL3(X,Y,Z)=-0.816492*X                     +0.57735*Z
00100     LL4(X,Y,Z)=                -0.816492*Y     -0.57735*Z
00110 * F IS DIRECTED TOWARD ORIGIN
00120     FF1(X,Y,Z)=                +0.612373*Y     -0.433013*Z+.25
00130     FF2(X,Y,Z)=+0.612373*X                     +0.433013*Z+.25
00140     FF3(X,Y,Z)=-0.612373*X                     +0.433013*Z+.25
00150     FF4(X,Y,Z)=                -0.612373*Y     -0.433013*Z+.25
00160     SS(A,B,C)=SQRT(A**2+B**2+C**2)
00170     K=17.
00180     C1=0.816492
00190     C2=0.57735
00200     C7=1.33
00210     C6=SQRT(K*C7*4.)
00220     C8=0.2
00230 * C6 DAMPING CONSTANT, C7 MASS(GR), C8 PRINT INTERVAL
00240 * RESERVED FOR VOLTS TO X,Y,Z, CONVERSION
00250 *
00260     PRINT 888
00270 888 FORMAT(15X,"OUTPUT FORMAT")/
00280    &       (15X,"DC=X, Y, Z, COMPONENTS , MAGNITUDE")/
00290    &     (15X," M=MAGNITUDES: CM OR DYNES OR AMPS")/
00300    &      //
00310    &   (2X,"TIME",9X,"-1*SPECIMEN POSITION DC")/
00320    &   (18X,"SPECIMEN VELOCITY DC")/
00330    &    (21X,"DESIRED FORCES DC")/
00340    &    (17X,"DESIRED COIL FORCES M")/
00350    &     (23X,"CURRENT INPUT M")/
00360    &    (19X,"DELIVERED FORCES DC")///)
```

```
00370      PRINT 35;PRINT 35
00380  * POSITION OF STING
00390      PRINT 35
00400      X=-0.67400
00410      Y=-0.51845
00420      Z=0.84321
00430      READ:IVEL,VMAG
00440      GO TO (91,92,93,94), IVEL
00450  *    V UNIT VECT PARALLEL TO COIL 3 CNTR LINE (IVEL=1)
00460    91 VX=0.816496 ;VY=0. ; VZ=-0.577350
00470      GO TO 99
00480  *   V UNIT VECT FROM STING TOWARD ORIGIN (IVEL=2)
00490    92 VX=0.56283 ;VY=0.43294 ; VZ=-0.70414
00500      GO TO 99
00510  * V UNIT VECT NORMAL TO STING (IVEL=3)
00520    93 VX=0.09120 ;VY=0.89397 ;VZ=-0.43867
00522      GO TO 99
00524  * V UNIT VECT. -OFF STING DUE TO MOUCH FORCES
00526    94    VX=0.8432 ; VY=-0.4672 ; VZ=-0.2658
00530    99 VX=VX*VMAG ; VY=VY*VMAG ; VZ=VZ*VMAG
00540  * INITIAL CONDITIONS: SPECIMEN AT X,Y,Z WITH VELOCITY
00550  *   VX,VY,VZ---AFTER DT SECONDS IS AT X1,Y1,Z1 WITH VELOCITY
00560  * VX,VY,VZ:---COIL ACTION BEGINS NOW
00570      T=0.0
00580      DT=.01
00590      MAGP=SS(X,Y,Z)
00600      MAGV=SS(VX,VY,VZ)
00610      IF(MAGV.EQ.0.0) GO TO 102
00620  * V UNIT VECTOR COMPONENTS
00630      VXU=VX/MAGV
00640      VYU=VY/MAGV
00650      VZU=VZ/MAGV
00660      GO TO 4
00670  102 VXU=0.;VYU=0.;VZU=0.
00680    4   PRINT 5
00690    5 FORMAT(1X,"INITIAL CONDITIONS  T=0.00",//)
00700      PRINT 30,X,Y,Z,MAGP
00710      PRINT 30,VX,VY,VZ,MAGV
00720      PRINT 6
00730    6 FORMAT(1X,"------------------",//)
00740  * COMPUTE INITIAL DISPLACEMENT
00750      X1=X+VX*DT
00760      Y1=Y+VY*DT
00770      Z1=Z+VZ*DT
00780      MAGP=SS(X1,Y1,Z1)
00790      IF(MAGP.EQ.0.0) GO TO 103
00800  * -P UNIT VECTOR COMPONENTS
00810      X1U=-X1/MAGP
00820      Y1U=-Y1/MAGP
00830      Z1U=-Z1/MAGP
00840      GO TO 10
00850  103 X1U=0.;Y1U=0.;Z1U=0.
00860  * END OF START UP SEQUENCE
```

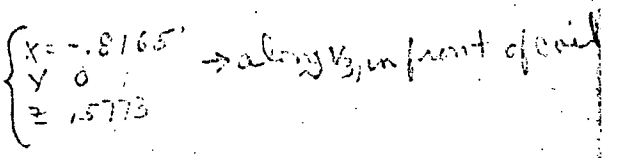

```
00870   10 CONTINUE
00880      T=T+DT
00890  * COMPUTE L'S(P PROJECTIONS ON COIL VECTORS)
00900      L1=LL1(X,Y,Z)
00910      L2=LL2(X,Y,Z)
00920      L3=LL3(X,Y,Z)
00930      L4=LL4(X,Y,Z)
00940      L11=LL1(X1,Y1,Z1)
00950      L21=LL2(X1,Y1,Z1)
00960      L31=LL3(X1,Y1,Z1)
00970      L41=LL4(X1,Y1,Z1)
00980  *--------COMPUTE F'S----------
00990      F1=FF1(X1,Y1,Z1)
01000      F2=FF2(X1,Y1,Z1)
01010      F3=FF3(X1,Y1,Z1)
01020      F4=FF4(X1,Y1,Z1)
01030  *   LOOK FOR SMALLEST -F
01040      ADD1=AMIN1(F1,F2,F3,F4)
01050  * COMPONENT VELOCITIES ALONG COIL AXES
01060      DL1DT=(L11-L1)/DT
01070      DL2DT=(L21-L2)/DT
01080      DL3DT=(L31-L3)/DT
01090      DL4DT=(L41-L4)/DT
01100  * ADJUST F'S
01110      F1=K*(F1-ADD1)+C6*DL1DT
01120      F2=K*(F2-ADD1)+C6*DL2DT
01130      F3=K*(F3-ADD1)+C6*DL3DT
01140      F4=K*(F4-ADD1)+C6*DL4DT
01150  * CHECK AND ADJUST FOR -F'S
01160      ADD2=AMIN1(F1,F2,F3,F4)
01170      F1=F1-ADD2
01180      F2=F2-ADD2
01190      F3=F3-ADD2
01200      F4=F4-ADD2
01210  * --------END OF F'S CALCULATIONS--------
01220  * CALL SUBROUTINE FOR COIL CURRENTS-"CURENT"
01230      CALL CURENT(F1,F2,F3,F4,L11,L21,L31,L41,I1,I2,I3,I4)
01240  * CALL SUBRT. FOR CONVERSION OF X1,Y1,Z1, TO
01250  *  X1P,Y1P,Z1P,-GRAY'S ORIENTATION OF THE TETRAH.
01260  *  "CNVRTX" IN WHICH GRAY'S COILS A,B,C,D ARE OPS'
01270  * COILS 4,3,1,2 RESPECTIVELY
01280      CALL CNVRTX(X1,Y1,Z1,X1P,Y1P,Z1P)
01290  * CALL SUBRT. "TETMFO"-MODIFIED "TETRA OF GRAY--
01300  * TAKES X1P,Y1P,Z1P AND CURRENTS AND COMPUTES FX,FY,FZ
01310  *  IN GRAY'S COORDINATE SYSTEM
01320      CALL TETMFO(X1P,Y1P,Z1P,I1,I2,I3,I4,FXP,FYP,FZP)
01330  * CALL SUBRT. "CNVRTF"- CONVERTS GRAY'S FORCE COMPONENTS
01340  *(FXP,...) TO OPS COMPONENTS(UNIT VECT. FORM) FFXU,...
01350      CALL CNVRTF(FXP,FYP,FZP,FFXU,FFYU,FFZU,MAGFF)
01360
```

```
01370 *  COMPUTE DESIRED FORCE VECTOR COMPONENTS
01380      FX=0.0*F1   -C1*F2   +C1*F3    +0.0*F4
01390      FY=-C1*F1   +0.0*F2 +0.0*F3   +C1*F4
01400      FZ=+C2*F1   -C2*F2   -C2*F3    +C2*F4
01410      MAGF=SS(FX,FY,FZ)
01420      IF(MAGF.EQ.0.0) GO TO 104
01430 * F UNIT VECTOR COMPONENTS
01440      FXU=FX/MAGF
01450      FYU=FY/MAGF
01460      FZU=FZ/MAGF
01470      GO TO 7
01480  104 FXU=0.;FYU=0.;FZU=0.
01491    7 IF(T.GT.0.0) C8=.01
01492      IF(T.GT.0.02) C8=.02
01494      IF(T.GT.0.1) C8=0.2
01496      IF(T.GT.1.5) C8=0.5
01498      TM=T/C8
01500      TRT=AINT(TM+.005)
01510      TEST=ABS(TRT-TM)
01520      IF(TEST.LE.0.0001)  GO TO 20
01530      GO TO 15
01540   20 PRINT 25,T,X1 ,Y1 ,Z1 ,MAGP
01550   25 FORMAT(2X,//,F8.2,1P4E14.3)
01560       PRINT 30,VX ,VY ,VZ ,MAGV
01570      PRINT 30,FX ,FY ,FZ ,MAGF
01580      PRINT 30,F1,F2,F3,F4
01590      PRINT 30,I1,I2,I3,I4
01600      PRINT 30,FFX ,FFY ,FFZ ,MAGFF
01610   30 FORMAT(8X,1P4E14.3)
01620      PRINT 35
01630   35 FORMAT(/)
01640 *
01650    15 CONTINUE
01660 *COMPUTE ACCELERATION COMPONENTS DUE TO ACTING FORCES
01670      AX=(FFXU*MAGFF)/C7
01680      AY=(FFYU*MAGFF)/C7
01690      AZ=(FFZU*MAGFF)/C7
01700 *  TRANSFER OLD POSITION AND COMPUTE NEW
01710 *     TRANSFER
01720      X=X1
01730      Y=Y1
01740      Z=Z1
01750 *     NEW POSITION
01760      X1=X1+(VX+0.5*AX*DT)*DT
01770      Y1=Y1+(VY+0.5*AY*DT)*DT
01780      Z1=Z1+(VZ+0.5*AZ*DT)*DT
01790      MAGP=SS(X1,Y1,Z1)
01800      IF(MAGP.EQ.0.0) GO TO 106
```

```
01810 * UNIT VECTOR COMPONENTS FOR -P
01820       X1U=-X1/MAGP
01830       Y1U=-Y1/MAGP
01840       Z1U=-Z1/MAGP
01850       GO TO 8
01860 106 X1U=0.;Y1U=0.;Z1U=0.
01870 * NEW VELOCITY
01880     8 VX=VX+AX*DT
01890       VY=VY+AY*DT
01900       VZ=VZ+AZ*DT
01910       MAGV=SS(VX,VY,VZ)
01920       IF(MAGV.EQ.0.0) GO TO 108
01930 * UNIT VECTOR COMPONENTS FOR V
01940       VXU=VX/MAGV
01950       VYU=VY/MAGV
01960       VZU=VZ/MAGV
01970       GO TO 10
01980 108 VXU=0.;VYU=0.;VZU=0.
01990       GO TO 10
02000       END
```

```
00010       SUBROUTINE CURENT(F1,F2,F3,F4,XL11,XL21,XL31,XL41,
00020 &                              XI1,XI2,XI3,XI4)
00030       XII(A,B,C)=(0.5*ALOG(A)-1.2464*B + C)
00040
00050        IF(F1.GT.0.0) GO TO 10
00060       XI1=1.E-6
00070        GO TO 12
00080    10 XI1=EXP(XII(F1,XL11,2.7764))
00090    12 IF(F2.GT.0.0) GO TO 20
00100       XI2=1.E-6
00110        GO TO 22
00120    20 XI2=EXP(XII(F2,XL21,2.7733))
00130    22 IF(F3.GT.0.0)  GO TO 30
00140       XI3=1.E-6
00150        GO TO 32
00160    30 XI3=EXP(XII(F3,XL31,2.7611))
00170    32 IF(F4.GT.0.0) GO TO 40
00180       XI4=1.E-6
00190        GO TO 42
00200    40 XI4=EXP(XII(F4,XL41,2.7663))
00210    42 CONTINUE
00215 * ADJUST CURRENTS; DO NOT EXCEED MAX BUT KEEP RATIO
00220       XMAX=45.
00230       XTRY=AMAX1(XI1,XI2,XI3,XI4)
00240       IF(XTRY.LE.XMAX) GO TO 50
00250       FACT=XMAX/XTRY
00260       XI1=XI1*FACT
00270       XI2=XI2*FACT
00280       XI3=XI3*FACT
00290       XI4=XI4*FACT
00300    50 CONTINUE
00310       RETURN
00320       END
```

```
00010       SUBROUTINE CNVRTX(X1,Y1,Z1,X1P,Y1P,Z1P)
00020       A=SQRT(1./3.)
00030       B=SQRT(2./3.)
00040       X1P= A*X1       +0.0*Y1       +  B*Z1
00050       Y1P=0.0*X1      +1.0*Y1       +0.0*Z1
00060       Z1P= -B*X1      +0.0*Y1        +  A*Z1
00070       RETURN
00080       END
00010       SUBROUTINE TETMFO(X,Y,Z,Z1,Z2,Z3,Z4,SUMX,SUMY,SUMZ)
00020       DIMENSION EYA(4),EYB(4),EYC(4),EYD(4),SK(4),FX(4),FY(4),FZ(4)
00024       IF(X.EQ.0.0)    X=1.E-6
00026       IF(Y.EQ.0.0)    Y=1.E-6
00028       IF(Z.EQ.0.0)   Z=1.E-6
00070       A=1.15
00080       DO 10 I=1,4
00090       EYA(I)=1.E-6
00100       EYB(I)=1.E-6
00110       EYC(I)=1.E-6
00120       EYD(I)=1.E-6
00130    10 CONTINUE
00140       EYC(3)=Z1
00150       EYD(1)=Z2
00160       EYB(4)=Z3
00170       EYA(2)=Z4
00180       RS=0.5
00185       SCM=3.05
00190       S=SCM*.01;X=X*.01;Y=Y*.01;Z=Z*.01
00200       AM=A*.01
00210       SK(1)=RS/0.0477
00220       SK(2)=RS/0.0436
00230       SK(3)=RS/0.0494
00240       SK(4)=RS/0.0406
00250       RS=RS*.01
00260       PI=3.1415926
00270       F1=0.5*SQRT(3.0)
00280       G1=(1.0/6.0)*SQRT(3.0)
00290       F2=0.5
00300       F3=1.0/6.0
00310       F4=(2.0/3.0)*SQRT(2.0)
00320       G2=(1.0/12.0)*SQRT(6.0)
00330       F5=(1.0/3.0)*SQRT(2.0)
00340       F6=(1.0/3.0)*SQRT(6.0)
00350       F7=1.0/3.0
00360       DO 59 J=1,4
00370       XA=F1*(X+G1*S)-F2*(Y+F2*S)
00380       YA=F3*(X+G1*S)+G1*(Y+F2*S)-F4*(Z+G2*S)
00390       ZA=F5*(X+G1*S)+F6*(Y+F2*S)+F7*(Z+G2*S)
00400       ZAC=ZA
00410       RHOA=SQRT(XA*XA+YA*YA)
00420       PHIA=ATAN2(YA,XA)
00430       BPHIA=0.0
```

```
00440       CALL MAG(J,AM,EYA,RHOA,ZAC,BRHO,BZAC)
00450       BRA1=BRHO
00460       IF(RHOA.LT.1.0E-05) BRA1=0.0
00470       BZA1=BZAC
00480       SIH=(EXP(2.0*SK(J))-EXP(-SK(J)))/2.0
00490       SIH1=(EXP(SK(J))-EXP(-SK(J)))/2.0
00500       Q=(SIH-SIN(2.0*SK(J)))/(SIH1*SIH1+SIN(SK(J))*SIN(SK(J)))
00510       GX=1.0-(0.75/SK(J))*Q
00520       DRHOA=.0001
00530       RHOA=RHOA+DRHOA
00540       CALL MAG(J,AM,EYA,RHOA,ZAC,BRHO,BZAC)
00550       BRA2=BRHO
00560       BZA2=BZAC
00570       DBDRHO=(BRA2-BRA1)/DRHOA
00580       RHOA=RHOA-DRHOA
00590       ZAC=ZAC+.0001
00600       CALL MAG(J,AM,EYA,RHOA,ZAC,BRHO,BZAC)
00610       BRA3=BRHO
00620       BZA3=BZAC
00630       EMU=4.0*PI*1.0E-07
00640       DBDZ=(BZA3-BZA1)/0.0001
00650       DBRDZ=(BRA3-BRA1)/0.0001
00660       DBDZR=(BZA2-BZA1)/0.0001
00670       BT=SQRT(BRA1*BRA1+BZA1*BZA1)
00680       SA=BZA1/BT
00690       CA=BRA1/BT
00700       DBTDS=SA*CA*DBDZR+SA*SA*DBDZ+CA*CA*DBDRHO+SA*CA*DBRDZ
00710       FS=(-BT)*(DBTDS)*GX*2.0*PI*(1.0/EMU)*RS**3
00720       EMU=4.0*PI*1.0E-07
00730       FRHOA=FS*CA
00740       FZACA=FS*SA
00750       FZAP=FZACA
00760       FYAP=FRHOA*SIN(PHIA)
00770       FXAP=FRHOA*COS(PHIA)
00780       FXA=F1*FXAP+F3*FYAP+F5*FZAP
00790       FYA=(-F2)*FXAP+G1*FYAP+F6*FZAP
00800       FZA=(-F4)*FYAP+F7*FZAP
00810       XC=F1*(X+G1*S)+F2*(Y-F2*S)
00820       YC=(-F3)*(X+G1*S)+G1*(Y-F2*S)+F4*(Z+G2*S)
00830       ZC=F5*(X+G1*S)-F6*(Y-F2*S)+F7*(Z+G2*S)
00840       ZCC=ZC
00850       RHOC=SQRT(XC*XC+YC*YC)
00860       PHIC=ATAN2(YC,XC)
00870       BPHIC=0.0
00880       CALL MAG(J,AM,EYC,RHOC,ZCC,BRHO,BZAC)
00890       BRC1=BRHO
00900       IF(RHOC.LT.1.0E-05) BRC1=0.0
00910       BZC1=BZAC
00920       RHOC=RHOC+0.0001
00930       CALL MAG(J,AM,EYC,RHOC,ZCC,BRHO,BZAC)
00940       BRC2=BRHO
00950       BZC2=BZAC
00960       DBDRHO=(BRC2-BRC1)/0.0001
00970       RHOC=RHOC-0.0001
00980       ZCC=ZCC+0.0001
```

```
00990       CALL MAG(J,AM,EYC,RHOC,ZCC,BRHO,BZAC)
01000       BRC3=BRHO
01010       BZC3=BZAC
01020       DBDZ=(BZC3-BZC1)/0.0001
01030       DBRDZ=(BRC3-BRC1)/0.0001
01040       DBDZR=(BZC2-BZC1)/0.0001
01050       BT=SQRT(BRC1*BRC1+BZC1*BZC1)
01060       SA=BZC1/BT
01070       CA=BRC1/BT
01080       DBTDS=SA*CA*DBDZR+SA*SA*DBDZ+CA*CA*DBDRHO+SA*CA*DBRDZ
01090       FS=(-BT)*(DBTDS)*GX*2.0*PI*(1.0/EMU)*RS**3
01100       FRHOC=FS*CA
01110       FZACC=FS*SA
01120       FZCP=FZACC
01130       FYCP=FRHOC*SIN(PHIC)
01140       FXCP=FRHOC*COS(PHIC)
01150       FXC=F1*FXCP-F3*FYCP+F5*FZCP
01160       FYC=F2*FXCP+G1*FYCP-F6*FZCP
01170       FZC=F4*FYCP+F7*FZCP
01180       XD=Y
01190       YD=(-F7)*(X-F7*SQRT(3.0)*S)-F4*(Z+G2*S)
01200       ZD=(-F4)*(X-F7*SQRT(3.0)*S)+F7*(Z+G2*S)
01210       ZDC=ZD
01220       RHOD=SQRT(XD*XD+YD*YD)
01230       PHID=ATAN2(YD,XD)
01240       BPHID=0.0
01250       CALL MAG(J,AM,EYD,RHOD,ZDC,BRHO,BZAC)
01260       BRD1=BRHO
01270       IF(RHOD.LT.1.0E-05) BRD1=0.0
01280       BZD1=BZAC
01290       RHOD=RHOD+.0001
01300       CALL MAG(J,AM,EYD,RHOD,ZDC,BRHO,BZAC)
01310       BRD2=BRHO
01320       BZD2=BZAC
01330       DBDRHO=(BRD2-BRD1)/.0001
01340       RHOD=RHOD-.0001
01350       ZDC=ZDC+.0001
01360       CALL MAG(J,AM,EYD,RHOD,ZDC,BRHO,BZAC)
01370       BRD3=BRHO
01380       BZD3=BZAC
01390       DBDZ=(BZD3-BZD1)/.0001
01400       DBRDZ=(BRD3-BRD1)/0.0001
01410       DBDZR=(BZD2-BZD1)/0.0001
01420       BT=SQRT(BRD1*BRD1+BZD1*BZD1)
01430       SA=BZD1/BT
01440       CA=BRD1/BT
01450       DBTDS=SA*CA*DBDZR+SA*SA*DBDZ+CA*CA*DBDRHO+SA*CA*DBRDZ
01460       FS=(-BT)*(DBTDS)*GX*2.0*PI*(1.0/EMU)*RS**3
01470       FRHOD=FS*CA
01480       FZACD=FS*SA
01490       FZDP=FZACD
01500       FYDP=FRHOD*SIN(PHID)
01510       FXDP=FRHOD*COS(PHID)
01520       FXD=(-F7)*FYDP-F4*FZDP
01530       FYD=FXDP
01540       FZD=(-F4)*FYDP+F7*FZDP
01550       XB=X
01560       YB=-Y
01570       ZB=-Z+0.25*SQRT(6.0)*S
01580       ZBC=ZB
```

```
01590       RHOB=SQRT(XB*XB+YB*YB)
01600       PHIB=ATAN2(YB,XB)
01610       BPHIB=0.0
01620       CALL MAG(J,AM,EYB,RHOB,ZBC,BRHO,BZAC)
01630       BRB1=BRHO
01640       IF(RHOB.LT.1.0E-05) BRB1=0.0
01650       BZB1=BZAC
01660       RHOB=RHOB+0.0001
01670       CALL MAG(J,AM,EYB,RHOB,ZBC,BRHO,BZAC)
01680       BRB2=BRHO
01690       BZB2=BZAC
01700       DBDRHO=(BRB2-BRB1)/.0001
01710       RHOB=RHOB-.0001
01720       ZBC=ZBC+.0001
01730       CALL MAG(J,AM,EYB,RHOB,ZBC,BRHO,BZAC)
01740       BRB3=BRHO
01750       BZB3=BZAC
01760       DBDZ=(BZB3-BZB1)/.0001
01770       DBRDZ=(BRB3-BRB1)/0.0001
01780       DBDZR=(BZB2-BZB1)/0.0001
01790       BT=SQRT(BRB1*BRB1+BZB1*BZB1)
01800       SA=BZB1/BT
01810       CA=BRB1/BT
01820       DBTDS=SA*CA*DBDZR+SA*SA*DBDZ+CA*CA*DBDRHO+SA*CA*DBRDZ
01830       FS=(-BT)*(DBTDS)*GX*2.0*PI*(1.0/EMU)*RS**3
01840       FRHOB=FS*CA
01850       FZACB=FS*SA
01860       FZBP=FZACB
01870       FYBP=FRHOB*SIN(PHIB)
01880       FXBP=FRHOB*COS(PHIB)
01890       FXB=FXBP
01900       FYB=-FYBP
01910       FZB=-FZBP
01930       FX(J)=FXA+FXB+FXC+FXD
01940       FY(J)=FYA+FYB+FYC+FYD
01950       FZ(J)=FZA+FZB+FZC+FZD
01970    59 CONTINUE
01980       SUMX=0.0
01990       SUMY=0.0
02000       SUMZ=0.0
02010       DO 60 M=1,4
02020       SUMX=SUMX+FX(M)
02030       SUMY=SUMY+FY(M)
02040       SUMZ=SUMZ+FZ(M)
02050    60 CONTINUE
02060       SUMX=SUMX*9.0*1.0E+05
02070       SUMY=SUMY*9.0*1.0E+05
02080       SUMZ=SUMZ*9.0*1.0E+05
02110       FTOT=SQRT(SUMX*SUMX+SUMY*SUMY+SUMZ*SUMZ)
02150      RETURN
02160       END
```

```
00010       SUBROUTINE MAG(J,A,EYE,RHO,Z,BRHO,BZ)
00020       DIMENSION EYE(6)
00030       PI=3.1415926
00040       EMU=4.0*PI*1.0E-07
00050       S1=A*A+RHO*RHO+Z*Z
00060       S2=(A-RHO)*(A-RHO)+Z*Z
00070       S3=(A+RHO)*(A+RHO)+Z*Z
00080       S4=A*A-RHO*RHO-Z*Z
00090       EKS=4.0*A*RHO/S3
00100       EK=SQRT(EKS)
00110       Y=CELI(1,EK)
00120       TK=Y
00130       Y=CELI(2,EK)
00140       E=Y
00150       S5=-TK+(S1/S2)*E
00160       S6=Z/(RHO*SQRT(S3))
00170       BRHO=((EYE(J)*EMU)/(2.0*PI))*S6*S5
00180       S7=TK+(S4/S2)*E
00190       BZ=((EYE(J)*EMU)/(2.0*PI))*(1.0/SQRT(S3))*S7
00200       RETURN
00210       END
```

```
00010      SUBROUTINE CNVRTF(FXP,FYP,FZP,FFXU,FFYU,FFZU,XMAGFF)
00020       A=SQRT(1./3.)
00030       B=SQRT(2./3.)
00040       FX=   A*FXP      +0.0*FYP      -B*FZP
00050      FY=0.0*FXP        +1.0*FYP      +0.0*FZP
00060       FZ=   B*FXP      +0.0*FYP      +A*FZP
00070       XMAGFF=SQRT(FX**2+FY**2+FZ**2)
00080       IF (XMAGFF.EQ.0.0)  GO TO 20
00090 * F UNIT VECTOR COMPONENTS
00100       FFXU=FX/XMAGFF
00110       FFYU=FY/XMAGFF
00120       FFZU=FZ/XMAGFF
00130       GO TO 15
00140   20 FFXU=0.0 ;FFYU=0.0 ;FFZU=0.0
00150    15 CONTINUE
00160       RETURN
00170       END
```

COMPUTER PROGRAM ABSTRACT

DATE OF ABSTRACT:	PROGRAM NUMBER:	TITLE:
1/26/72	NAS8-27228 (Task 15)	TETRA AND CUBE

SYMBOLIC NAME:	LANGUAGE:	SHARING	STATUS	MAN MONTHS:	COMPUTER TYPE:
TETRA CUBE	FORTRAN IV	[x] YES [ ] NO	[x] UNDER DEVELOPMENT [ ] OPERATIONAL [ ] COMPLETED	0.25 MACHINE HOURS: 25	GE 605

ABSTRACT

This abstract covers two separate computer programs, TETRA and CUBE. Program TETRA was written as part of Task IV to compute the force components and total force (as a function of position) exerted on a small sphere due to the magnetic field created by energizing a four coil system, the coils assumed located at the vertices of a tetrahedron. CUBE is a similar program, except that it is written for a six coil system, the coils assumed at the centers of each face. Forces are computed from an approximate formula which makes use of the magnetic induction at a point and its deviative.

MSFC - Form 3416-2 (February 1970)

```
$LIST TETRA

06/07/72  09.628

00005       DIMENSION EYA(4),EYB(4),EYC(4),EYD(4),SK(4),FX(4),FY(4),FZ(4)
00020    79 READ:X,Y,Z
00030       PRINT 1,X,Y,Z
00040     1 FORMAT(3X,2HX=F7.4,3X,2HY=F7.4,3X,2HZ=F7.4)
00050       PRINT 2
00060     2 FORMAT(/)
00070       A=1.15
00125       EYA(1)=1.0;EYA(2)=47.5;EYA(3)=0.8;EYA(4)=1.0E-06
00126       EYB(1)=0.94;EYB(2)=2.4;EYB(3)=0.31;EYB(4)=1.0E-06
00127       EYC(1)=1.82;EYC(2)=1.4;EYC(3)=45.0;EYC(4)=1.0E-06
00130       EYD(1)=45.0;EYD(2)=2.75;EYD(3)=2.11;EYD(4)=1.0E-06
00163       SCM=3.05
00180       READ:(SK(I),I=1,4)
00210       RS=0.5
00270       S=SCM*.01;X=X*.01;Y=Y*.01;Z=Z*.01
00280       AM=A*.01
00290       RS=RS*.01
00300       PI=3.1415926
00320       F1=0.5*SQRT(3.0)
00330       G1=(1.0/6.0)*SQRT(3.0)
00340       F2=0.5
00350       F3=1.0/6.0
00360       F4=(2.0/3.0)*SQRT(2.0)
00370       G2=(1.0/12.0)*SQRT(6.0)
00380       F5=(1.0/3.0)*SQRT(2.0)
00390       F6=(1.0/3.0)*SQRT(6.0)
00400       F7=1.0/3.0
00405       DO 59 J=1,4
00410       XA=F1*(X+G1*S)-F2*(Y+F2*S)
00420       YA=F3*(X+G1*S)+G1*(Y+F2*S)-F4*(Z+G2*S)
00430       ZA=F5*(X+G1*S)+F6*(Y+F2*S)+F7*(Z+G2*S)
00440       ZAC=ZA
00450       RHOA=SQRT(XA*XA+YA*YA)
00460       PHIA=ATAN2(YA,XA)
00520       BPHIA=0.0
00530       CALL MAG(J,AM,EYA,RHOA,ZAC,BRHO,BZAC)
00540       BRA1=BRHO
00545       IF(RHOA.LT.1.0E-05) BRA1=0.0
00550       BZA1=BZAC
00590       SIH=(EXP(2.0*SK(J))-EXP(-SK(J)))/2.0
00600       SIH1=(EXP(SK(J))-EXP(-SK(J)))/2.0
00610       0=(SIH-SIN(2.0*SK(J)))/(SIH1*SIH1+SIN(SK(J))*SIN(SK(J)))
00620       GX=1.0-(0.75/SK(J))*0
00630       DRHOA=.0001
00640       RHOA=RHOA+DRHOA
00650       CALL MAG(J,AM,EYA,RHOA,ZAC,BRHO,BZAC)
00660       BRA2=BRHO
00670       BZA2=BZAC
```

```
00680       DBDRHO=(BRA2-BRA1)/DRHOA
00690       RHOA=RHOA-DRHOA
00700       ZAC=ZAC+.0001
00710       CALL MAG(J,AM,EYA,RHOA,ZAC,BRHO,BZAC)
00720       BRA3=BRHO
00730       BZA3=BZAC
00735       EMU=4.0*PI*1.0E-07
00740       DBDZ=(BZA3-BZA1)/0.0001
00741       DBRDZ=(BRA3-BRA1)/0.0001
00742       DBDZR=(BZA2-BZA1)/0.0001
00743       BT=SQRT(BRA1*BRA1+BZA1*BZA1)
00744       SA=BZA1/BT
00745       CA=BRA1/BT
00746       DBTDS=SA*CA*DBDZR+SA*SA*DBDZ+CA*CA*DBDRHO+SA*CA*DBRDZ
00747       FS=(-BT)*(DBTDS)*GX*2.0*PI*(1.0/EMU)*RS**3
00750       EMU=4.0*PI*1.0E-07
00760       FRHOA=FS*CA
00770       FZACA=FS*SA
00780       FZAP=FZACA
00790       FYAP=FRHOA*SIN(PHIA)
00800       FXAP=FRHOA*COS(PHIA)
00810       FXA=F1*FXAP+F3*FYAP+F5*FZAP
00820       FYA=(-F2)*FXAP+G1*FYAP+F6*FZAP
00830       FZA=(-F4)*FYAP+F7*FZAP
00870       XC=F1*(X+G1*S)+F2*(Y-F2*S)
00880       YC=(-F3)*(X+G1*S)+G1*(Y-F2*S)+F4*(Z+G2*S)
00890       ZC=F5*(X+G1*S)-F6*(Y-F2*S)+F7*(Z+G2*S)
00900       ZCC=ZC
00910       RHOC=SQRT(XC*XC+YC*YC)
00920       PHIC=ATAN2(YC,XC)
00980       EPHIC=0.0
00990       CALL MAG(J,AM,EYC,RHOC,ZCC,BRHO,BZAC)
01000       BRC1=BRHO
01005       IF(RHOC.LT.1.0E-05) BRC1=0.0
01010       BZC1=BZAC
01050       RHOC=RHOC+0.0001
01060       CALL MAG(J,AM,EYC,RHOC,ZCC,BRHO,BZAC)
01070       BRC2=BRHO
01080       BZC2=BZAC
01090       DBDRHO=(BRC2-BRC1)/0.0001
01100       RHOC=RHOC-0.0001
01110       ZCC=ZCC+0.0001
01120       CALL MAG(J,AM,EYC,RHOC,ZCC,BRHO,BZAC)
01130       BRC3=BRHO
01140       BZC3=BZAC
01150       DBDZ=(BZC3-BZC1)/0.0001
01151       DBRDZ=(BRC3-BRC1)/0.0001
01152       DBDZR=(BZC2-BZC1)/0.0001
01153       BT=SQRT(BRC1*BRC1+BZC1*BZC1)
01154       SA=BZC1/BT
01155       CA=BRC1/BT
01156       DBTDS=SA*CA*DBDZR+SA*SA*DBDZ+CA*CA*DBDRHO+SA*CA*DBRDZ
01157       FS=(-BT)*(DBTDS)*GX*2.0*PI*(1.0/EMU)*RS**3
01160       FRHOC=FS*CA
```

```
01160       FRHOC=FS*CA
01170       FZACC=FS*SA
01180       FZCP=FZACC
01190       FYCP=FRHOC*SIN(PHIC)
01200       FXCP=FRHOC*COS(PHIC)
01210       FXC=F1*FXCP-F3*FYCP+F5*FZCP
01220       FYC=F2*FXCP+G1*FYCP-F6*FZCP
01230       FZC=F4*FYCP+F7*FZCP
01270       XD=Y
01280       YD=(-F7)*(X-F7*SQRT(3.0)*S)-F4*(Z+G2*S)
01290       ZD=(-F4)*(X-F7*SQRT(3.0)*S)+F7*(Z+G2*S)
01300       ZDC=ZD
01310       RHOD=SQRT(XD*XD+YD*YD)
01320       PHID=ATAN2(YD,XD)
01380       BPHID=0.0
01390       CALL MAG(J,AM,EYD,RHOD,ZDC,BRHO,BZAC)
01400       BRD1=BRHO
01405       IF(RHOD.LT.1.0E-05) BRD1=0.0
01410       BZD1=BZAC
01450       RHOD=RHOD+.0001
01460       CALL MAG(J,AM,EYD,RHOD,ZDC,BRHO,BZAC)
01470       BRD2=BRHO
01480       BZD2=BZAC
01490       DBDRHO=(BRD2-BRD1)/.0001
01500       RHOD=RHOD-.0001
01510       ZDC=ZDC+.0001
01520       CALL MAG(J,AM,EYD,RHOD,ZDC,BRHO,BZAC)
01530       BRD3=BRHO
01540       BZD3=BZAC
01550       DBDZ=(BZD3-BZD1)/.0001
01551       DBRDZ=(BRD3-BRD1)/0.0001
01552       DBDZR=(BZD2-BZD1)/0.0001
01553       BT=SQRT(BRD1*BRD1+BZD1*BZD1)
01554       SA=BZD1/BT
01555       CA=BRD1/BT
01556       DBTDS=SA*CA*DBDZR+SA*SA*DBDZ+CA*CA*DBDRHO+SA*CA*DBRDZ
01557       FS=(-BT)*(DBTDS)*GX*2.0*PI*(1.0/EMU)*RS**3
01560       FRHOD=FS*CA
01570       FZACD=FS*SA
01580       FZDP=FZACD
01590       FYDP=FRHOD*SIN(PHID)
01600       FXDP=FRHOD*COS(PHID)
01610       FXD=(-F7)*FYDP-F4*FZDP
01620       FYD=FXDP
01630       FZD=(-F4)*FYDP+F7*FZDP
01670       XB=X
01680       YB=-Y
01690       ZB=-Z+0.25*SQRT(6.0)*S
01700       ZBC=ZB
01710       RHOB=SQRT(XB*XB+YB*YB)
01720       PHIB=ATAN2(YB,XB)
01780       BPHIB=0.0
01790       CALL MAG(J,AM,EYB,RHOB,ZBC,BRHO,BZAC)
01800       BBR1=BRHO
```

```
01800        BRB1=BRHO
01805        IF(RHOB.LT.1.0E-05) BRB1=0.0
01810        BZB1=BZAC
01860        RHOB=RHOB+0.0001
01870        CALL MAG(J,AM,EYB,RHOB,ZBC,BRHO,BZAC)
01880        BRB2=BRHO
01890        BZB2=BZAC
01900        DBDRHO=(BRB2-BRB1)/.0001
01910        RHOB=RHOB-.0001
01920        ZBC=ZBC+.0001
01930        CALL MAG(J,AM,EYB,RHOB,ZBC,BRHO,BZAC)
01940        BRB3=BRHO
01950        BZB3=BZAC
01960        DBDZ=(BZB3-BZB1)/.0001
01961        DBRDZ=(BRB3-BRB1)/0.0001
01962        DBDZR=(BZB2-BZB1)/0.0001
01963        BT=SQRT(BRB1*BRB1+BZB1*BZB1)
01964        SA=BZB1/BT
01965        CA=BRB1/BT
01966        DBTDS=SA*CA*DBDZR+SA*SA*DBDZ+CA*CA*DBDRHO+SA*CA*DBRDZ
01967        FS=(-BT)*(DBTDS)*GX*2.0*PI*(1.0/EMU)*RS**3
01970        FRHOB=FS*CA
01980        FZACB=FS*SA
01990        FZBP=FZACB
02000        FYBP=FRHOB*SIN(PHIB)
02010        FXBP=FRHOB*COS(PHIB)
02020        FXB=FXBP
02030        FYB=-FYBP
02040        FZB=-FZBP
02060        PRINT 2
02080        FX(J)=FXA+FXB+FXC+FXD
02090        FY(J)=FYA+FYB+FYC+FYD
02100        FZ(J)=FZA+FZB+FZC+FZD
02120     50 FORMAT(3X,3HFX=E14.6,2X,3HFY=E14.6,2X,3HFZ=E14.6)
02125     59 CONTINUE
02130        SUMX=0.0
02140        SUMY=0.0
02150        SUMZ=0.0
02160        DO 60 M=1,4
02170        SUMX=SUMX+FX(M)
02180        SUMY=SUMY+FY(M)
02190        SUMZ=SUMZ+FZ(M)
02200     60 CONTINUE
02210        SUMX=SUMX*9.0*1.0E+05
02220        SUMY=SUMY*9.0*1.0E+05
02230        SUMZ=SUMZ*9.0*1.0E+05
02240        PRINT:"COMPUTE TOTAL FORCE COMPONENTS"
02250        PRINT 50,SUMX,SUMY,SUMZ
02260        FTOT=SQRT(SUMX*SUMX+SUMY*SUMY+SUMZ*SUMZ)
02270        PRINT 70,FTOT
02280     70 FORMAT(3X,12HTOTAL FORCE=E14.6,1X,5HDYNES)
02282        PRINT:"GO TO NEXT CASE"
02283        PRINT 2
```

```
02284       GO TO 79
02290       END


READY
```

$LIST CUBE

```
06/07/72  09.325

00010       DIMENSION EYA(6),EYB(6),EYC(6),EYD(6),EYE(6),EYF(6),
00020 &     SK(6),FX(6),FY(6),FZ(6)
00030    79 READ:X,Y,Z
00040       PRINT 1,X,Y,Z
00050     1 FORMAT(3X,2HX=F7.4,3X,2HY=F7.4,3X,2HZ=F7.4)
00060       PRINT 2
00070     2 FORMAT(/)
00080       A=1.15
00090       EYA(1)=1.0E-06;EYA(2)=1.0E-06;EYA(3)=45.0;EYA(4)=1.0E-06
00091       EYA(5)=1.0E-06;EYA(6)=1.0E-06
00100       EYB(1)=1.0E-06;EYB(2)=1.0E-06;EYB(3)=1.0E-06;EYB(4)=1.0E-06
00101       EYB(5)=1.0E-06;EYB(6)=1.0E-06
00110       EYC(1)=1.0E-06;EYC(2)=1.0E-06;EYC(3)=1.0E-06;EYC(4)=1.0E-06
00111       EYC(5)=1.0E-06;EYC(6)=1.0E-06
00120       EYD(1)=1.0E-06;EYD(2)=45.0;EYD(3)=1.0E-06;EYD(4)=1.0E-06
00121       EYD(5)=1.0E-06;EYD(6)=1.0E-06
00130       EYE(1)=1.0E-06;EYE(2)=1.0E-06;EYE(3)=1.0E-06;EYE(4)=1.0E-06
00131       EYE(5)=1.0E-06;EYE(6)=1.0E-06
00140       EYF(1)=45.0;EYF(2)=1.0E-06;EYF(3)=1.0E-06;EYF(4)=1.0E-06
00141       EYF(5)=1.0E-06;EYF(6)=1.0E-06
00150       SK(1)=14.7;SK(2)=15.6;SK(3)=16.7;SK(4)=1.0E-06
00151       SK(5)=1.0E-06;SK(6)=1.0E-06
00160       SCM=3.33
00170       RS=0.5
00180       S=SCM*0.01;X=X*0.01;Y=Y*0.01;Z=Z*0.01
00190       AM=A*0.01
00200       RS=RS*0.01
            PI=3.1415926
```

```
00210       PI=3.1415926
00220       DO 59 J=1,6
00230       XA=Z
00240       YA=Y
00250       ZA=S/2.0-X
00260       ZAC=ZA
00270       RHOA=SQRT(XA*XA+YA*YA)
00280       PHIA=ATAN2(YA,XA)
00290       BPHIA=0.0
00300       CALL MAG(J,AM,EYA,RHOA,ZAC,BRHO,BZAC)
00310       BRA1=BRHO
00320       IF(RHOA.LT.1.0E-05) BRA1=0.0
00330       BZA1=BZAC
00340       SIH=(EXP(2.0*SK(J))-EXP(-SK(J)))/2.0
00350       SIH1=(EXP(SK(J))-EXP(-SK(J)))/2.0
00360       Q=(SIH-SIN(2.0*SK(J)))/(SIH1*SIH1+SIN(SK(J))*SIN(SK(J)))
00370       GX=1.0-(0.75/SK(J))*Q
00380       RHOA=RHOA+0.0001
00390       CALL MAG(J,AM,EYA,RHOA,ZAC,BRHO,BZAC)
00400       BRA2=BRHO
00410       BZA2=BZAC
00420       DBDRHO=(BRA2-BRA1)/0.0001
00430       RHOA=RHOA-0.0001
00440       ZAC=ZAC+0.0001
00450       CALL MAG(J,AM,EYA,RHOA,ZAC,BRHO,BZAC)
00460       BRA3=BRHO
00470       BZA3=BZAC
00480       EMU=4.0*PI*1.0E-07
00490       DBDZ=(BZA3-BZA1)/0.0001
00500       DBRDZ=(BRA3-BRA1)/0.0001
00510       DBDZR=(BZA2-BZA1)/0.0001
00520       BT=SQRT(BRA1*BRA1+BZA1*BZA1)
00530       SA=BZA1/BT
00540       CA=BRA1/BT
00550       DBTDS=SA*CA*DBDZR+SA*SA*DBDZ+CA*CA*DBDRHO+SA*CA*DBRDZ
00560       FS=(-BT)*(DBTDS)*GX*2.0*PI*(1.0/EMU)*RS**3
00570       FRHOA=FS*CA
00580       FZACA=FS*SA
00590       FZAP=FZACA
00600       FYAP=FRHOA*SIN(PHIA)
00610       FXAP=FRHOA*COS(PHIA)
00620       FXA=-FZAP
00630       FYA=FYAP
00640       FZA=FXAP
00650       XB=X
00660       YB=-Z
00670       ZB=Y+S/2.0
00680       ZBC=ZB
00690       RHOB=SQRT(XB*XB+YB*YB)
00700       PHIB=ATAN2(YB,XB)
00710       BPHIB=0.0
00720       CALL MAG(J,AM,EYB,RHOB,ZBC,BRHO,BZAC)
00730       BRB1=BRHO
```

```
00740       IF(RHOB.LT.1.0E-05) BRB1=0.0
00750       BZB1=BZAC
00760       RHOB=RHOB+0.0001
00770       CALL MAG(J,AM,EYB,RHOB,ZBC,BRHO,BZAC)
00780       BRB2=BRHO
00790       BZB2=BZAC
00800       DBDRHO=(BRB2-BRB1)/0.0001
00810       RHOB=RHOB-0.0001
00820       ZBC=ZBC+0.0001
00830       CALL MAG(J,AM,EYB,RHOB,ZBC,BRHO,BZAC)
00840       BRB3=BRHO
00850       BZB3=BZAC
00860       DBDZ=(BZB3-BZB1)/0.0001
00870       DBRDZ=(BRB3-BRB1)/0.0001
00880       DBDZR=(BZB2-BZB1)/0.0001
00890       BT=SQRT(BRB1*BRB1+BZB1*BZB1)
00900       SA=BZB1/BT
00910       CA=BRB1/BT
00920       DBTDS=SA*CA*DBDZR+SA*SA*DBDZ+CA*CA*DBDRHO+SA*CA*DBRDZ
00930       FS=(-BT)*(DBTDS)*GX*2.0*PI*(1.0/EMU)*RS**3
00940       FRHOB=FS*CA
00950       FZACB=FS*SA
00960       FZBP=FZACB
00970       FYBP=FRHOB*SIN(PHIB)
00980       FXBP=FRHOB*COS(PHIB)
00990       FXB=FXBP
01000       FYB=FZBP
01010       FZB=-FYBP
01020       XC=-Z
01030       YC=Y
01040       ZC=X+S/2.0
01050       ZCC=ZC
01060       RHOC=SQRT(XC*XC+YC*YC)
01070       PHIC=ATAN2(YC,XC)
01080       BPHIC=0.0
01090       CALL MAG(J,AM,EYC,RHOC,ZCC,BRHO,BZAC)
01100       BRC1=BRHO
01110       IF(RHOC.LT.1.0E-05) BRC1=0.0
01120       BZC1=BZAC
01130       RHOC=RHOC+0.0001
01140       CALL MAG(J,AM,EYC,RHOC,ZCC,BRHO,BZAC)
01150       BRC2=BRHO
01160       BZC2=BZAC
01170       DBDRHO=(BRC2-BRC1)/0.0001
01180       RHOC=RHOC-0.0001
01190       ZCC=ZCC+0.0001
01200       CALL MAG(J,AM,EYC,RHOC,ZCC,BRHO,BZAC)
01210       BRC3=BRHO
01220       BZC3=BZAC
01230       DBDZ=(BZC3-BZC1)/0.0001
01240       DBRDZ=(BRC3-BRC1)/0.0001
01250       DBDZR=(BZC2-BZC1)/0.0001
01260       BT=SQRT(BRC1*BRC1+BZC1*BZC1)
01270       SA=BZC1/BT
```

```
01270       SA=BZC1/BT
01280       CA=BRC1/BT
01290       DBTDS=SA*CA*DBDZR+SA*SA*DBDZ+CA*CA*DBDRHO+SA*CA*DBRDZ
01300       FS=(-BT)*(DBTDS)*GX*2.0*PI*(1.0/EMU)*RS**3
01310       FRHOC=FS*CA
01320       FZACC=FS*SA
01330       FZCP=FZACC
01340       FYCP=FRHOC*SIN(PHIC)
01350       FXCP=FRHOC*COS(PHIC)
01360       FXC=FZCP
01370       FYC=FYCP
01380       FZC=-FXCP
01390       XD=X
01400       YD=Z
01410       ZD=S/2.0-Y
01420       ZDC=ZD
01430       RHOD=SQRT(XD*XD+YD*YD)
01440       PHID=ATAN2(YD,XD)
01450       BPHID=0.0
01460       CALL MAG(J,AM,EYD,RHOD,ZDC,BRHO,BZAC)
01470       BRD1=BRHO
01480       IF(RHOD.LT.1.0E-05) BRD1=0.0
01490       BZD1=BZAC
01500       RHOD=RHOD+0.0001
01510       CALL MAG(J,AM,EYD,RHOD,ZDC,BRHO,BZAC)
01520       BRD2=BRHO
01530       BZD2=BZAC
01540       DBDRHO=(BRD2-BRD1)/0.0001
01550       RHOD=RHOD-0.0001
01560       ZDC=ZDC+0.0001
01570       CALL MAG(J,AM,EYD,RHOD,ZDC,BRHO,BZAC)
01580       BRD3=BRHO
01590       BZD3=BZAC
01600       DBDZ=(BZD3-BZD1)/0.0001
01610       DBRDZ=(BRD3-BRD1)/0.0001
01620       DBDZR=(BZD2-BZD1)/0.0001
01630       BT=SQRT(BRD1*BRD1+BZD1*BZD1)
01640       SA=BZD1/BT
01650       CA=BRD1/BT
01660       DBTDS=SA*CA*DBDZR+SA*SA*DBDZ+CA*CA*DBDRHO+SA*CA*DBRDZ
01670       FS=(-BT)*(DBTDS)*GX*2.0*PI*(1.0/EMU)*RS**3
01680       FRHOD=FS*CA
01690       FZACD=FS*SA
01700       FZDP=FZACD
01710       FYDP=FRHOD*SIN(PHID)
01720       FXDP=FRHOD*COS(PHID)
01730       FXD=FXDP
01740       FYD=-FZDP
01750       FZD=FYDP
01760       XE=X
01770       YE=-Y
01780       ZE=S/2.0-Z
01790       ZEC=ZE
```

```
01800       RHOE=SQRT(XE*XE+YE*YE)
01810       PHIE=ATAN2(YE,XE)
01820       BPHIE=0.0
01830       CALL MAG(J,AM,EYE,RHOE,ZEC,BRHO,BZAC)
01840       BRE1=BRHO
01850       IF(RHOE.LT.1.0E-05) BRE1=0.0
01860       BZE1=BZAC
01870       RHOE=RHOE+0.0001
01880       CALL MAG(J,AM,EYE,RHOE,ZEC,BRHO,BZAC)
01890       BRE2=BRHO
01900       BZE2=BZAC
01910       DBDRHO=(BRE2-BRE1)/0.0001
01920       RHOE=RHOE-0.0001
01930       ZEC=ZEC+0.0001
01940       CALL MAG(J,AM,EYE,RHOE,ZEC,BRHO,BZAC)
01950       BRE3=BRHO
01960       BZE3=BZAC
01970       DBDZ=(BZE3-BZE1)/0.0001
01980       DBRDZ=(BRE3-BRE1)/0.0001
01990       DBDZR=(BZE2-BZE1)/0.0001
02000       BT=SQRT(BRE1*BRE1+BZE1*BZE1)
02010       SA=BZE1/BT
02020       CA=BRE1/BT
02030       DBTDS=SA*CA*DBDZR+SA*SA*DBDZ+CA*CA*DBDRHO+SA*CA*DBRDZ
02040       FS=(-BT)*(DBTDS)*GX*2.0*PI*(1.0/EMU)*RS**3
02050       FRHOE=FS*CA
02060       FZACE=FS*SA
02070       FZEP=FZACE
02080       FYEP=FRHOE*SIN(PHIE)
02090       FXEP=FRHOE*COS(PHIE)
02100       FXE=FXEP
02110       FYE=-FYEP
02120       FZE=-FZEP
02130       XF=X
02140       YF=Y
02150       ZF=Z+S/2.0
02160       ZFC=ZF
02170       RHOF=SQRT(XF*XF+YF*YF)
02180       PHIF=ATAN2(YF,XF)
02190       BPHIF=0.0
02200       CALL MAG(J,AM,EYF,RHOF,ZFC,BRHO,BZAC)
02210       BRF1=BRHO
02220       IF(RHOF.LT.1.0E-05) BRF1=0.0
02230       BZF1=BZAC
02240       RHOF=RHOF+0.0001
02250       CALL MAG(J,AM,EYF,RHOF,ZFC,BRHO,BZAC)
02260       BRF2=BRHO
02270       BZF2=BZAC
02280       DBDRHO=(BRF2-BRF1)/0.0001
02290       RHOF=RHOF-0.0001
02300       ZFC=ZFC+0.0001
02310       CALL MAG(J,AM,EYF,RHOF,ZFC,BRHO,BZAC)
02320       BRF3=BRHO
02330       BZF3=BZAC
```

```
02330        BZF3=BZAC
02340        DBDZ=(BZF3-BZF1)/0.0001
02350        DBRDZ=(BRF3-BRF1)/0.0001
02360        DBDZR=(BZF2-BZF1)/0.0001
02370        BT=SQRT(BRF1*BRF1+BZF1*BZF1)
02380        SA=BZF1/BT
02390        CA=BRF1/BT
02400        DBTDS=SA*CA*DBDZR+SA*SA*DBDZ+CA*CA*DBDRHO+SA*CA*DBRDZ
02410        FS=(-BT)*(DBTDS)*GX*2.0*PI*(1.0/EMU)*RS**3
02420        FRHOF=FS*CA
02430        FZACF=FS*SA
02440        FZFP=FZACF
02450        FYFP=FRHOF*SIN(PHIF)
02460        FXFP=FRHOF*COS(PHIF)
02470        FXF=FXFP
02480        FYF=FYFP
02490        FZF=FZFP
02500        PRINT 2
02510        FX(J)=FXA+FXB+FXC+FXD+FXE+FXF
02520        FY(J)=FYA+FYB+FYC+FYD+FYE+FYF
02530        FZ(J)=FZA+FZB+FZC+FZD+FZE+FZF
02540    50  FORMAT(3X,3HFX=E14.6,2X,3HFY=E14.6,2X,3HFZ=E14.6)
02550    59  CONTINUE
02560        SUMX=0.0
02570        SUMY=0.0
02580        SUMZ=0.0
02590        DO 60 M=1,6
02600        SUMX=SUMX+FX(M)
02610        SUMY=SUMY+FY(M)
02620        SUMZ=SUMZ+FZ(M)
02630    60  CONTINUE
02640        SUMX=SUMX*9.0*1.0E+05
02650        SUMY=SUMY*9.0*1.0E+05
02660        SUMZ=SUMZ*9.0*1.0E+05
02670        PRINT:"COMPUTE TOTAL FORCE COMPONENTS"
02680        PRINT 50,SUMX,SUMY,SUMZ
02690        FTOT=SQRT(SUMX*SUMX+SUMY*SUMY+SUMZ*SUMZ)
02700        PRINT 70,FTOT
02710    70  FORMAT(3X,12HTOTAL FORCE=E14.6,1X,5HDYNES)
02720        PRINT:"GO TO NEXT CASE"
02730        PRINT 2
02740        GO TO 79
02750        END


READY
```

APPENDIX C

UNITS AND CONVERSIONS

For magnetic field computations, CGS and gaussian units are most convenient. In this system of units based on the centimeter, gram and second the magnetic field strength H in vacuum (or air) along the axis of a single turn coil of radius a is given by $H = \frac{2\pi a}{r^2} i$, where H is the field strength in oersteds and r is the slant range to the coil winding, a and r are both measured in centimeters, and i is the current flowing measured in abamperes (10 amperes = 1 abampere). All of the coil configurations considered in this study can be resolved into a summation of such single turn elements. In a vacuum the field strength H and the magnetic induction have, in CGS units, the same numerical value, i.e., B = H. B is measured in gauss. The force on a conductor carrying a current density $\vec{j}$ is given by $\frac{1}{c} \vec{j} \times \vec{H}$ dynes per cubic centimeter, where $\vec{j}$ is measured in abamperes per square centimer and c is the speed of light measured in centimeters per second.

In MKS units, which are most convenient in discussing practical electrical circuitry and which are also becoming more widely used in all phases of electrical theory, the field strength H due to a single current carrying coil turn of radius a is given by $H = \frac{a}{2r^2} i$ along the axis of the winding at a slant distance r. The coil radius a and the slant range r must be expressed in meters and the current i in amperes. The unit of field

strength H is the Maxwell (or ampere turn per meter). In this set of units B and H have a different numerical value in a vacuum. In MKS units the vacuum relation between B and H is given by $B = 4\pi \cdot 10^{-7} H$. B is measured in webers per square meter.

The conversion between these units is given in the brief list which should suffice for the limited scope of the present report.

CGS-Gauss		MKS
1 gauss	=	10^{-4} w-m^{-2}
1 oersted = $\frac{10^3}{4\pi}$ Maxwells	=	79.5 Maxwells
1 abampere	=	10 amperes
1 cm	-	10^{-2} m